AN ALGORITHM FOR THE EXTRACTION OF OCEAN WAVE SPECTRA FROM NARROW BEAM HF RADAR BACKSCATTER

RANDY KEITH HOWELL, B.Eng.

AN ALGORITHM FOR THE EXTRACTION OF OCEAN WAVE SPECTRA FROM NARROW BEAM HF RADAR BACKSCATTER

by

©Randy Keith Howell, B.Eng.

A thesis submitted to the School of Graduate Studies
in partial fulfillment of the requirements for the
degree of Master of Engineering

Faculty of Engineering and Applied Science
Memorial University of Newfoundland
March, 1990
St. John's Newfoundland

ISBN 0-315-61786-1

Abstract

An algorithm is developed and tested to interpret ocean wave spectra from the backscatter return of one or more narrow beam HF radars. The basis of this measurement is the inversion of the integral equation representing the second order radar cross section of the ocean surface (Barrick and Lipa, 1986; Srivastava, 1984; Walsh and Howell, 1990). This equation is numerically inverted by approximating it as a matrix equation and factorizing the resultant kernel matrix using a singular value decomposition to obtain its pseudo-inverse.

Due to the limitations of the assumption used to linearize the integral equation, the proposed inversion algorithm is best suited for general use at high HF frequencies ($\approx$ 20 to 30 MHz). However, this algorithm may still be applied for the crucial task of monitoring large sea state conditions at even very low HF frequencies ($<$ 10 MHz).

As a test of this algorithm, comparisons are made between wave spectrum estimates obtained from a WAVEC buoy and a set of two 25.4 MHz ground wave radars that were deployed during the 1986 Canadian Atlantic Storms Program (CASP). Overall, the results of this experiment have been positive and have demonstrated both the basic feasibility of the inversion algorithm and the wave sensing capability of HF radar.

When using the data of a single radar, the principal information that can be obtained is the nondirectional or one-dimensional (1-D) wave spectrum. Although directional information may be obtained from a single radar it suffers from a left/right directional ambiguity. In general, the comparison of single radar estimates for the 1-D spectrum with those of the buoy at CASP have been good. This is demonstrated by the reasonable average difference from the buoy of $\approx$ 15% for significant waveheight estimates. This figure is roughly the same for all cross section models.

When using the data of two radars, not only can more accurate estimates of the

1-D spectrum be obtained but full directional information as well. The comparison of dual-radar wave spectrum estimates with those of the buoy at CASP have been very good. For the Walsh and Howell (1990) cross section model, dual-radar significant waveheight estimates differed from the buoy by only 4.6% on average. For the Barrick and Lipa (1986) and Srivastava (1984) models this average difference is 9.1%. For all models, the average difference for dominant direction estimates is $\approx 10°$.

Although all cross section models produced estimates that correlated well with the buoy, it was the Walsh and Howell (1990) model which consistently provided the best agreement. This would seem to indicate that the Walsh and Howell theory provides a better model for the radar spectrum. Due to the somewhat small size of the CASP data set it is not yet possible to be statistically confident of this finding.

Acknowledgements

The author is indebted to his supervisor, Dr. John Walsh, Professor, Faculty of Engineering and Applied Science, for the advice and guidance he has given throughout the course of this study. Although it may be preliminary, the author would also like thank Dr. Walsh for giving him the opportunity to continue the work started in this thesis as his Ph.D. student.

Thanks are also owed to Dr. J. Clark, Director, Centre for Cold Ocean Resources Engineering (C-CORE), for providing graduate student support in the form of a C-CORE fellowship and for providing office space at C-CORE. The additional support provided by Dr. Walsh through his NSERC strategic grant is also gratefully acknowledged.

The use of the CASP data set has been important to this work and the time and effort invested in furnishing this data to the author is greatly appreciated. The wave spectra measured by the WAVEC buoy was provided to the author by Dr. William Perrie and Mr. Bechara Toulany of the Bedford Institute of Oceanography. The author's principal contact with C-CORE for the CASP radar data has been Mr. Kenneth Hickey Jr. who, in addition to providing this data in a convenient form, has been instrumental in familiarizing the author with the experiment. Special thanks are due to Mr. Hickey for this effort.

The assistance and helpful suggestions provided by Dr. Satish Srivastava, Dr. Rafaat Khan, Mr. Eric Gill, Mr. Barry Dawe, and Mr. William Winsor is also appreciated.

Contents

List of Figures

List of Tables

List of Symbols

Roman Letters

$[a_o(f), b_o(f)]$	[even, odd] wave Fourier coefficients
$[a_o(F), b_o(F)]$	Normalized [even, odd] Fourier coefficients, $= [a_o(f), b_o(f)]\,(2k_o)^{5/2}$
C	Kernel function of the second order integral equation
$\boldsymbol{C}$	Kernel matrix
d	Water depth
D	Normalized water depth, $= 2k_o d$
$e(f)$	One-dimensional temporal wave spectrum
$e(f, \theta)$	Two-dimensional temporal wave spectrum
$E(F, \theta)$	Normalized 2-D temporal wave spectrum, $= e(f, \theta)(2k_o)^{5/2}$
f	Ocean frequency
F	Normalized ocean frequency, $= f\sqrt{2k_o}$
g	Acceleration due to gravity
$g(\theta)$	Ocean directional distribution function
f_p	Peak frequency of the wave spectrum
h	rms waveheight
h_s	Significant waveheight, $= 4h$
$H(\theta)$	$= .5$ for $\theta = 0$ or π, $= 1$ otherwise
I	Number of Doppler points per sideband for $0.15 < u < 0.36$
J	Number of ocean frequency bands

J_t	Jacobian of transformation
k_o	Radar wavenumber
$\hat{k}_o$	Look direction of radar
$\vec{k}, k$	Ocean wavenumber vector and magnitude
$\vec{K}, K$	Normalized ocean wavenumber vector and magnitude, $= 2k_o(\vec{k}, k)$
$\vec{k}'$	$\vec{k} + \vec{k}' = -2\vec{k}_o$
$\vec{K}'$	$= 2k_o\vec{k}', \vec{K} + \vec{K}' = -\hat{k}_o$
K_d	$= K\tanh(KD)$
K'_d	$= K'\tanh(K'D)$
L	$= mm'$
m, m'	Set of indices identifying a second order sideband
r	Number of singular values retained
$R_{m'}$	Total first order power for the m' Doppler half of the spectrum
s	Spread parameter of the cardioid distribution
$s(k,\theta)$	Two-dimensional spatial wave spectrum
$S(K,\theta)$	Normalized 2-D spatial wave spectrum, $= s(k,\theta)(2k_o)^4$
T	$E(F,\theta) = TS(K,\theta)$
u	normalized Doppler shift from first order peak
U_w	Wind speed
$\boldsymbol{U}$	Orthogonal matrix containing the right singular vectors of $\boldsymbol{C}$
$\boldsymbol{V}$	Orthogonal matrix containing the left singular vectors of $\boldsymbol{C}$
$\boldsymbol{x}$	Solution vector of $\boldsymbol{Cx} = \boldsymbol{\sigma}$

Greek Letters

α	Direction of wave vector $m\vec{k}$
α'	Direction of wave vector $m'\vec{k'}$
β	Angular separation between $\hat{k_o}$ and $\vec{k'}$
Γ	Gamma function
Γ_1	Normalized single scatter coupling coefficient
Γ_2	Normalized double scatter coupling coefficient
Γ_s	Total coupling coefficient, $= \Gamma_1 + \Gamma_2$
$\delta(x)$	Dirac delta function
Δ	Average value of the normalized surface impedance
$\Delta\theta$	Half-power beamwidth of cardioid distribution
Δu	Normalized Doppler resolution of radar spectrum
η	Normalized Doppler frequency, $= \omega_d/\omega_B$
θ	Direction of wave vector $\vec{k}$
θ'	Direction of wave vector $\vec{k'}$
$\overline{\theta}$	Mean direction parameter of the cardioid distribution
θ_d	Dominant direction of the wavefield
μ_i	ith singular value, also the ith diagonal element of $\boldsymbol{\Sigma}$
σ^n	nth order radar cross section
σ_n	Normalized nth order radar cross section, $= \omega_B \sigma^n$

σ_{2L}	Linearized second order radar cross section
${}_n\sigma_{2L}$	σ_{2L} corresponding to radar # n
$\boldsymbol{\sigma}$	Data vector of radar spectral values
$\boldsymbol{\Sigma}$	Diagonal matrix containing the singular values of $\boldsymbol{C}$
ϕ	One-half the angular separation between radar beams
ϕ_c	Wave crossing angle
ω	Ocean radian frequency
ω_d	Doppler frequency
ω_B	Bragg frequency, $= \sqrt{2gk_o \tanh(2k_o d)}$

Special Symbols

$\boldsymbol{C}^+$	Pseudo-inverse of matrix $\boldsymbol{C}$
$\boldsymbol{C}^{-1}$	Inverse of matrix $\boldsymbol{C}$

Abbreviations

1-D	One-dimensional
2-D	Two-dimensional
BL/S	Barrick and Lipa (1986) and Srivastava (1984)
CASP	Canadian Atlantic Storms Program
SVD	Singular value decomposition
WH	Walsh and Howell (1990)

Chapter 1

Introduction

1.1 General Introduction

The measurement of ocean wave information is of great importance for a variety of marine applications. Among its uses include: the preparation of marine forecasts; oceanographic and fisheries research; vessel navigation; and the planning and operation of many ocean engineering projects and activities (e.g., resource development). Reliable and economic monitoring of ocean surface conditions over large areas is of considerable interest and importance.

A remote sensing device which has the potential to help meet this important need is HF Doppler radar. On the basis of its radio propagation mode, two types of HF radars may be identified that are applicable to this problem, namely ground wave and sky wave radars.

Ground wave radars employ the ground wave mode of radio propagation where the radar signal is guided by a good conducting surface such as the ocean to follow a path that essentially matches the earth's curvature. Consequently, ground wave signals may reach well beyond the normal line-of-sight horizon that limits conventional radar systems. Operation in the HF band (3 - 30 MHz) not only permits efficient ground wave propagation so that large detection ranges are obtained (potentially 200 km for wave measurements) but causes the transmitted signal to react strongly with the ocean surface. The resulting echo return will contain a wealth of information

concerning ocean surface conditions. The use of these radars for the mapping of surface currents is now a well established practice. A new challenge for these systems is the measurement of wave spectra.

Sky wave radars take advantage of the mirror-like properties of the charged particle layer of the atmosphere called the ionosphere to reflect a HF radio wave out to ranges up to 3000 km. Although great range is achieved by ionospheric propagation, the variable motions of the ionosphere present a problem for wave sensing due to the (often considerable) smearing of the radar Doppler spectrum it introduces. This contamination generally precludes sky wave radars from measuring ocean currents and often prevents them from extracting detailed wave information from the radar return. However, it is still possible to obtain many important statistical parameters regarding the wave spectrum from sky wave returns.

HF radars offer several advantages over conventional *in situ* wave measurement techniques (e.g., wave buoys). Perhaps the most important of these is the ability of these radars to monitor a large region of ocean (subdivided into cells) out to considerable distances from shore. This clearly differs from *in situ* devices which would require the expensive deployment of many such units to match the coverage of a single radar. *In situ* sensors are also generally less reliable than HF radars since they are difficult to access for maintenance and sometimes experience data loss during high sea states. They are also generally constrained to operate near the coast in order to find safe anchorage.

An excellent discussion of the benefits offered by HF radars may be found in van Heteren et al. (1986). This paper discusses the Netherlands' interest in using HF ground wave radars for its wave and current measurement program which is already one of the most sophisticated in the world.

Much progress has been made in understanding the relationship between the Doppler spectrum of the backscattered radar signal and the ocean wave spectrum.

The echo return is in the form of a Doppler spectrum due to the Doppler frequency shifts induced to the incident radio wave by the moving ocean waves. The physical mechanism for the interaction of the radar signal with the ocean surface is that of Bragg scattering (Crombie (1955)). Theoretical formulations for the backscatter spectrum have been developed by Barrick (1972), Srivastava (1984), and Walsh and Howell (1990). It was found from these analyses that wave information may be interpreted from the second order component of the received Doppler spectrum. This requires the inversion of a two-dimensional integral equation of the first kind. Although this integral equation is nonlinear, it may be easily approximated as a linear equation for the Doppler region of interest.

Integral equations arise frequently in many remote sensing problems. However, these are often such that an analytical solution is not feasible. The usual recourse is to employ model fitting or numerical inversion techniques to obtain the solution. Model fitting techniques attempt to solve the equation by fitting a parametric model of the unknown quantity to the measured data (usually in a least squares manner). Numerical inversion for linear problems involves the discretization of the integral equation so that it may be expressed in matrix form. By inverting this matrix equation, whether directly or iteratively, the solution may be found. Since it provides a more general solution method, numerical inversion using matrix methods is generally preferred over model fitting techniques.

In this thesis, a numerical inversion method is employed to extract ocean wave information from the return of one or more narrow beam radars, i.e., a radar whose receive beam pattern is highly directive. This same inversion technique has been adapted elsewhere for wide beam (Gill, 1990) and omnidirectional (Howell and Walsh, 1990) antenna configurations. The solution for the matrix equation of this problem is found in a direct manner by computing its pseudo-inverse from the matrix's singular value decomposition (with all small singular values set to zero). Once this inverse

matrix is calculated, it may be stored in computer memory where it may be called upon again and again to process radar data.

Using this solution method, radar data processing to extract wave information becomes a simple and computationally swift task. Given a set of inverted matrices corresponding to different radar operation parameters (e.g., water depth, angular separation between receive beams of two radars, etc.), processing work will only involve retrieving the appropriate inverse matrix from memory and multiplying it with a column vector of radar spectral values. As such, relatively little time will be required to carry out this simple procedure.

The amount of processing time that is required to to perform wave measurements is an important consideration due to the large coverage that HF radars may provide. In order to map wave conditions over the radar's extensive coverage area in near real-time, the inversion algorithm that is applied must be fast. If this were not so, the radar would lose much of its operational practicality for a number of applications.

As with any other inversion method designed to recover detailed information it may only be successfully applied to data of reasonably good resolution and quality. This is generally not so much of a problem for ground wave radars with their good success rate in obtaining high quality data, however, for sky wave radars it may be crucial due to ionospheric contamination. Hence, the inversion algorithm proposed in this thesis is perhaps more suited for usage with ground wave radars then it is for sky wave radars.

Although this problem is not considered in this thesis, algorithms may be developed that can be applied to poor quality data to obtain only statistical parameters of the wave spectrum (e.g., significant waveheight). A possible means of accomplishing this is to examine only integrated quantities (moments) of the radar Doppler spectrum's sidebands. Such an algorithm may then be relatively insensitive to the condition of the data.

1.2 Literature Review

1.2.1 Radar Spectrum Models

Presently, three separate models exist that describe electromagnetic scatter from the ocean surface at HF. Based upon Rice's (1951) perturbation technique, Barrick (1972) was the first to derive expressions for the first and second order radar cross section of the ocean surface. These expressions were later updated by Barrick and Lipa (1986) to take into account finite water depth. In developing this model for the backscatter return, a plane wave transmitting source was assumed.

Using a scattering analysis based upon the general formulation of Walsh (1980) (also Walsh and Srivastava, 1987a), Srivastava (1984) also derived expressions for the radar cross section to second order. Although these expressions were derived assuming deep water, they may be easily modified for the case of arbitrary depth using Hasselmann's (1962) expression for the second order component of the height profile of the ocean. In applying the Walsh scattering analysis technique to this problem, a pulsed dipole was assumed for the transmitting source. The use of this finite source to model the transmitter is preferred as it is more representative of actual HF radar systems (e.g., CODAR and OSCR) than the less realistic plane wave source used by Barrick.

From Srivastava's analysis, the second order cross section is shown to consist of three parts. The first part, known as the onpatch term, is equivalent to Barrick's result and the other two parts may be viewed as the interaction of the transmitting source with the surrounding ocean surface and a multipathing effect commonly known as offpatch scatter. The source interaction component has been analysed by Walsh and Srivastava (1987b) while offpatch second order scatter has been analysed by Howell et al. (1987) and Srivastava (1987). From these studies, it has been determined that these two terms do not significantly affect the critical regions of the radar Doppler spectrum near the first order peaks. It is these regions of the radar spectrum that

are targeted for extracting ocean wave parameters (the reasons for which will be discussed later). Thus, for the purpose of wave measurements, these last two parts may be neglected so that only that part of Srivastava's result which is equivalent to Barrick's result needs to be taken to represent the second order return. These last two terms, however, may be important for target detection problems.

In a recent approach, Walsh and Howell (1990) employed the Walsh scattering analysis technique to develop cross section equations up to third order in interaction. Like the Srivastava approach, a pulsed dipole is assumed for the transmitting source. The second order component of this cross section model differs slightly from the mutually agreeing results developed by both Barrick and Srivastava. However, there is still strong agreement between this second order model and the other two. The very fact that these widely different approaches have produced results that largely agree lends a degree of confidence to the overall second order theory.

One of the important new results of the Walsh and Howell analysis is the expression for the third order cross section. Walsh and Howell (1990) have studied the contribution of the third order term to the overall cross section and have found that for the region of the radar spectrum near the first order peaks the third order component may, as a first approximation, be neglected. However, the importance of this term to the radar spectrum increases with distance from the first order peaks. Hence, if one desires to interpret wave data from a greater portion of the radar spectrum it would be crucial to include third order interactions in the analysis.

1.2.2 Data Interpretation Techniques for Estimation of Wave Spectra

The interpretation of ocean wave information from HF radar sea echo has been treated by a number of investigators using a variety of methods. An important aspect of most of the methods to be discussed here is the initial linearization of the second order integral equation through use of the first-order return. As it shall be seen later,

this linearization leads to a convenient normalization of the radar spectrum which removes the need to quantify the path gains or losses of the received signal.

Using a solution method similar to that presented in this thesis for narrow beam (i.e., large aperture) systems, Gill (1990) and Howell and Walsh (1990) developed techniques to extract wave data from smaller aperture HF radars. In Gill's analysis, broad beam antennas are considered with particular emphasis on 4-element square arrays. In Howell and Walsh's analysis, the problem of extracting the nondirectional waveheight spectrum from an omnidirectional ship-mounted radar is considered. For both techniques, very good inversion results have been obtained.

In another numerical inversion approach, Lipa and Barrick (1980) developed an iterative solution method for the narrow beam integral equation based upon the regularization methods of Phillips (1962) and Twomey (1963). A similar technique is also used by Barrick and Lipa (1979) to solve the integral equation corresponding to a broad beam system composed of a cross-loop antenna mounted on a monopole. Although regularization allows the formulation of a well posed problem it imposes additional constraints, such as smoothness, on the solution. As yet, this inversion algorithm has been tested with only one measured radar spectrum (Lipa et al., 1981). For this case, reasonable results were found.

In a different approach, Lipa and Barrick (1982) developed a model fitting technique to analyse narrow beam radar data. The model used for the wave spectrum is that of an amplitude spectrum multiplied by a cardioid directional distribution function where all model parameters are a function of ocean frequency. In order to perform a practical least squares fit to the radar data the assumption is made that there is an effective one-to-one mapping of ocean frequency to a set of radar Doppler frequencies. This assumption is generally only valid for those Doppler frequencies very close to the first-order peaks where the range of ocean frequencies that maps onto the radar spectrum is small. Consequently, information may only be extracted

for the low frequency end of the wave spectrum.

Recognizing the need to be able to perform measurements for a greater range of ocean frequencies, Wyatt (1986) extended the Lipa and Barrick model fitting technique. It was determined that, for many circumstances, the range of ocean frequencies that contribute significantly to a given Doppler frequency may be small compared to the total range. Information for higher ocean frequencies may then be obtained in much the same manner as for the lower frequencies. This approximation is best suited, however, for cases where the angular separation between the dominant wave direction and the radar look direction is less than approximately 45°. If significant amounts of energy are propagating orthogonally to the radar beam this assumption will not hold. This assumption also implies a reasonably smooth variation of the model parameters over frequency.

A variety of tests have been performed upon the Wyatt model fitting technique using both simulated and measured radar data. When using the data of a single radar (Wyatt, 1986; Wyatt et al., 1986) good results were found in many circumstances. However, waveheight results degraded when significant amounts of wave energy were travelling perpendicular to the radar beam. Typical mean discrepancies in significant waveheight estimates using real data were observed to be +16% with a 21% standard deviation.

Wyatt (1987) later extended the technique to analyse the data of two radars viewing the same patch of ocean from different vantage points. Tests of this method using simulated data demonstrate the increased accuracy that two radars may provide. The use of two radars also eliminates the left/right ambiguity of wave direction estimates inherent to a single radar.

In another model fitting approach, Maresca and Georges (1980) performed a least squares fit to narrow beam radar data to determine the five parameters of the JONSWAP spectrum (Hasselmann et al., 1976) using an assumed directional distribution

for the ocean waves. The JONSWAP spectrum is a model for the waveheight spectrum of a fetch-limited sea corresponding to a set of given wind conditions. Hence, this model spectrum may not be fully representative of a sea if it contains significant amounts of swell. For the two cases presented, corresponding to principally wind generated sea with little swell, good results were found.

A number of techniques have also been developed to extract only a few statistical parameters of the wave spectrum (e.g., significant waveheight) by examining integrated parameters of the radar spectrum. Such methods include the use of approximate closed-form (Barrick, 1977) or semiempirical (Maresca and Georges, 1980; Wyatt, 1984) formulae to relate these statistical parameters to the radar return, and the use of least squares fitting techniques to extract such parameters for the swell region of the wave spectrum (Lipa and Barrick, 1980, 1982). Although it is preferred to obtain detailed wave spectra information, situations may arise where the quality of the radar data is such that there may be no choice but to apply methods which examine only integrated parameters. This problem is especially acute for sky wave radars due to the contamination imparted to the sky wave return by ionospheric motion.

1.3 Scope of the Thesis

In this thesis, a data interpretation algorithm is developed and tested to extract directional ocean wave spectra from the backscatter return of one or more narrow beam HF Doppler radars. The basis of this algorithm is the numerical inversion of the integral equation representing the second order radar cross section of the ocean surface at HF. This inversion will take place for that region of the radar spectrum close to the first order peaks. Within this region, the second order integral equation may be easily linearized thus allowing it to be expressed as a matrix equation.

The inclusion of third order interactions in the inversion solution will not be considered here as they do not contribute significantly to the region of interest (Walsh

and Howell, 1990). However, it does represent a goal of future work for refinement of the inversion algorithm to include such higher order effects.

Initially, the second order integral equation is linearized using Lipa and Barrick's (1982) method. This linearization also serves as a convenient normalization for the data that removes the need to account for the path gains or losses of the backscatter. The overall accuracy of this linearization method depends upon the radar operating frequency. For high HF frequencies it may be accurately applied for almost any general sea state whereas for low HF frequencies it may only be applied for large sea state conditions. As the only measured radar data available to test the inversion algorithm in this thesis corresponds to a high HF frequency (25.4 MHz), the development of a new and more general linearization method will not be considered here. Its development, however, represents an important goal for future refinement of the algorithm.

The matrix equation is derived from the linearized integral equation by discretizing the ocean wave spectrum. This is done by expanding the ocean spectrum in a truncated Fourier series over angle and assuming that the Fourier coefficients remain constant within equal length bands of ocean frequency. The variables of this system of equations are these coefficients. Due to symmetries in the mapping of the ocean wave spectrum onto the radar spectrum, the integral equation has negligible dependence upon the odd Fourier coefficients of the series expansion. Consequently, only ambiguous directional information regarding the wavefield may be obtained from the data of a single radar. The use of two or more radars viewing the same area of ocean from different directions overcomes this problem and permits the extraction of odd Fourier coefficients. The level of accuracy of wave spectra estimates provided by two radars will, of course, depend upon the angular separation between radar beams with the best case occurring when the beams are orthogonal.

The solution to this equation is found, in a direct manner, by calculating its

generalized inverse from the singular value decomposition of the kernel matrix with all small singular values set to zero. A general procedure is outlined which may be used to determine the required number of singular values to be retained to create the inversion solution. As a direct solution is found to the integral equation, the task of processing a large number of radar spectra on a routine basis becomes inexpensive in computation time. This contrasts with iterative solution techniques which would require an inordinate amount of time to converge to a solution for a large number of cases.

The performance of the algorithm is tested for both single and dual- radar usage by comparing its results to those of a WAVEC buoy using data collected during the 1986 Canadian Atlantic Storms Program (CASP). Simulated data is also used to test the algorithm and to help confirm some of the general properties of the solution that were observed from the CASP data. In the CASP experiment, two 25.4 MHz ground wave radars were deployed on the coast of Nova Scotia, Canada so that their beams intersected at the location of the buoy. The angular separation between radar beams was 56°.

The CASP data set also affords the opportunity to conduct an initial study on each of the various models for the second order cross section (Barrick, 1972; Srivastava, 1984; Walsh and Howell, 1990) to see which better represents the radar return. This will be done by substituting each model into the inversion algorithm in turn and determining which leads to the best agreement with the buoy for wave spectral estimates.

Chapter 2

The Radar Cross Section of the Ocean Surface at HF

2.1 General

In this chapter, the expressions for the first and second order radar cross section of the ocean surface at HF are presented. As all three cross section models are of very similar form, full first and second order expressions need be presented for only one model of this set. The cross section model chosen for this task is that developed by Barrick and Lipa (1986). The other two cross section models (Srivastava, 1984; Walsh and Howell, 1990) will be introduced by comparing their first and second order expressions with those of Barrick and Lipa. All manipulations performed on the Barrick and Lipa equations presented here apply to the other cross section models as well.

To better understand the significance of these equations and some of their basic properties, a discussion is first made regarding the underlying physical mechanism responsible for the backscatter return. This discussion also serves as a means of introducing several important properties regarding the physics of ocean gravity waves.

After performing some elementary reductions on the second order equation, it is linearized using the method of Lipa and Barrick (1982). Due to the limitations of this linearization technique and for several other reasons discussed within, the inversion

is restricted to those Doppler frequencies close to the first order peaks. This is the principal Doppler region of interest for inversion as it contains the most important information regarding the wave spectrum.

In preparation for the inversion of the integral equation, a study is made of its mapping properties to determine what implications they may hold for inversion. Of particular interest is the amount of wave information that may be obtained from a HF radar and what factors may affect the accuracy of the inversion.

2.2 Description of the Interaction Mechanism

Electromagnetic backscatter from the ocean surface has been a topic of investigation since the inception of radar. The first major advance in the understanding of the underlying physical interaction process came about from the discovery made by Crombie (1955) as a result of his pioneering experiment. From examination of measured radar Doppler spectra he observed that the principal features of the signal return were the two well defined spikes symmetrically placed about the radar carrier frequency, but not necessarily of the same amplitude (Fig. 2.1). These resonant peaks were later to be known as the first order or Bragg peaks. Crombie also observed that the placement of these peaks was proportional to the square root of the radar wavenumber.

Insight into the nature of this phenomenon may be obtained from examination of that fundamental property of ocean wave physics known as wave dispersion. As the ocean surface acts as a dispersive medium, the phase speed of an ocean wave will be proportional to its wavelength with longer ocean waves travelling faster. Based upon the governing hydrodynamic equations and boundary conditions (Kinsman, 1965, ch. 2), the relationship between the radian frequency of a ocean wave, ω, and its wavenumber, k, may be derived as (Kinsman, 1965, ch. 3)

$$\omega = \sqrt{gk \tanh(kd)} \tag{2.1}$$

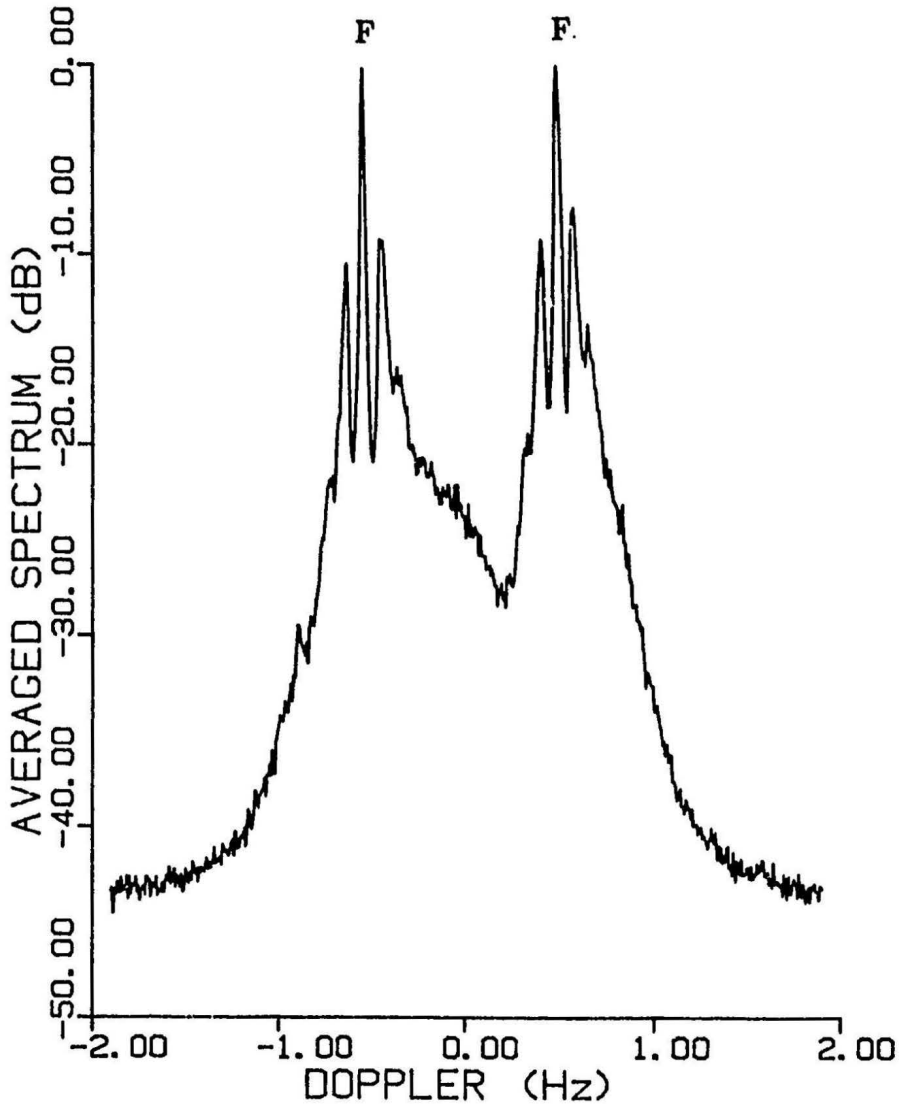

Figure 2.1: Example of a radar Doppler spectrum recorded by a 25.4 MHz narrow beam system. First order peaks are designated by F.

where d is water depth and g is the acceleration due to gravity. The above equation is the well known *dispersion relationship* for ocean gravity waves. For the limiting case when kd is large the dispersion relationship becomes

$$\omega = \sqrt{gk} \tag{2.2}$$

Equation (2.2) is commonly referred to as the *deep water dispersion relationship.* This approximation is satisfied, in general, if the water depth is greater than half the wavelength.

Based upon the dispersive properties of ocean waves, Crombie found that the placement of these peaks was consistent with a target velocity that matches that of an ocean wave whose wavelength is equal to one-half the radar wavelength. It is then logical to conclude that these narrow first order peaks are the result of resonant backscatter from ocean waves of this length that are either advancing directly towards (positive Doppler peak) or receding directly from (negative Doppler peak) the radar. Since these waves satisfy the geometry for coherent Bragg scatter, Crombie correctly deduced that it was this diffraction-grating mechanism which is responsible for ocean backscatter. The two ocean waves that are responsible for the Bragg peaks are commonly referred to as the Bragg waves.

Based upon the dispersion relationship (2.1), the radian Doppler shift of the first order peaks, ω_B, is given by

$$\omega_B = \sqrt{2gk_o \tanh(2k_o d)} \tag{2.3}$$

where k_o is the radar wavenumber. The above equation holds for monostatic operation of the radar (transmitter and receiver co-located) with the transmitted signal directed at near grazing incidence.

From Fig. 2.1 it may be seen that there is a complicated sideband structure surrounding the first order peaks. It is generally accepted that this continuum is the result of higher order interactions of which second order forms the dominant contribu-

tion. The radar cross section equation for the ocean surface, $\sigma(\omega_d)$, may be expressed as

$$\sigma(\omega_d) = \sigma^{(1)}(\omega_d) + \sigma^{(2)}(\omega_d) + \cdots \tag{2.4}$$

where $\sigma^{(\ )}(\omega_d)$ represents the contribution to the overall cross section from each order of interaction and ω_d is Doppler frequency.

In order for two ocean waves to produce second order return their corresponding wavenumber vectors, say $\vec{k}$ and $\vec{k'}$, must satisfy the geometry for Bragg scattering, i.e.,

$$\vec{k} + \vec{k'} = -2\vec{k_o} \tag{2.5}$$

where the vector $\vec{k_o}$ lies in the direction of the boresight of the narrow beam radar pointing out to sea. The radian Doppler shift from the carrier frequency, ω_d, of the scattered electromagnetic field is given by

$$\omega_d = m\omega + m'\omega' \tag{2.6}$$

where the ocean frequencies ω and ω' correspond respectively to ocean wavenumbers k and k' through the dispersion relationship (2.1). The coefficients m and m' take on the values ± 1 to represent the four possible combinations of direction that the two scattering wave vectors may take, with wavenumber magnitudes unchanged, that satisfies (2.6).

From consideration of equations (2.5) and (2.6) it may be observed that the second order return will form a continuous spectrum and will involve the entire ocean gravity wave spectrum. Consequently, this makes it a desirable quantity to analyse for the extraction of wave information.

Two possible sources for second order interactions may be identified (Hasselmann, 1971). One such mechanism involves hydrodynamic effects and consists of a single scattering from a second order ocean wave with wave vector $\vec{k} + \vec{k'}$ produced from the nonlinear interaction of two crossing waves. Although these "interference" waves are

not freely propagating they will produce radio backscatter if they match the Bragg wavelength and direction. The other mechanism involves two scatterings. For this multiple scattering effect, a portion of the radio energy scattered from a first order ocean wave $\vec{k}$ is scattered from another first order ocean wave $\vec{k}'$. If this wave vector combination satisfies (2.5), backscatter will be directed towards the transmitting source.

2.3 Basic Equations

By definition, the distribution of wave energy as a function of frequency (or wavenumber) and direction is the ocean wave spectrum. In this thesis we shall distinguish between two such spectral density functions. These are the temporal ocean wave spectrum $e(f,\theta)$ and the spatial ocean wave spectrum $s(k,\theta)$. The quantities f and θ represents temporal frequency and wave direction respectively. These wave spectral quantities are defined such that the mean square waveheight (h^2) of the ocean surface is

$$h^2 = \int_0^\infty \int_0^{2\pi} e(f,\theta)\, df\, d\theta = \int_0^\infty \int_0^{2\pi} k\, s(k,\theta)\, dk\, d\theta \tag{2.7}$$

where h is the root-mean-square (rms) waveheight of the ocean surface above the mean level.

Based upon the above equation, a physical interpretation can be given to each of the two wave spectrum forms as they are defined here. Whereas the temporal spectrum follows oceanographic convention and is directly related to wave energy, the spatial spectrum contains wave slope information which in turn depends on wave energy. This definition for the spatial spectrum was useful in analysing electromagnetic scatter from the ocean as it is wave slope rather than wave amplitude which is primarily responsible for the scattering to take place.

The relationship between the temporal and spatial wave spectrum may be found through use of the dispersion relationship (2.1) and (2.7). Using these equations, it

can be shown that

$$s(k,\theta) = \left[\frac{g\tanh(kd) + gkd\,\mathrm{sech}^2(kd)}{4\pi k\sqrt{gk\tanh(kd)}}\right] e(f,\theta) \tag{2.8}$$

As mentioned before, this thesis will focus on the first and second order expressions of the Barrick and Lipa (1986) model in presenting the radar cross section of the ocean surface. This simplifies the presentation of all three models as they are all closely related. The other two models will be described by comparing their first and second order expressions with those of Barrick and Lipa.

For convenience, the first and second order radar cross section equations will be expressed in dimensionless form. To accomplish this the following normalized variables are defined:

$$\begin{aligned}
\text{water depth:} \quad & D = && 2k_o d \\
\text{wave vector:} \quad & \vec{K} = && \vec{k}/2k_o \\
\text{wavenumber:} \quad & K = && k/2k_o \\
\text{ocean frequency:} \quad & F = && f/\sqrt{2k_o} \\
\text{Doppler frequency:} \quad & \eta = && \omega_d/\omega_b \\
\text{first order cross section:} \quad & \sigma_1(\eta) = && \omega_b\,\sigma^{(1)}(\omega_d) \\
\text{second order cross section:} \quad & \sigma_2(\eta) = && \omega_b\,\sigma^{(2)}(\omega_d) \\
\text{spatial ocean wave spectrum:} \quad & S(K,\theta) = && (2k_o)^4 s(k,\theta) \\
\text{temporal ocean wave spectrum:} \quad & E(F,\theta) = && (2k_o)^{5/2} e(f,\theta)
\end{aligned} \tag{2.9}$$

Applying the above definitions to the form of the cross section equations presented in Lipa and Barrick (1986), the dimensionless form of the average first and second order radar spectral cross section of the ocean surface per unit surface area for vertical polarization at HF, grazing incidence, and narrow beam reception may be given as

$$\sigma_1(\eta) = 4\pi \sum_{m'=\pm 1} S(1,(1+m')\pi/2)\delta(\eta - m') \tag{2.10}$$

$$\sigma_2(\eta) = 8\pi \sum_{m,m'=\pm 1} \int_0^{\infty} \int_{-\pi}^{\pi} |\Gamma_s|^2 \, S(K,\alpha) S(K',\alpha') \delta(\eta - m\sqrt{K_d} - m'\sqrt{K'_d}) K dK d\theta \quad (2.11)$$

with the restriction that

$$K' \geq K \quad (2.12)$$

and where

$$K_d = K \tanh(KD) \quad (2.13)$$

$$K'_d = K' \tanh(K'D) \quad (2.14)$$

All directions for the above set of cross section equations are with respect to the look direction of the narrow beam radar looking out to sea. δ is the Dirac delta function. It is interesting to note that the argument of the delta function in (2.11) represents the dimensionless form of (2.6) after substitution of the dispersion relationship (2.1). This is assuming that $\tanh(D) \simeq 1$ as it will be for all but the shallowest water depths which are excluded from this analysis.

The form of the first order expression differs for each cross section model. The Barrick and Lipa model represents the first order return as two impulse functions located at the Bragg frequencies whereas Srivastava (1984) and Walsh and Howell (1990) has the first order return as a continuum. This continuum, however, consists primarily of two narrow spikes also located at the Bragg frequencies. In any event, the exact form of the first order cross section is not pertinent to this thesis as the first order return is only used to linearize the second order expression. For this purpose, the only quantity of interest from the first order return is the total power contained in each first order peak which is virtually the same for all models. For all three models then, the total energy contained in each of the two first order peaks is given by

$$R_{m'} = 4\pi S(1, (1 + m')\pi/2) \quad (2.15)$$

where the sign of m' identifies whether R, the energy of the peak, is for the positive or negative Doppler half of the radar spectrum.

The second order equation (2.11) may be classified as a nonlinear, two-dimensional integral equation of the first kind (Delves and Mohamed, 1985). The two-dimensional nature of this equation is a result of the fact that the ocean spectrum is a two-dimensional quantity. The presence of the product of two wave spectra terms in this equation's integrand is the source of its nonlinearity.

A number of integrable singularities (of the square root type) appear in the second order spectrum for reasons explained by Barrick (1972). These occur in the radar spectrum at Doppler shifts of $\pm\sqrt{2}$ and $\pm 2^{3/4}$ times the Bragg frequency. Fig. 2.2 is an example of a radar spectrum in which the peaks these singularities produce may be clearly seen for the negative Doppler half of the spectrum. Although these singularities are not readily apparent in Fig. 2.1 they are detectable nevertheless. Other second order peaks are present in Figs. 2.1 and 2.2 which lie adjacent to the first order peaks. These arise simply because the wave spectrum is maximum for the wavenumber range corresponding to these Doppler shifts.

The two scattering wave vectors $\vec{K}$ and $\vec{K}'$ responsible for the second order return obey the dimensionless form of (2.5), i.e.,

$$\vec{K} + \vec{K}' = -\hat{k}_o \tag{2.16}$$

In polar form, the wave vectors $\vec{K}$ and $\vec{K}'$ have coordinates (K, θ) and (K', θ') respectively. Using (2.16) and the law of cosines and sines, the polar coordinates of the wave vector $\vec{K}'$ may be expressed in terms of the coordinates of $\vec{K}$ as

$$K' = \sqrt{K^2 + 2K\cos(\theta) + 1} \tag{2.17}$$

$$\theta' = \beta + \pi \tag{2.18}$$

where

$$\beta = \arcsin(K\sin(\theta)/K') \tag{2.19}$$

The angles α and α' represent the direction of the wave vectors $m\vec{K}$ and $m'\vec{K}'$

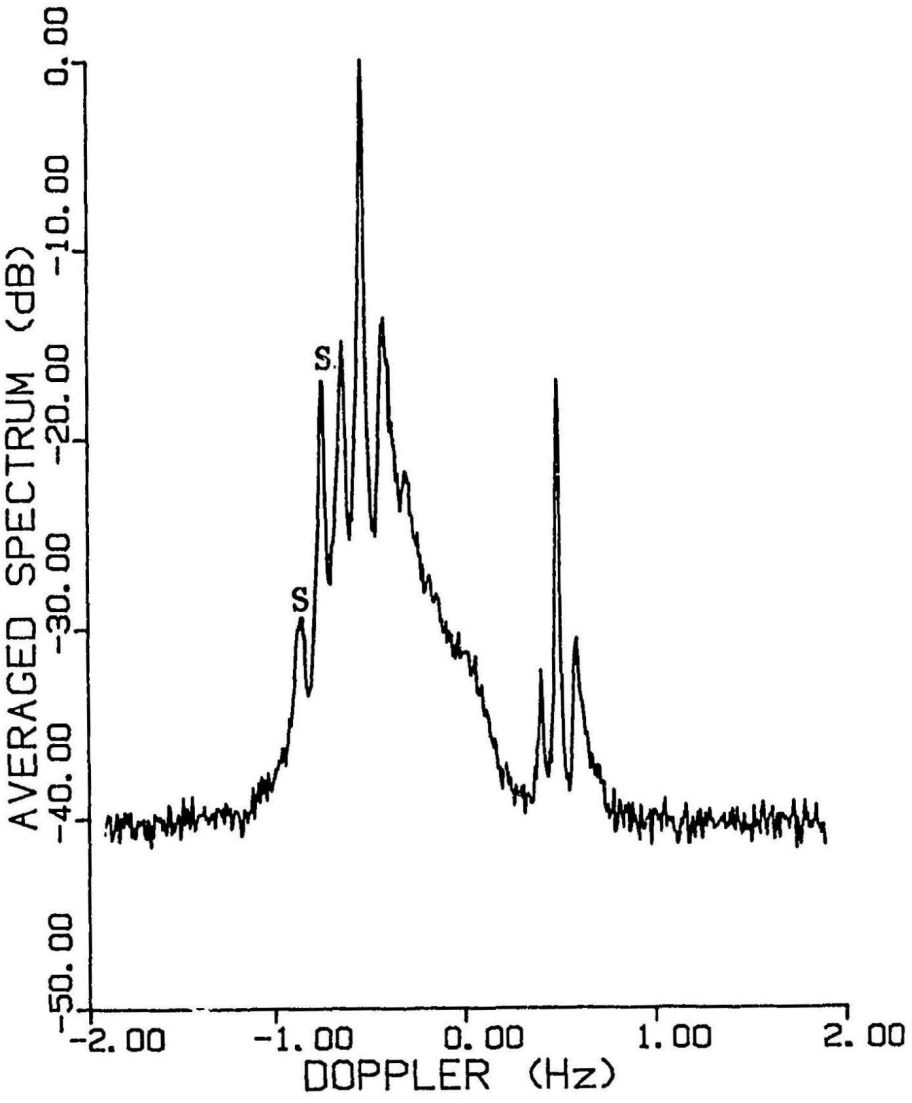

Figure 2.2: Example of a 25.4 MHz narrow beam radar Doppler spectrum with strong second order singularities. These singularities, designated by S, are readily apparent in the negative Doppler half of the spectrum.

respectively. In terms of θ and θ' these angles may be defined as

$$\alpha = \theta \pm (1-m)\pi/2 \tag{2.20}$$

$$\alpha' = \theta' \pm (1-m')\pi/2 \tag{2.21}$$

The two alternate definitions for α and α' are, in fact, equivalent since either adding or subtracting π to an angle will give the same result.

The quantity Γ_s is a coupling coefficient that includes contributions from both second order mechanisms, i.e., a single scattering from a second order wave (Γ_1) and double scatter from two first order waves (Γ_2):

$$\Gamma_s = \Gamma_1 + \Gamma_2 \tag{2.22}$$

For the Barrick and Lipa model the individual coupling coefficient terms have the form

$$\begin{aligned}\Gamma_1 = \frac{-i}{2}\Bigg[& K_d + K_d' + \frac{L(K_d K_d' - \vec{K}\cdot\vec{K}')}{\sqrt{K_d K_d'}}\left(\frac{1+\eta^2}{1-\eta^2}\right) \\ & - \frac{(\sqrt{K_d} + L\sqrt{K_d'})(K_d^{3/2}\mathrm{csch}^2(KD) + LK_d'^{3/2}\mathrm{csch}^2(K'D))}{1-\eta^2}\Bigg]\end{aligned} \tag{2.23}$$

$$\Gamma_2 = \frac{1}{2}\left[\frac{(\vec{K}\cdot\hat{k}_o)(\vec{K}'\cdot\hat{k}_o) - 2\vec{K}\cdot\vec{K}'}{\sqrt{\vec{K}\cdot\vec{K}' - \Delta/2}}\right] \tag{2.24}$$

where

$$L = mm' \tag{2.25}$$

$$i = \sqrt{-1} \tag{2.26}$$

The Δ term appearing in the denominator of Γ_2 refers to the normalized surface impedance at the air-sea interface. It has been found adequate (Lipa and Barrick, 1986) to use the following constant value for Δ across the HF band:

$$\Delta = 0.011 - i\,0.012 \tag{2.27}$$

A more accurate choice for Δ is not required as it exerts negligible influence on the second order cross section for the Doppler region of interest for inversion (close to the first order peaks).

For all three cross section models, Γ_1 is the same. Although Srivastava (1984) derived his radar cross section expressions assuming deep water, his analysis may be easily modified for the case of arbitrary depth using Hasselmann's (1962) derivation for the second order correction to the height profile of the ocean. The resulting new expression for Γ_1 will agree exactly with that presented here.

Except for the $-\Delta/2$ term appearing in the denominator of Γ_2, the onpatch component of Srivastava's (1984) second order cross section is identical to Barrick and Lipa's result after accounting for finite water depth. The $-\Delta/2$ term did not arise from Barrick's (1972) analysis for the scattering problem; instead, it was added to the denominator of Γ_2 after the analysis for reasons put forward in Lipa and Barrick (1986). For the same reasons then, this term could be included in Srivastava's result if one so desires. Hence, there is no intrinsic difference between this component of Srivastava's second order cross section and that developed by Barrick and Lipa.

The Walsh and Howell (1990) expression for Γ_2 differs significantly from both Srivastava's and Barrick and Lipa's result. This difference lies in the numerator term of Γ_2 and not in its denominator which, with the exception of the surface impedance term, must be the same for all models. The physical source for this difference is the fact that the Walsh and Howell expression for Γ_2 is zero if the wave vectors $\vec{K}$ and $\vec{K}'$ are aligned or opposed to one another whereas Γ_2 for the other models is maximum for this case.

Although the Walsh and Howell second order expression differs from the other two due to its Γ_2 term, the overall difference is actually only slight. This is due to the fact that, in general, the contribution of Γ_2 to the total coupling coefficient is small in comparison to Γ_1. This is to be expected as Γ_1 represents a physical process that

involves a lower number of scatters than Γ_2.

Having established the close relationship between all three cross section models for their second order component, this thesis will treat (2.11) from this point on as being a general expression which applies to all cross section models. To this end, the coupling coefficient Γ_s will be considered as being an arbitrary function whose form depends on what cross section model is being examined.

In applying (2.11) for the problem of interpreting wave information from the radar spectrum, its limitations in representing the total radar cross section outside of the first order peaks must be established. It is known that for increasing distance from the first order peaks other cross section terms, particularly third order (Walsh and Howell, 1990), become the dominant contributors to the overall cross section spectrum. From studies of the second and third order cross section (Walsh and Howell, 1990), it has been found that the overall cross section may, in general, be well approximated by the second order term only for $0.6 < |\eta| < 0.9$ and $1.1 < |\eta| < 1.4$. This set of limits has the advantage that they avoid the singularities occurring at $|\eta| = \sqrt{2}$ which would greatly complicate the inversion problem if they were included. It should also be noted that the linearization method to be employed on this integral equation applies best within these limits.

2.4 Simplification and Reduction of the Integral Equation

Using the sifting properties of the Dirac delta function, one of the integrals in (2.11) may be evaluated in closed form. The K integral is chosen for this purpose. The second order equation now becomes

$$\sigma_2(\eta) = 16\pi \sum_{m,m'=\pm 1} \int_{-\pi}^{\pi} |\Gamma_s|^2 J_t S(K,\alpha) S(K',\alpha') K^{3/2}\, d\theta \tag{2.28}$$

where the restrictions

$$\eta - m\sqrt{K\tanh(KD)} - m'\sqrt{K'\tanh(K'D)} = 0 \tag{2.29}$$

and (2.12) apply. Equation (2.29) will be referred to in this thesis as the *delta function constraint.* In evaluating (2.28) the above constraint equation must be solved for each θ to determine the values of K that satisfy it. Once K is found the value of K' may be determined from it using (2.17). As (2.29) is a nonlinear equation its solution for K must be found using numerical techniques. For the case of deep water however, the constraint equation becomes linear and a closed form solution may be easily obtained.

The Jacobian of transformation, J_t, used in evaluating the outer integral may be derived as

$$J_t = \frac{1}{\left|\frac{K_d}{\sqrt{K}} + \frac{K^{3/2}D\mathrm{sech}^2(KD)}{K_d} + L\sqrt{K}(\cos(\theta) + K)\left(\frac{K'_d}{K'^2} + \frac{D\mathrm{sech}^2(K'D)}{K'_d}\right)\right|} \tag{2.30}$$

Lipa and Barrick (1986) proved in closed form, for the case of deep water, that different combinations of m and m' define disjoint ranges of Doppler frequency. These disjoint ranges shall be referred to here as "sidebands". For a given Doppler the deep water version of the delta function constraint (2.29) will yield solutions for the wave vectors $\vec{K}$ and $\vec{K}'$ for only one combination of (m,m'). This proof is not transferable for the case of arbitrary depth, however, as the the nonlinear form of (2.29) does not make it amenable for a closed form proof. It is simple to prove numerically though, that this property holds for arbitrary depth. The values of m and m' corresponding to each of the four second order sidebands are as follows:

$$\begin{aligned} m = m' = 1 \quad &\text{for} \quad \eta > 1 \\ m = -1, m' = 1 \quad &\text{for} \quad 0 < \eta < 1 \\ m = 1, m' = -1 \quad &\text{for} \quad -1 < \eta < 0 \\ m = m' = -1 \quad &\text{for} \quad \eta < -1 \end{aligned} \tag{2.31}$$

It is interesting to note that as a result of these conditions m' and η will have the same sign.

From the above set of conditions it may be seen that the delta function constraint is an even function of η. This is so since both m and m' changes sign if η changes sign so that (2.29) remains effectively the same. Using (2.31) the parameter L takes on the value -1 for the region between the first order peaks and $+1$ outside. This is equivalent to

$$L = \begin{cases} 1 & \text{for } |\eta| > 1 \\ -1 & \text{for } |\eta| < 1 \end{cases} \tag{2.32}$$

Those second order sidebands that lie between the first order peaks ($L = -1$) shall be referred to as the "inner" sidebands while those who lie outside this region ($L = 1$) shall be referred to as the "outer" sidebands.

Another important property of the delta function constraint is that it is also an even function of θ as K' depends only upon $\cos(\theta)$ by virtue of (2.17). Since the coupling coefficient and the Jacobian of transformation are also even functions of θ, the closed integral of (2.28) may then have its integration points occurring at $\pm\theta$ summed to yield the second order equation

$$\sigma_2(\eta) = 16\pi \int_0^{\pi} |\Gamma_s|^2 J_t H \left\{ S(K,\alpha) S(K',\alpha') + S(K,-\alpha) S(K',-\alpha') \right\} K^{3/2}\, d\theta \tag{2.33}$$

with restrictions (2.12), (2.29) and (2.31). The function H appearing above prevents the integral from having its integration points occurring at $\theta = 0$ and $\theta = \pi$ from being summed twice. It is defined as

$$H = \begin{cases} \frac{1}{2} & \text{for } \theta = 0 \text{ or } \pi \\ 1 & \text{otherwise} \end{cases} \tag{2.34}$$

The second order integral (2.33) was written without the summation over the indices m, m' as (2.31) now makes this unnecessary. Since (2.31) represents a restriction on (2.33) it demonstrates an important feature of the second order integral, i.e., it is not one integral equation but in fact four such equations, one for each second order

sideband. The inversion of radar sea echo therefore involves the solution of a system of independent integral equations.

2.5 Linearization of the Integral Equation

In this section the second order integral equation (2.33) is linearized using the method of Lipa and Barrick (1982). To understand the basis of this linearization technique it is first necessary to examine the properties of the wave vector $\vec{K}'$ which along with the wave vector $\vec{K}$ are the two scattering waves responsible for the second order return. In analysing the wave vector $\vec{K}'$ it shall be useful to define a dimensionless parameter, u which is the magnitude of the normalized Doppler frequency shift from the first order peaks:

$$u = m(\eta - m') \tag{2.35}$$

In terms of the parameter u, the Doppler frequency limits for the second order equation (Section (2.3)) may be conveniently expressed as $0.1 < u < 0.4$.

As the delta function constraint is an even function of η, its solution for both K and K' for a given value of θ will be the same for all Doppler frequency points having the same value of u and L. For every such set of Doppler frequencies, there is a distinct range of values for both K and K' that solutions to the delta function constraint for all θ may take. The endpoints for both of these continuous ranges are given by the solution for K and K' at θ equal to 0° and 180°.

Fig. 2.3 is a set of curves showing the deep water solution for the wavenumber K' up to $u = 0.4$ for θ equal to 0°, 90° and 180°. The family of solution curves for all values of θ are bounded by the θ equal to 0° and 180° curves.

From these solutions curves, it may be observed for all sidebands that the range of values for the normalized wavenumber K' at each u is approximately centered about a value of one. This is a significant result as it means that the scattering wave represented by K' is of comparable length to the Bragg waves, i.e., those waves

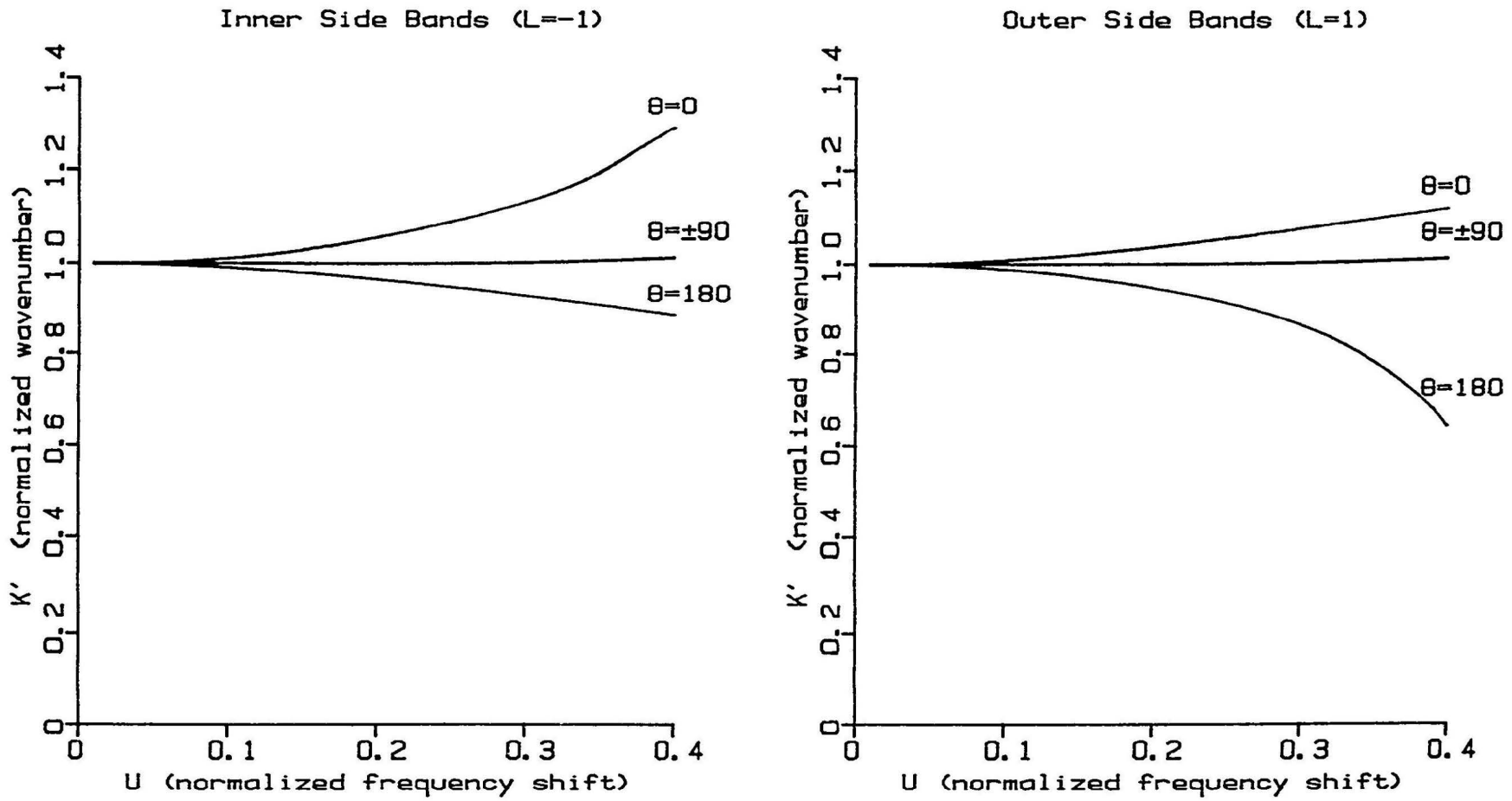

Figure 2.3: Deep water solution (up to $u = 0.4$) for the normalized wavenumber K' at $\theta = 0°$, $90°$ and $180°$. The family of solution curves for all θ are bounded by the $\theta = 0°$ and $180°$ curves.

responsible for the first order return. Although the width of the range of values for K' at each u may increase substantially for increasing values of u the value for K' at the lower extent of this range still remains large.

As both K' and the Bragg waves are substantially large wavenumbers they will generally lie in the saturated region of the gravity wave spectrum. At this equilibrium stage where no further growth is possible, the wave spectrum will depend upon wavenumber as k^{-4} or correspondingly upon frequency as f^{-5} (Phillips, 1966). As these short saturated waves are essentially wind driven they tend to share the same directional properties. Typically, the distribution of wave energy over direction for these short waves is very broad.

By making this assumption of saturation and further assuming that saturated waves share the same broad directional distribution, spectral components with wavenumber K' may be related to those having the Bragg wavelength as

$$S(K', \alpha') = \frac{S(1, \alpha')}{K'^4} \tag{2.36}$$

The suitability of the above approximation depends upon the radar operating frequency. At higher HF frequencies ($\approx$ 20 to 30 MHz) the assumption of saturation is valid for all but the lowest sea states. As the operating frequency decreases the Bragg wave becomes longer with the result that a larger sea state is required in order to drive this wave to saturation. This approximation will then need to be modified so that it may be used with generality at lower HF frequencies. This thesis will not concern itself with this problem as the only measured data available to test the inversion algorithm is from the 1986 CASP experiment which had an operating frequency of 25.4 MHz.

From examination of (2.18) it may also be observed that the direction of the wave vector $\vec{K}'$ is also closely matched to that of the Bragg waves as well. The difference in direction between the wave vector $\vec{K}'$ and the Bragg waves is represented by the parameter β (equation (2.19)). Fig. 2.4 is a plot showing the maximum value of β

for each Doppler point up to $u = 0.4$. It may be observed from this diagram that β is generally small. For a broad directional distribution there will be little difference between wave components having this difference in direction. It is then appropriate to assume

$$\beta \approx 0 \tag{2.37}$$

Using (2.21) this approximation may be reexpressed as

$$\alpha' \approx \pm(1 + m')\pi/2 \tag{2.38}$$

The alternate definitions for α' are equivalent as adding or subtracting π to an angle gives the same result.

Substituting (2.36) and (2.38) into (2.33) the second order equation may be approximated as

$$\sigma_2(\eta) \approx 16\pi \int_0^{\pi} |\Gamma_s|^2 J_t H \frac{S(1,(1+m')\pi/2)}{K'^4} \{S(K,\alpha) + S(K,-\alpha)\} K^{3/2} d\theta \tag{2.39}$$

The above equation may be linearized to remove the Bragg wave spectral term $S(1,(1+m')\pi/2)$ by dividing each Doppler half of the spectrum by the energy contained in the local first order peak ($R_{m'}$). This linearization approach has the elegant advantage that it also serves as a convenient normalization for the data that removes the need to account for unknown path gains or losses of the received radar signal. The resulting linearized second order equation, $\sigma_{2L}(\eta)$, is given by

$$\sigma_{2L}(\eta) = \frac{\sigma_2(\eta)}{R_{m'}} \approx 4 \int_0^{\pi} \frac{|\Gamma_s|^2 J_t H}{K'^4} \{S(K,\alpha) + S(K,-\alpha)\} K^{3/2} d\theta \tag{2.40}$$

In preparation for the inversion of (2.40), its spatial wave spectrum terms will be converted to temporal spectra using (2.8) and (2.9). The temporal spectrum is preferred over the spatial spectrum for inversion purposes as it follows oceanographic convention and has a much simpler physical interpretation in terms of wave energy. Performing this conversion the linearized second order equation becomes

$$\sigma_{2L}(\eta) = \int_0^{\pi} C \{E(F,\alpha) + E(F,-\alpha)\} d\theta \tag{2.41}$$

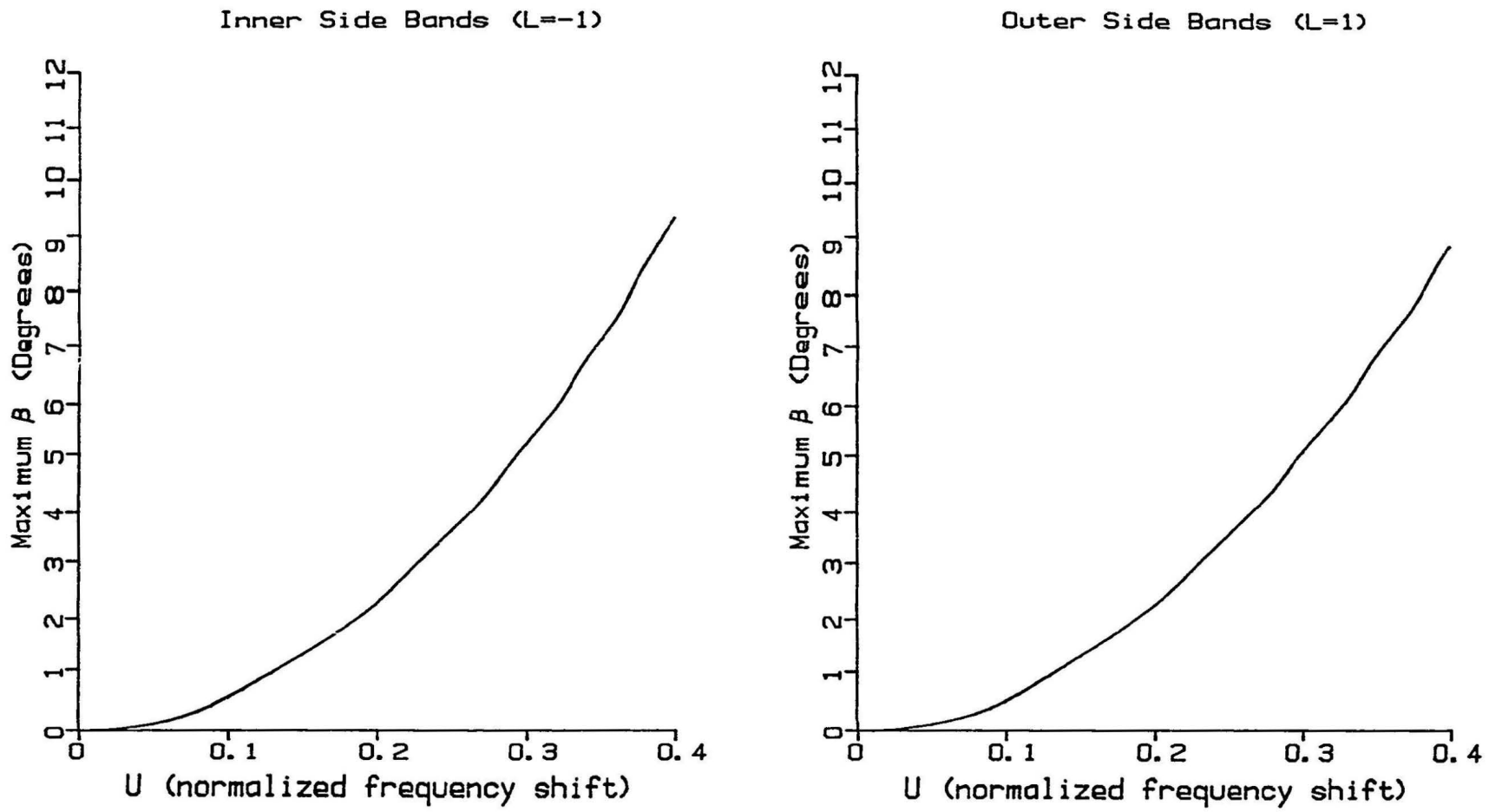

Figure 2.4: Maximum value of β for all Doppler up to $u = 0.4$.

where

$$C = \frac{4\,|\Gamma_s|^2\, J_t H T K^{3/2}}{K'^4} \tag{2.42}$$

and T represents the dimensionless form of (2.8), i.e.,

$$T = \frac{g\tanh(KD) + gKD\mathrm{sech}^2(KD)}{4\pi K\sqrt{gK\,\tanh(KD)}} \tag{2.43}$$

By definition, C is the kernel of the integral equation. The above expression for the second order cross section has the constraint conditions (2.12), (2.29) and (2.31). In general, this integral equation will represent the radar spectrum by itself for $0.1 < u < 0.4$.

2.6 Mapping Properties of the Integral Equation

In this section, several important properties are described regarding the mapping of the ocean wave spectrum onto the second order cross section. The properties of the $\vec{K}'$ wave vector were examined in the last section. Attention is restricted to the regions of the radar spectrum close to the first order peaks as the inversion algorithm is to be applied there only. The structure of this mapping is determined by both the delta function constraint (2.29) and the kernel of the integral equation (2.42). The delta function constraint governs what ocean wave vectors may contribute to a given Doppler frequency of the radar spectrum while the kernel function determines how strongly each wave vector pair contributes to this Doppler point.

Perhaps the most important aspect of this mapping is the folding of the ocean spectrum about the radar beam as a result of the delta function constraint being an even function of θ. Stated another way, the radar spectrum does not depend so much upon the wave spectrum quantity $E(F,\alpha)$ as it depends upon $E(F,\alpha) + E(F,-\alpha)$ which itself corresponds to a folded wave spectrum. As a result of this folding about the radar beam, a single narrow beam radar may only provide ambiguous information regarding the direction of the wavefield. This directional ambiguity is left/right in

nature as a single radar may determine the angle a moving target makes with its beam but cannot tell which side it is arriving from relative to this beam. The use of two radars viewing the same patch of ocean from different vantage points overcomes this ambiguity and permits the extraction of full directional information.

Shown in Fig. 2.5 is a set of curves showing the deep water solution for the wavenumber K up to $u = 0.4$ for θ equal to 0^o, 90^o and 180^o. The family of solution curves for all values of θ are bounded by the θ equal to 0^o and 180^o curves.

From these solution curves, it may be observed that the normalized wavenumber K occupies the important long wave region of the ocean wave spectrum. It is this region of the wave spectrum which is targeted for measurement as the longer waves contain the bulk of the total wave energy. It may be further observed from these solution curves that the range of values for K at each u becomes wider and the values larger as u increases. At $u = 0.4$ and $L = 1$, K has its maximum value of 0.36 for $\theta = 180^o$.

Although the radar spectrum up to $u = 0.4$ will contain information for a substantial range of ocean wavenumbers, this information is incomplete as the only directional components present for large values of K will be those that are travelling along the radar beam. This is a consequence of the fact that the $\theta = 0$ and 180^o solution curves in Fig. 2.5 diverge rapidly for large values of u. This divergence is indeed fast when one considers that for the outer sidebands ($L = 1$) the maximum value of K at $u = 0.36$ is 0.24 while only a short distance away at $u = 0.4$ it jumps by 50 % to 0.36.

It is doubtful whether much useful information can be extracted for these large wavenumbers as they are only represented by their radial components. As the kernel function for the outer sidebands ($L = 1$) is maximum at $\theta = 180^o$, it may not be possible to ignore these wavenumber components when analysing radar data. As a result, it may be more practical to forego any attempt to extract information for these large wavenumbers and concentrate on a lesser range of values for u in performing

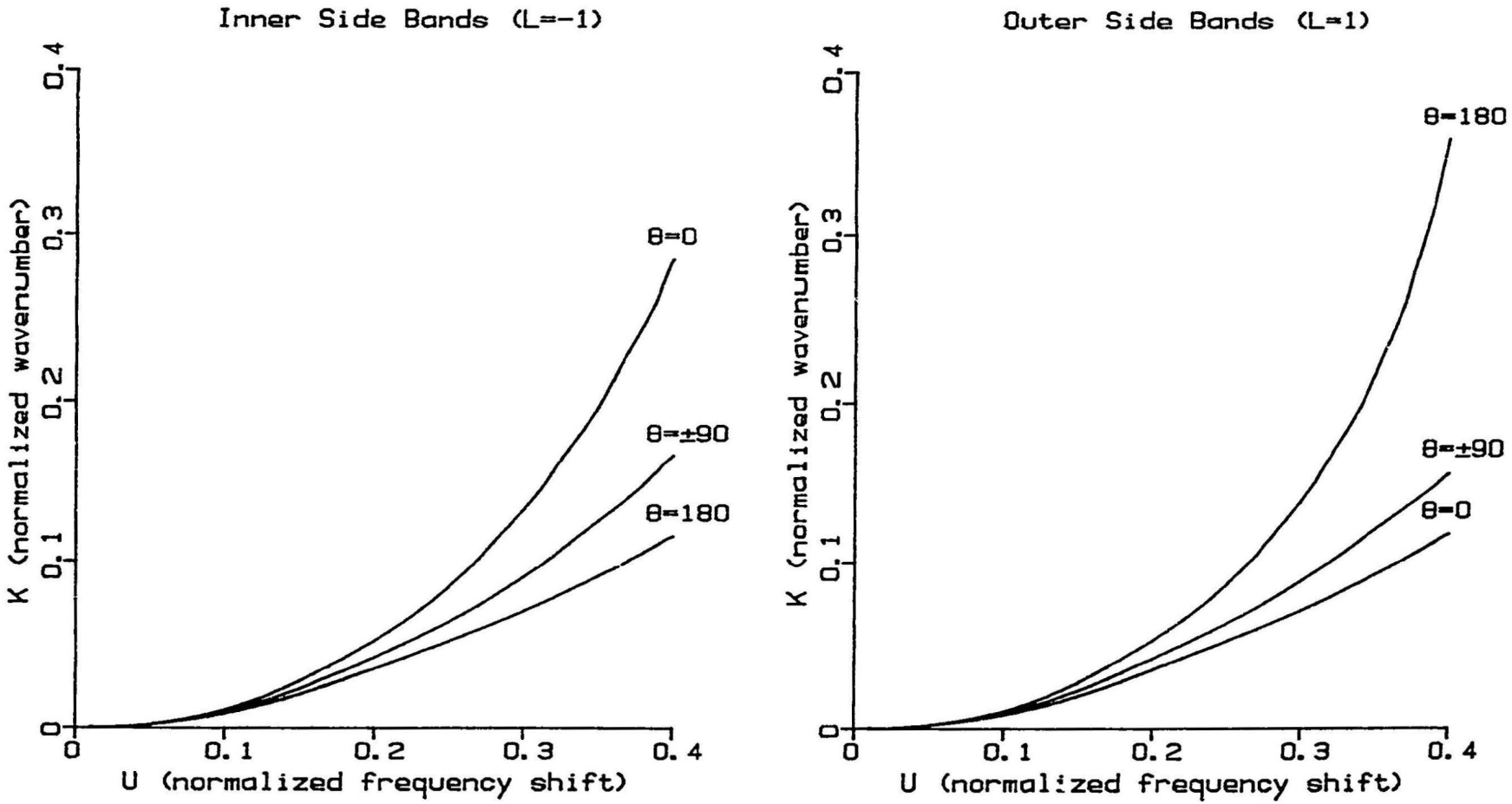

Figure 2.5: Deep water solution (up to $u = 0.4$) for the normalized wavenumber K at $\theta = 0°$, $90°$ and $180°$. The family of solution curves for all θ are bounded by the $\theta = 0°$ and $180°$ curves.

the inversion (perhaps up to $u = 0.36$ only).

Although the overall shape and size of the kernel function C may differ for each value of u, it consists primarily of two main lobes which have their maxima at θ equal to 0° or 180°. This property holds for all cross section models. As a demonstration of this behaviour, Fig. 2.6 shows polar plots of the Barrick and Lipa (1986) expression for C for various values of u. From these plots, it may be observed that, in general, a narrow beam radar is most strongly coupled to those long ocean waves which are travelling along the radar beam while most weakly coupled to those long ocean waves which are travelling roughly perpendicular to the beam.

This property of narrow beam radars has important implications for the accuracy of the inversion as it will mean that results may depend upon the orientation of the wavefield with respect to the radar beam. For cases when the waves are predominantly travelling in a direction that lies along the receive beam, the radar return will be strongly coupled to the bulk of the wave spectrum's energy. It is expected then that the radar should be able to estimate this energy with good accuracy. However, if large amounts of wave energy are travelling in a direction perpendicular to the receive beam the narrow beam radar will not clearly "see" this energy as its contribution to the radar spectrum will be weighted such that it will be of similar importance as the weaker radial waves. It is then likely that the radar may underpredict the total wave energy. This underestimation of waveheight estimates should increase progressively as the wavefield direction relative to the beam approaches orthogonality.

This variation in waveheight accuracy can be greatly reduced by using two or more narrow beam radars viewing the same patch of ocean from different directions. The additional information that two or more radars can provide will do much to eliminate this directional dependence on results as each radar will act to complement one another so that one can effectively monitor waves travelling in one direction that the other cannot. More accurate results will be achieved as the inversion must satisfy

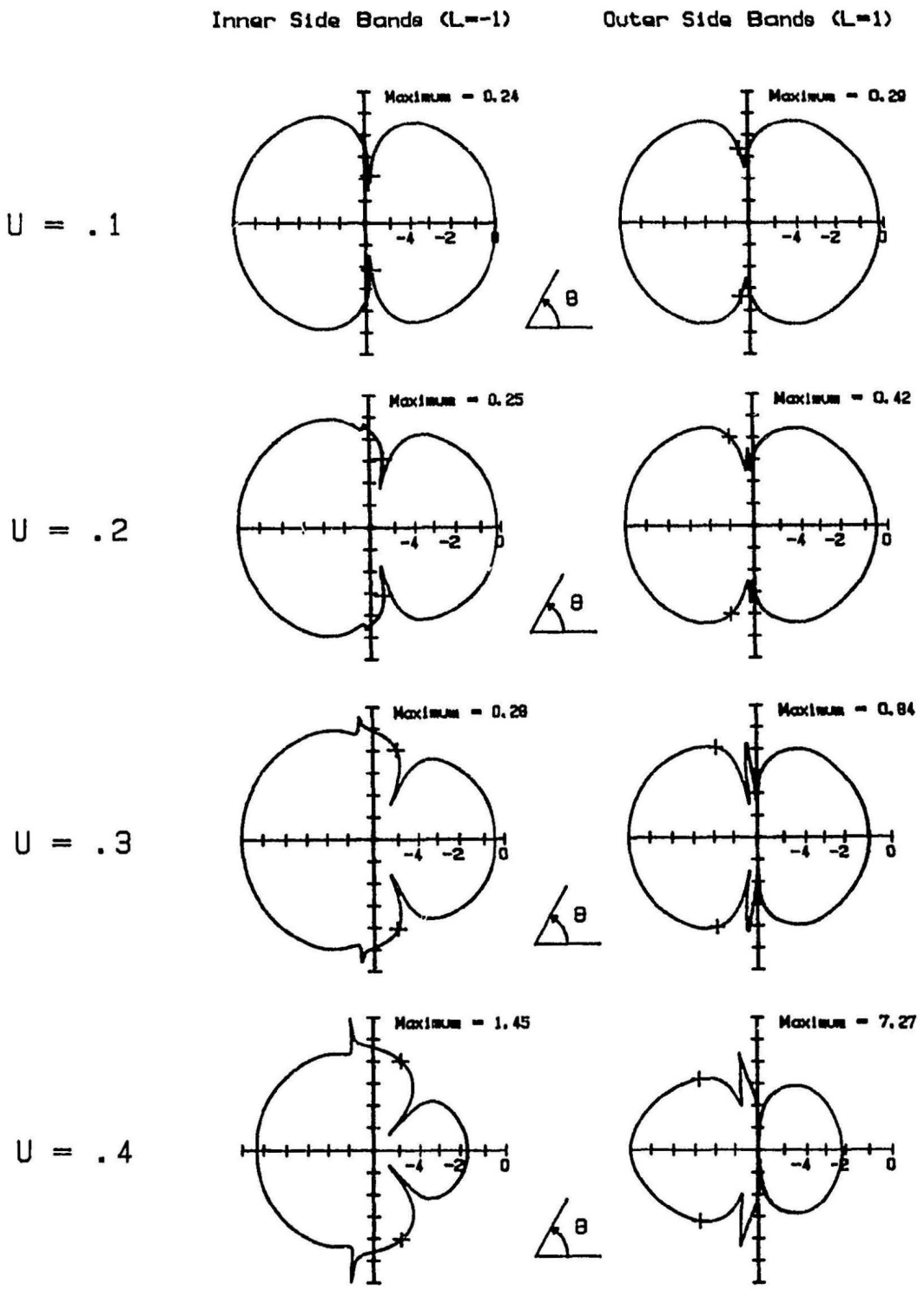

Figure 2.6: Logarithmic polar plots of the Barrick and Lipa expression for the kernel function C at $u = 0.1$, 0.2, 0.3, and 0.4. Each plot has been normalized by its maximum value. The marker + designates the angles at which β is maximum.

all radars. The use of two radars also serves to eliminate the left/right directional ambiguity inherent in a single radar.

Chapter 3

Solution of the Integral Equation

3.1 General

In this chapter, the linearized second order integral equation (2.41) is inverted, using matrix methods, for the region of the radar spectrum close to the first order peaks ($u < 0.4$) and for one or two narrow beam radars. For two radars viewing the same patch of ocean from different directions there will be two such equations as (2.41), both having a common frame of reference. The extension of the inversion algorithm to the set of equations resulting from three or more radars is straightforward.

Prior to calculating the solution of (2.41) for one or two radars, several practical considerations in analysing HF radar data must be first addressed and plans made for their incorporation into the inversion algorithm. One such problem is the lesser range of Doppler that can be examined due to the enlarged width of the first order peaks occurring in actual radar observations. Another more important concern is that of noise. In many circumstances, poor signal-to-noise ratios for some of the second order sidebands will make their data unavailable for use in calculating the inversion solution. Consequently, the solution must be found using the remaining sidebands.

The matrix equation is formed by discretizing the integral equation. In order to express the integral equation at each Doppler point as a finite term algebraic equation, the wave spectrum needs to be represented by a finite number of variables. This is accomplished by expanding the wave spectrum in a truncated Fourier series versus

angle and assuming that the Fourier coefficients are constant over equal length bands of ocean frequency. For a single radar the systems of equations for all Doppler points will have only even Fourier coefficients as its variables. This is a result of the fact that (2.41) folds the wave spectrum about the radar beam. For two radars the number of equations will double and both even and odd coefficients will be present in the matrix equation.

The solution to the matrix equation for either one or two radars is found by calculating its generalized (pseudo-) inverse using a singular value decomposition (SVD). In computing this inverse, all small singular values are set to zero.

As integral equations of the first kind are inherently ill-posed (Delves and Mohamed, 1985) it is expected that the matrix equation of this problem will be of less than full rank and that it will also experience conditioning problems. SVDs are particularly suited for problems such as this as they provide the solution which is of smallest norm even if the matrix is not of full rank. In addition, it is also possible to explore, in a qualitative sense, the condition of the matrix equation by studying the rate at which the singular values go to zero.

3.2 Preliminaries

3.2.1 The Integral Equation for Two Radars

The second order equation (2.41) was written with respect to the look direction of the narrow beam radar. For two such radars it is necessary to adopt a common frame of reference in describing the equation for each. A convenient reference for this task is the line bisecting the two narrow beams. It will also be convenient to distinguish between the two radars by assigning each a number.

Proceeding in this manner, the convention will be adopted that if the two receive beams have an angular separation of 2ϕ, radar # 1 will be that radar whose receive beam is separated from the bisector by an angle of ϕ while radar # 2 will be that radar

having an angular separation of $-\phi$. The system of second order integral equations for two radars may then be expressed as

$$
\begin{aligned}
{}_1\sigma_{2L}(\eta) &= \int_0^{\pi} C\left\{E(F,\phi+\alpha)+E(F,\phi+-\alpha)\right\}\,d\theta \qquad (3.1)\\
{}_2\sigma_{2L}(\eta) &= \int_0^{\pi} C\left\{E(F,-\phi+\alpha)+E(F,-\phi+-\alpha)\right\}\,d\theta \qquad (3.2)
\end{aligned}
$$

where the left subscript of each second order equation identifies the radar. As with (2.41) the above obeys the constraints (2.12), (2.29) and (2.31). By virtue of (2.31) each of the above equations will represent a set of four integral equations, one for each second order sideband. Combined, the above represents a set of eight integral equations.

3.2.2 Doppler Limits and Noise Effects

Prior to performing the inversion of the set of integral equations for both one and two radars, it will first be necessary to establish practical limits on what range of Doppler frequencies may be used for the analysis and also what effects noise may have on the radar spectrum. Of particular interest, is the reduction of the number of second order sidebands that may be used due to poor signal-to-noise ratios.

In the last chapter it was established that the second order cross section may be used to represent the total cross section by itself for $0.1 < u < 0.4$. In studying the mapping properties of the integral equation it was decided that an upper limit of 0.36 for u would be more practical for the analysis. This has the advantage of excluding those large wavenumber terms which are only represented by their radial directional components.

In many circumstances, it may not be possible to achieve a lower limit of 0.1 for u in performing the inversion due to the enlarged width of the first order peaks encountered in actual radar observations. The widening of these peaks are the result of smearing effects associated with currents and the problem of finite sample size in calculating the estimate for the Doppler spectrum from the radar time series.

Although it will generally be possible to still approach $u = 0.1$ for many cases, a more general (and perhaps conservative) restriction of $u \geq 0.15$ will be applied in this thesis. As a result, the total range of Doppler that will be used in the present inversion is $0.15 < u < 0.36$.

An important consideration for any inversion problem is that, because of noise, the measured data is often only imprecisely known. For integral equations of the first kind this problem can be acute due to their poorer condition, i.e., an arbitrarily small perturbation in the data may give rise to a large perturbation in the solution. To combat the problem of noise for equations of the first kind, regularization methods have been developed (see Delves and Mohamed, 1985) to impose stability on the solution. A drawback to regularization however, is that it also constrains the solution to be smooth.

Although the HF band is often very congested and hence noisy, the problem of noise in performing wave measurements using HF radars may be overcome so that at least one-half of the radar spectrum may still be inverted. The crux of this solution lies in the fact that, unlike many other radar systems, HF radars operate as a *coherent* device. That is, a HF radar monitors its target for a long period of time (typically one-half hour for wave measurements) and collects a time series of its observations. With this lengthy time series a substantial amount of incoherent averaging may be performed so that the noise level for the estimate of the radar spectrum will be greatly reduced. From this point on it shall be assumed that enough averaging has been performed on the data so that the noise level of the radar spectrum is fairly low (approximately 40 dB down from the largest first order peak).

Although the noise level of the radar spectrum may be brought down, it will still have a significant impact on the radar spectrum as some second order sidebands may still be only slightly above the noise level or perhaps buried beneath it. Shown in Fig. (3.1) is a plot of a measured radar Doppler spectrum which illustrates this

problem.

It may be observed from this example spectrum that except for its first order peak, the positive half of the radar spectrum lies at such a low level that it has been buried in noise. As a result, this half of the radar spectrum is not accessible for processing. On the other hand, the negative half of the spectrum stands well above the noise and may still be used for the inversion.

The loss of the positive Doppler half of the radar spectrum for this case is a direct result of the fact that the short ocean waves had far more energy propagating away from the radar than towards it. This fact can be confirmed from the much greater height of the negative Doppler first order peak over the positive Doppler peak. In general, the mismatch in height between each Doppler half of the first order return will be approximately the same for the second order spectrum. This is so as one of the two scattering waves that produce the second order return for a given Doppler will always be very much like the Bragg wave that produced the nearby first order peak.

The dependence of each half of the radar spectrum upon the height of its local first order peak is also demonstrated in Figs. 2.1 and 2.2. In Fig. 2.1 the heights of the two Bragg waves are nearly equal and as a consequence the radar spectrum is nearly symmetric about zero Doppler. In Fig. 2.2 the disparity between the heights of the two Bragg waves is not so great as it was for Fig. 3.1 and as a result second order peaks may be clearly observed in the positive half of the spectrum. However, these peaks are only marginally above the noise floor and may still not be suitable for inclusion in the inversion algorithm. As a general rule, in order for second order data to be of use for inversion it should stand about 10 dB above the noise floor.

On the basis of the above discussion, it is generally reasonable to expect that at least one-half of the radar spectrum will be available for processing. The other two sidebands corresponding to the weaker half of the spectrum may be excluded from

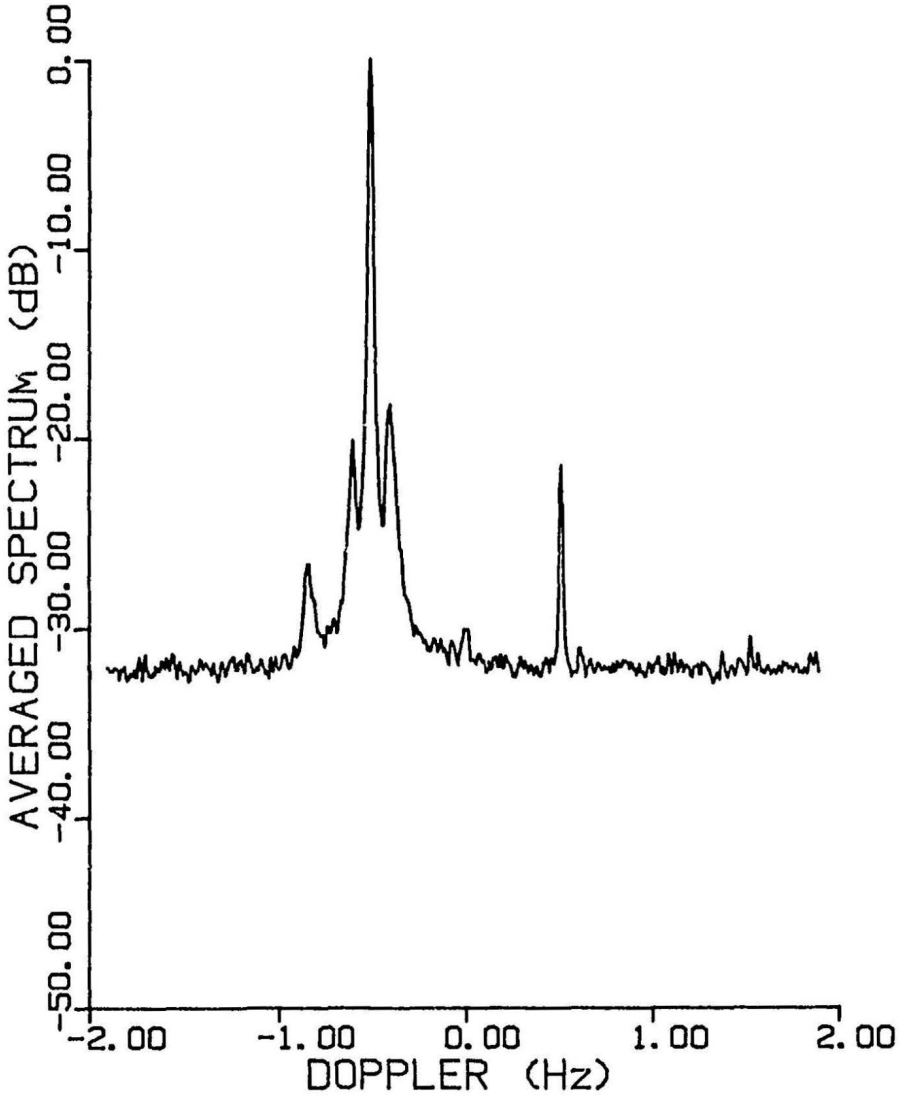

Figure 3.1: Example of a 25.4 MHz narrow beam radar Doppler spectrum showing strong noise contamination. Except for its first order peak, the positive Doppler half of the spectrum has been buried in noise.

the analysis depending upon their signal-to-noise levels.

If any sidebands are indeed discarded then the integral equations they represent must also be removed from the total system of integral equations. The solution must then be found using the remaining equations. Solutions must then be prepared for several different cases, each case being identified by what pairs of sidebands are available for analysis from the spectra of one or more radars.

3.3 Discretization of the Integral Equation

3.3.1 Fourier Series Expansion for the Wave Spectrum

A common and very useful representation for the ocean wave spectrum is to expand it into a Fourier series versus angle. Such an expansion has the form

$$e(f,\theta) = \sum_{n=0}^{\infty} \{a_n(f)\cos(n\theta) + b_n(f)\sin(n\theta)\} \tag{3.3}$$

where each Fourier coefficient is a function of frequency. These coefficients are defined such that

$$a_n(f) = \begin{cases} \dfrac{2}{\pi}\displaystyle\int_0^{2\pi} e(f,\theta)\,d\theta & \text{for } n = 0 \\ \dfrac{1}{\pi}\displaystyle\int_0^{2\pi} e(f,\theta)\cos(n\theta)\,d\theta & \text{otherwise} \end{cases} \tag{3.4}$$

$$b_n(f) = \begin{cases} 0 & \text{for } n = 0 \\ \dfrac{1}{\pi}\displaystyle\int_0^{2\pi} e(f,\theta)\sin(n\theta)\,d\theta & \text{otherwise} \end{cases} \tag{3.5}$$

The Fourier coefficient $a_0(f)$ is of special interest for many applications. It is directly related to the spectral density function $e(f)$ which is commonly referred to as the one-dimensional (or simply 1-D) wave spectrum. The 1-D wave spectrum $e(f)$ is defined such that its represents the distribution of wave energy as a function of frequency only, i.e., it is equivalent to the integration of the 2-D wave spectrum $e(f,\theta)$ over angle. Hence,

$$e(f) = \int_0^{2\pi} e(f,\theta)\,d\theta \tag{3.6}$$

Comparing the above with (3.4) it may be seen that

$$e(f) = a_0(f)\pi/2 \tag{3.7}$$

By and large, the most sought after information for wave studies is the 1-D wave spectrum. From this spectral density function the most important ocean spectral parameters may be determined (e.g., rms waveheight). Indeed, most wave buoys have been designed to measure $e(f)$ only.

Using (2.9) and (3.3) the Fourier series expansion for the normalized wave spectrum $E(F,\theta)$ may be written as

$$E(F,\theta) = \sum_{n=0}^{\infty} \{a_n(F)\cos(n\theta) + b_n(F)\sin(n\theta)\} \tag{3.8}$$

where the normalized Fourier coefficients $(a_n(F), b_n(F))$ are defined such that

$$(a_n(F), b_n(F)) = (2k_0)^{5/2}(a_n(f), b_n(f)) \tag{3.9}$$

Using the above representation for $E(F,\theta)$, the set of integral equations for one radar (2.41) may be rewritten as

$$\sigma_{2L}(u,m,m') = 2\sum_{n=0}^{\infty} \int_0^{\pi} Cm^n a_n(F)\cos(n\theta)\,d\theta \tag{3.10}$$

As a result of the folding of the wave spectrum about the radar beam, the cross section equation for one radar depends only upon the even Fourier coefficients of the expansion. Without the odd coefficients it is impossible to resolve the left/right directional ambiguity inherent in (3.10).

For future convenience, the η argument of the above second order equation has been replaced with the parameters u, m, and m' which are related to η by virtue of (2.35) as

$$\eta = m' + mu \tag{3.11}$$

In a similar fashion, the set of integral equations for two radars ((3.1) and (3.2)) may be reexpressed as

$${}_1\sigma_{2L}(u,m,m') = 2\sum_{n=0}^{\infty} \int_0^{\pi} Cm^n \{a_n(F)\cos(n\phi) + b_n(F)\sin(n\phi)\}\cos(n\theta)\,d\theta \tag{3.12}$$

$$_2\sigma_{2L}(u,m,m') = 2\sum_{n=0}^{\infty}\int_0^{\pi} Cm^n \{a_n(F)\cos(n\phi) - b_n(F)\sin(n\phi)\}\cos(n\theta)\,d\theta \quad (3.13)$$

With the data of two radars it is possible to extract information for both even and odd Fourier coefficients. Hence, unambiguous directional information may be obtained.

Two radars, however, may still not provide full spectral information as both (3.12) and (3.13) will not depend upon certain coefficients for a given value of ϕ. For example, if ϕ were equal to 30° then the set of even coefficients $a_3, a_9, a_{15}, \ldots$ and the set of odd coefficients $b_6, b_{12}, b_{18}, \ldots$ will be missing from (3.12) and (3.13). Even if ϕ was not exactly 30° it may be unwise to attempt to extract information for these coefficients as they may be weighted by such a small value that the integral equations will only weakly depend upon them. A choice must then be made to determine what coefficients should be excluded from the analysis for a given value of ϕ.

In the following sections the Fourier series is to be truncated after $n = 2$. Therefore, the only case of concern in trying to determine if a Fourier coefficient is to be excluded from (3.12) and (3.13) is when the two radar beams are almost orthogonal ($\phi = 45°$). For this case it shall be considered acceptable, in general, to exclude the $a_2(F)$ Fourier coefficient if $85° < 2\phi < 95°$.

Some of the $n = 1$ coefficients may also be excluded if the angle of intersection between the two radars is equal to 0 or 180°, however, these are not practical situations. If the angle between the radar beams were close to zero then the Doppler spectrum observed by each radar will be essentially equivalent. Hence, there will have been no effective increase in information in using two radars over one. In a similar manner, little additional information over that of one radar will be obtained if the two radars are opposed to one another. For this case it is easy to show that the Doppler spectrum observed by each radar will be the mirror image of one another.

The preceding paragraph brings to attention an important limitation in using two radars, i.e., the success of the inversion will depend upon the angular separation between the two receive beams. In all likelihood, the best inversion results should be

obtained when the two beams are orthogonal. The accuracy of the results should also decrease as the two receive beams approach alignment or opposition to one another. This property will be examined further in the next chapter.

3.3.2 Matrix Equation for One and Two Radars

The matrix equation for both one and two radars is formed by approximating (3.10), (3.12), and (3.13) as finite term algebraic equations. The set of discretized integral equations for each Doppler point will then represent a system of equations (or equivalently, a matrix equation). The variables of this system are the Fourier coefficients of the wave spectrum.

As the radar spectrum will exist over discrete values of η there will be also a discrete set of values which u may take over the range $0.15 < u < 0.36$. These discrete values u_i are given by

$$u_i = u_1 + (i-1)\Delta u \text{ for } i = 1, \ldots, I \tag{3.14}$$

where Δu is the resolution of the Doppler spectrum, I is the total number of Doppler points per sideband for $0.15 < u < 0.36$, and u_1 is the smallest discrete value of u lying within this range for u.

In order to express the equation for each Doppler point as a finite term algebraic equation, the ocean wave spectrum must be discretized into a finite number of variables. As a first step towards this end, $E(F,\theta)$ will be assumed constant over equal length bands of frequency F. Hence, the values of the Fourier coefficients for each band will be assumed constant as well. The total number of bands will be represented by the number J.

The total range of frequencies which is to be divided up in J bands has as its lower endpoint the value of F occurring at $(u = u_1, L = -1, \theta = \pi)$ and an upper endpoint corresponding to the value of F occurring at $(u = u_I, L = 1, \theta = \pi)$. At 25.4 MHz the resulting total (unnormalized) range of ocean frequencies will be approximately

$0.07 < f < 0.25$ Hz. This is a particularly advantageous range of frequencies for measurement as it will contain the bulk of the total ocean spectral energy.

This range becomes more restricted however, as the operating frequency decreases. At 10 MHz this range becomes approximately $0.044 < f < 0.157$ Hz which may not be sufficient to produce an estimate for the rms waveheight h. The range of values for other operating frequencies may be calculated by multiplying the endpoints of the 25.4 MHz range by the square root of the ratio of the operating frequency to 25.4×10^6.

To complete the discretization of the wave spectrum into a finite number of variables its Fourier series expansion needs to be truncated after a certain value of n. In general, this Fourier series may be well approximated by its first nine terms only ($n = 4$). As to how many terms may be practically retained to represent the wave spectrum will depend upon Δu, the resolution of the radar spectrum. If too many terms are retained such that the number of variables exceeds the number of available equations (Doppler points), the matrix equation will become underdetermined and thus difficult to solve.

Owing to the sampling rate limits of the radar equipment used at CASP, this thesis will truncate the Fourier series after $n = 2$. For other reasons, this limitation also applies to most wavebuoy systems including those used at CASP. This can be considered an acceptable compromise as, for many circumstances, the main features of the directional distribution will still be preserved if the series is approximated by its first five terms only. However, some accuracy will be sacrificed from the inversion if this done. This will be especially true for those frequency bands which have a narrow directional distribution. This topic will be explored in more detail in the next chapter.

Following the discretization scheme for $E(F, \theta)$ described above, the set of dis-

cretized integral equations for one radar (3.10) may be rewritten as

$$\sigma_{2L}(u_i, m, m') = 2\sum_{n=0}^{2}\int_0^{\pi} Cm^n{}_j a_n(F)\cos(n\theta)\,d\theta \tag{3.15}$$

where ${}_j a_n$ (also ${}_j b_n$) are Fourier coefficients for the jth frequency band. The value of j in the above integral depends upon θ by virtue of the delta function constraint (2.29). This constraint equation in turn controls the value of F.

In order to express the above integral equation in terms of an algebraic equation, the overall contribution to the integral from each frequency band must be isolated. As a given frequency band j will correspond to a continuous range of values for θ, the second order integral may be reexpressed as the algebraic equation

$$\sigma_{2L}(u_i, m, m') = 2\sum_{j=0}^{J}\sum_{n=0}^{2}\int_{\theta_{i,j,L}} Cm^n{}_j a_n(F)\cos(n\theta)\,d\theta \tag{3.16}$$

where $\theta_{i,j,L}$ represents the θ limits for band j for a given u_i and L. For this set of Doppler points, if there are no values of θ ranging from 0 to π which will have a solution F to (2.29) that belongs to band j then the θ integral will be zero for that j.

In practice, it is a simple matter to determine $\theta_{i,j,L}$ for a given Doppler point. This may be done numerically by reviewing the solutions for F to the delta function constraint for values of θ ranging from 0 to π. A closed form expression for $\theta_{i,j,L}$ may also be derived using the delta function constraint if it is assumed that $\tanh(K'D) \approx 1$. In general, this can be considered to be a very good approximation for all but very low HF frequencies.

In a similar fashion, the set of integral equations for two radars ((3.11) and (3.12)) may be reexpressed in discretized form as

$${}_1\sigma_{2L}(u_i, m, m') = 2\sum_{j=0}^{J}\sum_{n=0}^{2}\int_{\theta_{i,j,L}} Cm^n\left\{{}_j a_n(F)\cos(n\phi) + {}_j b_n(F)\sin(n\phi)\right\}\cos(n\theta)\,d\theta \tag{3.17}$$

$${}_2\sigma_{2L}(u_i, m, m') = 2\sum_{j=0}^{J}\sum_{n=0}^{2}\int_{\theta_{i,j,L}} Cm^n\left\{{}_j a_n(F)\cos(n\phi) - {}_j b_n(F)\sin(n\phi)\right\}\cos(n\theta)\,d\theta \tag{3.18}$$

Having expressed the integral equations in discretized form, the set of algebraic equations for all u_i, m and m' may be directly expressed in matrix form for both one and two radars as

$$\boldsymbol{C}\boldsymbol{x} = \boldsymbol{\sigma} \tag{3.19}$$

where $i = 1, \ldots, I$ and $j = 1, \ldots, J$

The solution vector $\boldsymbol{x}$ of the equation is defined as

$$\boldsymbol{x} = \begin{bmatrix} \boldsymbol{x}_1 \\ \boldsymbol{x}_2 \\ \vdots \\ \boldsymbol{x}_J \end{bmatrix} \tag{3.20}$$

where

$$\boldsymbol{x}_j = \begin{cases} \begin{bmatrix} {}_ja_2 \\ {}_ja_1 \\ {}_ja_0 \end{bmatrix} & \text{for one radar} \\ \begin{bmatrix} {}_ja_2 \\ {}_ja_1 \\ {}_ja_0 \\ {}_jb_1 \\ {}_jb_2 \end{bmatrix} & \text{for two radars} \end{cases} \tag{3.21}$$

The data vector of the problem is represented by $\boldsymbol{\sigma}$ which is composed of normalized radar spectral values. This data vector has the form

$$\boldsymbol{\sigma} = \begin{bmatrix} \boldsymbol{\sigma}_1 \\ \boldsymbol{\sigma}_2 \\ \vdots \\ \boldsymbol{\sigma}_I \end{bmatrix} \tag{3.22}$$

where each element $\boldsymbol{\sigma}_i$ of $\boldsymbol{\sigma}$ represent the grouping of all Doppler points having the

same value of u_i:

$$\boldsymbol{\sigma}_i = \begin{cases} \begin{bmatrix} \sigma_{2L}(u_i,-1,-1) \\ \sigma_{2L}(u_i,1,-1) \\ \sigma_{2L}(u_i,-1,1) \\ \sigma_{2L}(u_i,1,1) \end{bmatrix} & \text{for one radar} \\ \begin{bmatrix} {}_1\sigma_{2L}(u_i,-1,-1) \\ {}_1\sigma_{2L}(u_i,1,-1) \\ {}_1\sigma_{2L}(u_i,-1,1) \\ {}_1\sigma_{2L}(u_i,1,1) \\ {}_2\sigma_{2L}(u_i,-1,-1) \\ {}_2\sigma_{2L}(u_i,1,-1) \\ {}_2\sigma_{2L}(u_i,-1,1) \\ {}_2\sigma_{2L}(u_i,1,1) \end{bmatrix} & \text{for two radars} \end{cases} \tag{3.23}$$

The rectangular matrix $\boldsymbol{C}$ represents the kernel matrix of this problem. The elements of $\boldsymbol{C}$ are defined as

$$\boldsymbol{C}_{i,j} = \begin{cases} \begin{bmatrix} p_1 & -p_2 & p_3 \\ q_1 & q_2 & q_3 \\ q_1 & -q_2 & q_3 \\ p_1 & p_2 & p_3 \end{bmatrix} & \text{for one radar} \\ \begin{bmatrix} r_1 & -r_2 & r_3 & -r_4 & r_5 \\ s_1 & s_2 & s_3 & s_4 & s_5 \\ s_1 & -s_2 & s_3 & -s_4 & s_5 \\ r_1 & r_2 & r_3 & r_4 & r_5 \\ r_1 & -r_2 & r_3 & r_4 & -r_5 \\ s_1 & s_2 & s_3 & -s_4 & -s_5 \\ s_1 & -s_2 & s_3 & s_4 & -s_5 \\ r_1 & r_2 & r_3 & -r_4 & -r_5 \end{bmatrix} & \text{for two radars} \end{cases} \tag{3.24}$$

where

$$(p_1, q_1) = 2\int_{\theta_{i,j,L}} C\cos(2\theta)\,d\theta \quad \text{for } L = (1,-1) \tag{3.25}$$

$$(p_2, q_2) = 2\int_{\theta_{i,j,L}} C\cos(\theta)\,d\theta \quad \text{for } L = (1,-1) \tag{3.26}$$

$$(p_3, q_3) = 2\int_{\theta_{i,j,L}} C\,d\theta \quad \text{for } L = (1,-1) \tag{3.27}$$

and

$$(r_1, s_1) = (p_1, q_1)\cos(2\phi) \tag{3.28}$$

$$(r_2, s_2) = (p_2, q_2)\cos(\phi) \tag{3.29}$$

$$(r_3, s_3) = (p_3, q_3) \tag{3.30}$$

$$(r_4, s_4) = (p_2, q_2)\sin(\phi) \tag{3.31}$$

$$(r_5, s_5) = (p_1, q_1)\sin(2\phi) \tag{3.32}$$

If poor signal-to-noise ratios for some second order sidebands prevent their use for inversion, those rows of $\boldsymbol{\sigma}_i$ corresponding to these sidebands will have to be deleted. The rows of $\boldsymbol{C}_{i,j}$ having the same row numbers as the deleted rows of $\boldsymbol{\sigma}_i$ will also have to be deleted.

3.4 The Pseudo-Inverse of the Matrix Equation

Having expressed the set of integral equations in matrix form (equation (3.19)) it is now desired to solve this equation. The problem of finding a solution to a matrix equation falls within that well known category of matrix problems referred to as "inversion". Ideally, the inversion of a matrix equation can be achieved if it were multiplied by an inverse operator $\boldsymbol{C}^{-1}$. The solution vector $\boldsymbol{x}$ for this problem would then be simply $\boldsymbol{C}^{-1}\boldsymbol{\sigma}$. However, it is often the case as it is for this problem that this inverse matrix does not exist. As a result, there will be no unique solution to the problem. The matrix equation is then said to be singular.

In practice, a somewhat more general notion of inversion is usually applied to find the solution of a matrix equation. Instead of insisting that (3.19) has a solution, it shall only be required that there is some vector $\boldsymbol{x}$ which is "solution-like" in the sense that it minimizes

$$\|\boldsymbol{\sigma} - \boldsymbol{C}\boldsymbol{x}\|_2^2$$

where $\|\cdot\|_2$ is the vector two-norm. Such a vector $\boldsymbol{x}$ is called a *linear least squares*

solution. The problem of determining this solution is called the *linear least squares problem.*

As with any least squares problem it is desired to find the solution of smallest norm (length). It has been proven by (among others) Strang (1983) that the optimal solution to the linear least squares problem is

$$\boldsymbol{x} = \boldsymbol{C}^{+}\boldsymbol{\sigma} \tag{3.33}$$

where the matrix $\boldsymbol{C}^{+}$ is the *pseudo-inverse* or *Moore-Penrose generalized inverse* of $\boldsymbol{C}$. Even if the matrix $\boldsymbol{C}$ is not of full rank (singular) the above is still the optimal solution for the problem. It is of interest to note that if $\boldsymbol{C}$ were not singular then its pseudo-inverse $\boldsymbol{C}^{+}$ would be equivalent to its left-inverse $\boldsymbol{C}^{-1}$.

The pseudo-inverse of a matrix is obtained from a simple but valuable matrix factorization technique called *singular value decomposition* (SVD), which according to Gilbert Strang (1983, ch.3) is a method that is

not nearly as famous as it should be.

It has been shown by Stewart (1973, ch.6) and others that by using the method of singular value decomposition any general m by n matrix $\boldsymbol{C}$ can be factored into the diagonal form

$$\boldsymbol{C} = \boldsymbol{U}\begin{pmatrix} \boldsymbol{\Sigma} & \mathbf{0} \\ \mathbf{0} & \mathbf{0} \end{pmatrix}\boldsymbol{V}^{T} \tag{3.34}$$

where $\boldsymbol{U}$ is an m by m orthogonal matrix, $\boldsymbol{V}$ is a n by n orthogonal matrix, and $\boldsymbol{\Sigma}$ is a diagonal matrix having the form

$$\boldsymbol{\Sigma} = diag(\mu_1, \mu_2, \ldots, \mu_n) \tag{3.35}$$

with

$$\mu_1 \geq \mu_2 \geq \cdots \geq \mu_n \geq 0 \tag{3.36}$$

The numbers $\mu_1, \mu_2, \ldots, \mu_n$ are called the *singular values* of $\boldsymbol{C}$. The columns of $\boldsymbol{U}$ are called the *right singular vectors* of $\boldsymbol{C}$ while the columns of $\boldsymbol{V}$ are called the *left*

singular vectors of C. There is a close relationship between the singular values and vectors of a matrix and its eigenvalues and eigenvectors.

Library routines are available to calculate the SVD of a general matrix. One such **FORTRAN** routine is **SSVDC** which is part of the public domain **LINPACK** library (Dongarra et al., 1979). This same routine was also used as a basis for the **IMSL** subroutine **LSVRR** (IMSL Math/Library User's Manual, 1987). In this thesis, the SVD of the kernel matrix C is calculated using the **IMSL** routine **DLSVRR** which is a double precision version of **LSVRR**.

Having calculated the SVD of C, its pseudo-inverse follows immediately by inverting the right hand side of (3.34) after all small singular values have been set to zero. It is important to truncate these small values as the inverse of Σ is simply the reciprocal of its non-zero elements. If a singular value μ_i were very small then μ_i^{-1} would be very large and may possibly overwhelm the pseudo-inverse. Assuming that only the first r singular values have been retained and that $\mu_{r+1} = \mu_{r+2} = \cdots = \mu_n = 0$, the pseudo-inverse of C may be written as

$$C^+ = V \begin{pmatrix} \Sigma^{-1} & \mathbf{0} \\ \mathbf{0} & \mathbf{0} \end{pmatrix} U^T \tag{3.37}$$

where, of course, the inverse of an orthogonal matrix is simply its transpose. The parameter r should be close in value to the rank of the matrix Σ which in turn is equivalent to the rank of C.

With (3.37), the solution to the integral equation has been formulated. What is now required to calculate this solution is a choice for r.

3.5 Selection of r and the Condition of the Kernel Matrix

The only remaining problem to overcome in completing the inversion algorithm is to determine how many singular values should be retained for the inversion. This will be done by exploring what values of r give the most accurate results for simulated

radar data. A sample of these wave spectrum solutions for the selected value of r will be presented in the next chapter.

An important aspect of the problem of selecting r is the stability of the inversion solution, i.e., how sensitive is it to changes in r. If there a good amount of flexibility available in the choice of r to achieve the "best" solution, for a given set of conditions, the problem of choosing r is greatly simplified. However, if this is not the case, much care must be taken in the choice of r.

Another possible concern is if r is dependent on sea state. If this is so, the selection of r may become very difficult as *a priori* knowledge of the wave spectrum will probably be required. However, if it is not, the inversion algorithm will become robust as it may be applied in the same manner each time for the same radar deployment.

To illustrate the general properties of the selected value of r, consider the decomposition of the single and dual-radar kernel matrix $\boldsymbol{C}$ for the case of deep water, $I = J = 30$, and $2\phi = 60°$ for two radars. If only two sidebands are available from the data of a single radar, J will be set to 15. Except for the water depth, these parameter values are the same as, or very close to, that used for the CASP data set.

Shown in Fig. 3.2 is a set of logarithmic plots for the singular values resulting from the double precision decomposition of the single radar kernel matrix (with two or four sidebands). Fig. 3.3 is a similar set of plots for the dual-radar singular values (with six or eight sidebands). Both Figs. 3.2 and 3.3 were generated using the Barrick and Lipa (1986) second order model. The properties of the decomposition to be discussed here as well as the selection method for r is the same for all three second order models.

It may be observed from these singular value plots that the logarithm of the singular values of this problem is characterized by an initial linear descent of small slope which eventually undergoes a relatively sharp downturn with the singular values rapidly approaching zero. For all cases, except the single radar case with only two

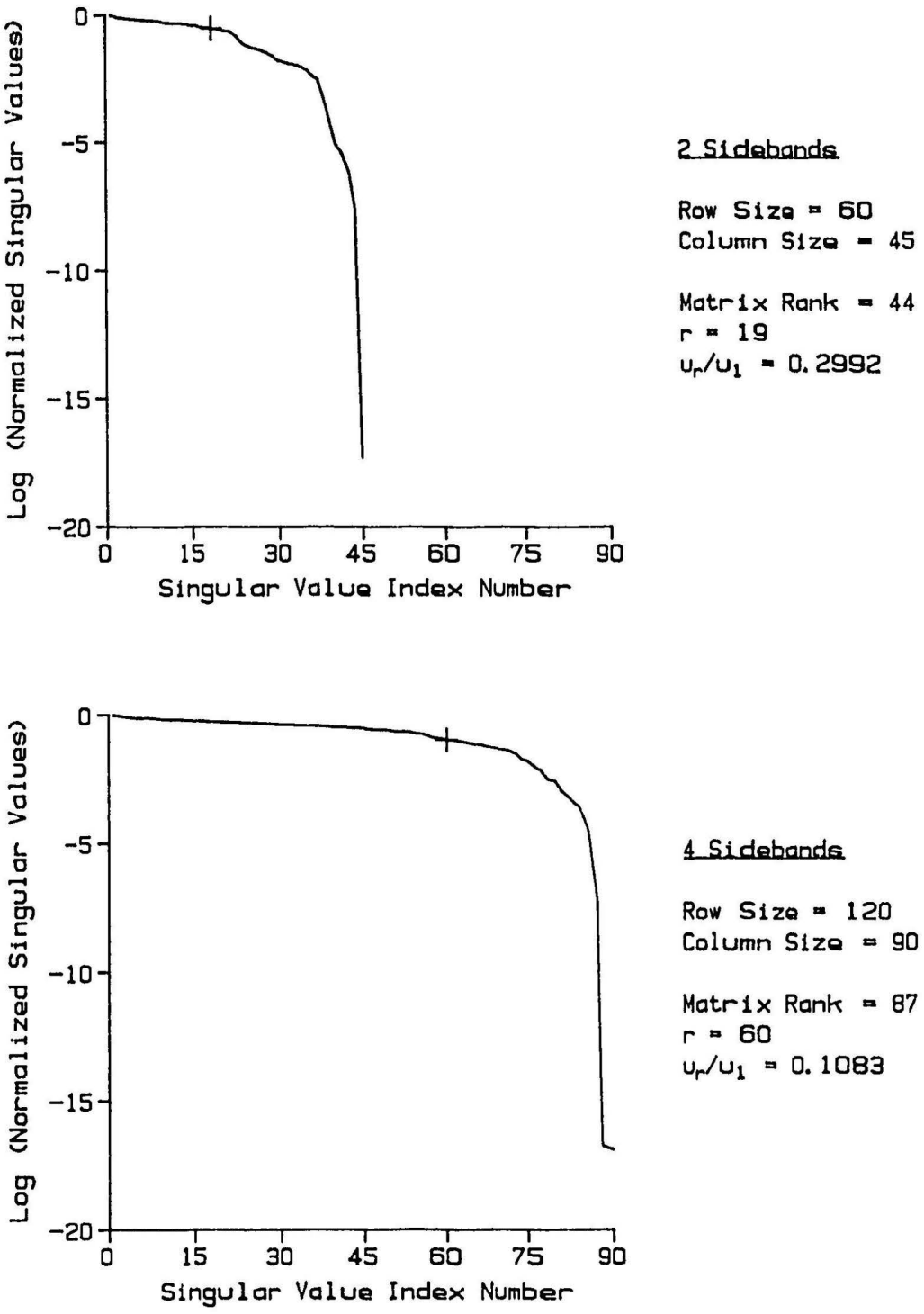

Figure 3.2: Logarithmic plot of the singular values resulting from the decomposition of the single radar kernel matrix for the case of deep water, $I = 30$, and $J = 15$ (two sidebands) or 30 (four sidebands). All singular values have been normalized by the first singular value. The marker + indicates the cut-off point after which singular values are discarded.

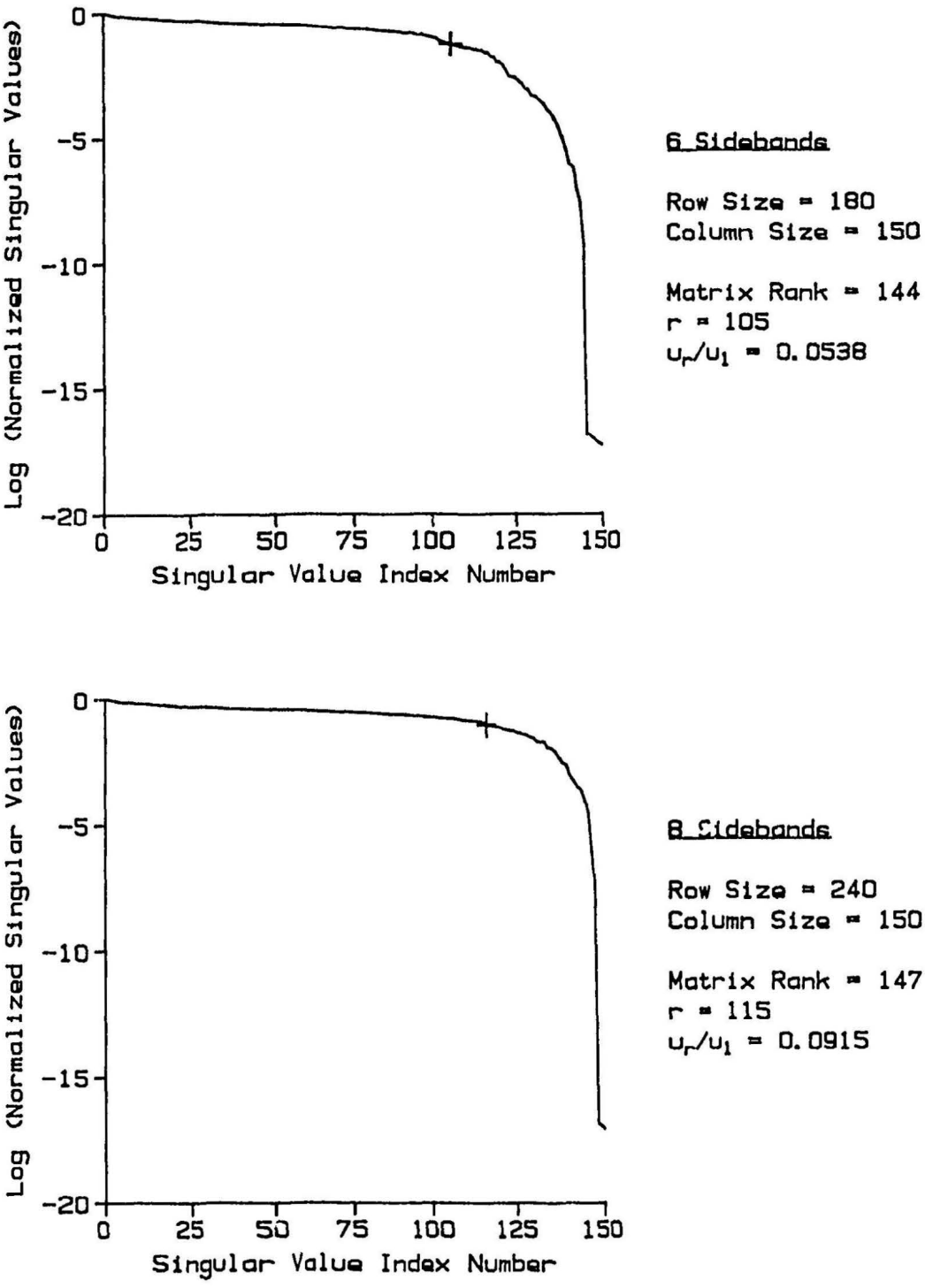

Figure 3.3: Logarithmic plot of the singular values resulting from the decomposition of the dual-radar kernel matrix for the case of deep water, $2\phi = 60°$, and $I = J = 30$. All singular values have been normalized by the first singular value. The marker + indicates the cut-off point after which singular values are discarded.

sidebands, the initial linear portion of the curve contains the bulk of the singular values.

Also shown in Figs. 3.2 and 3.3 is a marker indicating the position of that r which resulted in the best inversion solution for simulated data. The value of this optimal r for each case is listed next to the diagram. It has been found from these simulation tests that the choice of r is independent of sea state or wave direction. For actual radar data, this same property also holds. As a matter of fact, the value of r used for these cases also gave the best results for the CASP data.

That r remains the same irrespective of sea state or wave direction greatly simplifies the problem of choosing r. All that r does depend upon are radar operation parameters such as water depth, number of radars and ϕ, I and J, number of available sidebands, etc.

From the singular value plots shown in Figs. 3.2 and 3.3, it may be observed that the choice of r for each case demonstrates a consistent trend, i.e., r lies very close to, but usually just a little past, the end of the linear portion of the curve. This same property also holds for the CASP data. From examination of a similar set of plots corresponding to an extensive range of operation parameters, it was found that the choice of r also lies in the same general location. Hence, it is now known, in general terms, where r should lie. How precise a specific choice for r should be will depend upon how sensitive the inversion solution is to changes in r from the optimal value.

As is turns out, an exacting choice for r is not required as the inversion solution remains stable over an extensive range of values for r. For example, for the four sideband case of Fig. 3.2 where r was selected to be 60, single radar estimates for $e(f)$ will change only upon the order of a few percent for $20 < r < 65$. The same property also holds for dual-radar estimates of $e(f)$. For the eight sideband case of Fig. 3.3 where r was selected to be 115, $e(f)$ estimates remain stable over the range $30 < r < 120$. In general, $e(f)$ estimates will be virtually the same for all but the

smallest value of r that lies on the linear portion of the curve.

With regards to the measurement of directional information, a more restricted range for r is required. For the eight sideband case of Fig. 3.3, directional parameter estimates remain steady for approximately $90 < r < 120$. It is of interest to note that for frequencies near the spectral peak, these parameters remain stable for a much larger range of r. In any case, even for this more restricted, although still very wide range, there is a great amount of flexibility for the choice of r.

That the inversion solution demonstrates such good stability with respect to r may be indicative of the kernel matrix's conditioning. An elegant benefit of factorizing a matrix using a SVD is that it gives insight into its rank and conditioning. This information may be obtained from its singular values.

An estimate for the rank of a matrix may be easily determined from its singular values (Gladwell, 1974). This is accomplished by testing the singular values against a small tolerance value. The rank of the matrix will simply be the number of singular values that exceed this tolerance.

To study the rank of this problem, a tolerance of 10^{-6} will be applied against the double precision examples presented in Figs. 3.2 and 3.3. The resulting estimate for the rank is listed next to each diagram. It may be observed from these estimates that the kernel matrices of this problem are very close to full rank, i.e., almost equal to the number of columns. Although this does not mean that the problem is well conditioned, it is encouraging nonetheless as it suggests that it is not badly conditioned.

A qualitative measure of the conditioning of this problem may be obtained from the rate that the sequence of singular values go to zero (Baker, 1977, ch. 15.5; Miller, 1974). In general, the faster the rate of decay of the singular values the more ill-conditioned the problem.

Based upon this rationale, it would seem that this problem is relatively well conditioned as the initial sequence of singular values has a slow rate of decay. Listed

next to each of the diagrams of Figs. 3.2 and 3.3 is the singular value ratio μ_r/μ_1. For this problem, this ratio is rather large and is typically of the order of 10^{-1}. As r is rather large and is close to the total number of singular values, this large singular value ratio demonstrates that the singular values do indeed fall off at a very slow rate for the linear region. From a practical point of view this problem may be considered to be reasonably well conditioned.

Chapter 4

Test Results

4.1 General

In this chapter, the inversion algorithm is tested. The principal source of data which will be used to test this algorithm are the 25.4 MHz dual-radar observations collected during the 1986 Canadian Atlantic Storms Program (CASP). The "groundtruth" information for this experiment is provided by a WAVEC directional wave buoy.

With this data set, the algorithm can be tested for both single and dual-radar usage. The angular separation between the two receive beams at CASP is 56^{o}. Some of the results presented here from CASP have already appeared in Howell and Walsh (1988, 1989).

The CASP data set also provides the opportunity to test the various models for the second order cross section to see which better fits the measured data. This will be done by comparing the inversion results for each model to the WAVEC's estimate for the wave spectrum to see which model provides the best agreement. For convenience, the mutually agreeing Barrick and Lipa (1986) and Srivastava (1984) models shall be collectively referred to from this point as simply the BL/S model. Likewise, the Walsh and Howell (1990) model shall be referred to as the WII model.

Another means by which the algorithm will be tested is to use simulated radar data. The model for the wave spectrum used to create this simulated data is that of a

Pierson-Moskowitz (1964) spectrum multiplied by a cardioid directional distribution function (Longuet-Higgins et al., 1963).

Although measured radar data is preferred for analysis, the use of simulated data in addition to the CASP data set will provide a more comprehensive test of the inversion algorithm. Specifically, it is desired from these simulation tests to:

1. Examine the accuracy of the dual-radar inversion for angular separations between receive beams other than 56°.

2. Confirm some of the trends observed in the inversion solution at CASP. Of particular interest is the apparent linear dependence on wave direction for the accuracy of $e(f)$ estimates made by a single radar.

3. Assess the effects of using only the first five Fourier coefficients in performing the inversion.

All simulation tests presented here were made using the BL/S second order model. It is not necessary to present the simulation results for the closely related WH model as these results are virtually identical to that obtained using the other models. This is not to say however that the WH model is indistinguishable from the other two. Quite the contrary, it is only logical that these results should be so similar since if a set of data was created using one theory and inverted using the same theory, then all that was tested was the inversion algorithm. Hence, all that can be expected from these simulation tests is to examine the properties of the algorithm.

The operating frequency at which these simulation tests will be performed is the same as the CASP operating frequency of 25.4 MHz. To better compare with the CASP inversion results, the values assigned to the Doppler resolution of the radar spectrum, Δu, and the number of ocean frequency bands, J, will also be the same as that used for the CASP data. These values are: $\Delta u = 7.245 \times 10^{-3}$ (hence, $J = 30$);

and $J = 30$. If only two sidebands are available when processing the data of a single radar, J will be set to 15.

For an operating frequency of 25.4 MHz, wave information can be measured using the algorithm for the frequency range 0.07 to 0.25 Hz. The frequency resolution of the radar estimated wave spectrum is 0.006 Hz for $J = 30$ and 0.012 Hz for $J = 15$.

In general, the properties and accuracy of the inversion solution remains constant over the upper extent of the HF band ($\approx$ 20 to 30 MHz). Although the proposed inversion algorithm may be applied for lower operating frequencies if the sea state is sufficiently high to satisfy the linearization assumption of saturation, the main focus of this chapter will be on high HF frequencies. The inversion of the integral equation for lower operating frequencies is, in fact, a different problem than the one addressed here, since a different linearization technique is required and third order effects will probably have to be accounted for. It is a future goal, however, to generalize the inversion technique for a greater range of radar frequencies.

Prior to examining the inversion results, some background information is required on how the measured Fourier coefficients are interpreted to yield directional information and several important statistical parameters. In this thesis, directional information is interpreted from these coefficients by fitting them to the parameters of the cardioid directional distribution model. This same model was used to interpret the five Fourier coefficients provided by the WAVEC buoy. A short description of this model is provided here.

4.2 Interpretation of Ocean Spectral Parameters from the Measured Fourier Coefficients

4.2.1 Definition of Common Statistical Parameters

For many applications, the information required from measured wave data corresponds to a few statistical parameters that summarize the properties of the wave

spectrum. The most important parameter of this set has already been introduced, i.e., rms waveheight, h. For many, h is the essence of sea state.

Although the most important statistical descriptor of the ocean spectrum is its rms waveheight, it is more common to describe the wave spectrum in terms of its *significant waveheight*, h_s, instead. Significant waveheight is defined in terms of rms waveheight as

$$h_s^2 = (4h)^2 = 4^2 \int_0^\infty e(f)\, df \tag{4.1}$$

The Fourier coefficient $a_0(f)$ is directly related to $e(f)$ by (3.7). Physically, significant waveheight is a close approximation to the wave heights estimated by trained observers at sea.

In order to provide a better comparison between all sensors at CASP, h_s will be calculated in this thesis using the frequency range 0.07 to 0.25 Hz. Since most of the ocean spectral energy will be contained in this range the difference between the values of h_s calculated here and the "full range" values will be only on the order of a few percent.

Other parameters of interest include: peak frequency (f_p); and dominant direction (θ_d). f_p is simply the value of ocean frequency at which $e(f)$ is maximum. θ_d is defined here as the direction of maximum energy propagation for the wave spectrum. The value of θ which achieves this will be the one which results in a maximum value for the integral

$$\int_0^\infty e(f,\theta)\, df$$

where $c(f,\theta)$ will be approximated here by its first five Fourier terms only.

4.2.2 The Cardioid Model for the Directional Distribution of Ocean Waves

A currently popular model for the ocean wave spectrum is to express it as the product of its 1-D spectrum $e(f)$ and a directional factor $g(\theta)$:

$$e(f,\theta) = e(f)g(\theta) \tag{4.2}$$

In writing the above the assumption of separability has been made so that $e(f)$ and $g(\theta)$ can be treated as independent quantities.

A parametric model for $g(\theta)$, originally proposed by Longuet-Higgins et al. (1963), has the form

$$g(\theta) = A(s)\left|\cos\left(\frac{\theta-\bar{\theta}}{2}\right)\right|^{2s} \tag{4.3}$$

where the parameter s is called the *spreading function* and $\bar{\theta}$ is called the *mean wave direction.* Both s and $\bar{\theta}$ are functions of frequency. $A(s)$ is a normalization factor such that

$$\int_0^{2\pi} g(\theta)\,d\theta = 1$$

This normalization criterion will be satisfied if

$$A(s) = \frac{\Gamma(s+1/2)}{2\sqrt{\pi}\Gamma(s+1)} \tag{4.4}$$

where Γ is the gamma function.

As the above expression for $g(\theta)$ is similar to a cardioid function it is commonly referred to as the *cardioid directional distribution model.* In general, this symmetric model will provide a good fit to actual wave spectra. However, this model may not accurately represent frequency components that are multi-modal in direction or are highly directive (e.g., swell).

An appealing feature of this model is that each parameter has an immediate physical interpretation. The mean direction parameter $\bar{\theta}$ represents the direction of maximum energy propagation for each frequency. The directional distribution will

be symmetric about this direction. The spreading function s determines the width of this distribution. For large s this distribution is narrow and concentrated. For small s this distribution is wide and diffuse.

Another common representation for the width of the cardioid model is its *half-power beamwidth* $\Delta\theta$. By definition, $\Delta\theta$ is simply the half-power width of the distribution. It is related to the spreading function s as

$$s = \frac{\ln(0.5)}{2\ln(\cos(\Delta\theta)/4)} \tag{4.5}$$

In many ways, $\Delta\theta$ is a more meaningful physical parameter than s as it provides a direct measure of the angular width of the distribution.

An estimate for the cardioid parameters s and $\overline{\theta}$ may be obtained from the wave spectrum's Fourier coefficients. Based upon (3.3) and (4.2), it is simple to show that the relationship between these parameters and the Fourier coefficients is

$$\frac{a_n(f)}{a_0(f)} = \frac{s(s-1)\cdots(s-n+1)}{2(s+1)(s+2)\cdots(s+n)}\cos(n\overline{\theta}) \tag{4.6}$$

$$\frac{b_n(f)}{a_0(f)} = \frac{s(s-1)\cdots(s-n+1)}{2(s+1)(s+2)\cdots(s+n)}\sin(n\overline{\theta}) \tag{4.7}$$

In this thesis, the cardioid parameters are interpreted from the Fourier coefficients by performing a least squares fit to the set of four nonlinear equations corresponding to the above for both $n = 1$ and 2.

4.3 Results Using Simulated Data

4.3.1 Data Simulation

For the purpose of creating simulated data to test the inversion algorithm, the wave spectrum will be represented by (4.2) with $g(\theta)$ being represented by (4.3). For simplicity, $g(\theta)$ will be modelled as being the same for all frequencies. Therefore, only one value of $\overline{\theta}$ and s need be taken to represent the spectrum. This simple model for

the wave spectrum will be adequate to demonstrate some of the basic properties of both the inversion algorithm and the radar spectrum.

To complete the description of the wave spectrum, a model is required to represent the 1-D wave spectrum $e(f)$. Based upon observed wave spectra, Pierson and Moskowitz (1964) proposed the following form for $e(f)$ for the case of a fully developed sea with no swell:

$$e(f) = 2\pi\ C_p g^2 \omega^{-5} \exp\left[-0.74\left(\frac{g}{\omega U_w}\right)^4\right] \tag{4.8}$$

where U_w represents the wind speed 19.5 m above the ocean surface and C_p is an experimentally determined dimensionless constant. In this thesis, 0.0081 will be used for C_p (see Earle and Bishop, 1984).

This model for $e(f)$ has become widely accepted as a reasonable approximation to the limiting spectrum of a simple wind-driven sea (Hasselmann et al., 1976). It may be observed for the high frequency limit of this model that the spectrum will essentially have an ω^{-5} dependence. This agrees with Phillips (1966) finding for the characteristic falloff of saturated ocean waves.

Using these parametric models for the wave spectrum as input into (2.15) and (2.33), simulated first and second order radar data may be calculated. For the purpose of inversion, the second order spectrum calculated using (2.33) must be divided by the first order power calculated using (2.15).

As mentioned before, these simulation tests will be performed using the BL/S second order model. For the purpose of exploring the properties of the inversion algorithm, it matters little which of these closely related theories are used to create the data so long as the inversion algorithm uses the same theory to interpret it. Hence, the results presented here will be very much the same for all cross section models.

4.3.2 Results Using One Radar

Prior to analysing the results for one radar, it is worthwhile to first examine the symmetry existing between some of the simulated radar spectra to be treated here. As $g(\theta)$ for the simulation tests has been modelled as being the same for all frequencies, the dominant direction of the wavefield, θ_d, will be equivalent to $\overline{\theta}$.

One such important symmetry is that the simulated radar spectrum will be the same for wavefield directions $\pm\theta_d$. This property is a direct result of the fact that (2.41) folds the wave spectrum about the radar beam, i.e., the radar spectrum depends only upon the even Fourier terms of the ocean wave expansion. Since the wave spectra corresponding to these two wavefield directions are identical after folding about the radar beam, the resulting radar spectra will be identical as well.

Another important symmetry is the mirror symmetry that exists between simulated radar spectra for wavefield directions θ_d and $\theta_d + \pi$. For this case, it is intuitively obvious that these radar Doppler spectra will be mirror images of one another since their corresponding wave spectra are also mirror images.

Due to these two symmetries, inversion results will also demonstrate symmetry. Of particular interest is the symmetry of estimates for the $a_o(f)$ Fourier coefficient that exist for $\pm\theta_d$ and $\pm\theta_d + \pi$. These four different wavefield directions have one important property in common, i.e., they all have the same angle of intersection with the radar beam. This angle of intersection shall be referred to here as the *wave crossing angle*. The symbol ϕ_c shall be used to describe it.

Shown in Fig. 4.1 are the inversion results for $c(f)$ corresponding to a single 25.4 MHz radar for $U_w = 30$ knots, $s = 2$, and $\phi_c = 0^o$, 30^o, 60^o, and 90^o. Recall that $e(f)$ is directly proportional to $a_o(f)$ by (3.7). A similar set of test results are shown in Fig. 4.2 for $s = 4$.

It should be mentioned that the inversion performed for the $\phi_c = 0^o$ case for both Figs. 4.1 and 4.2 used only two sidebands. This was done to reflect actual operating

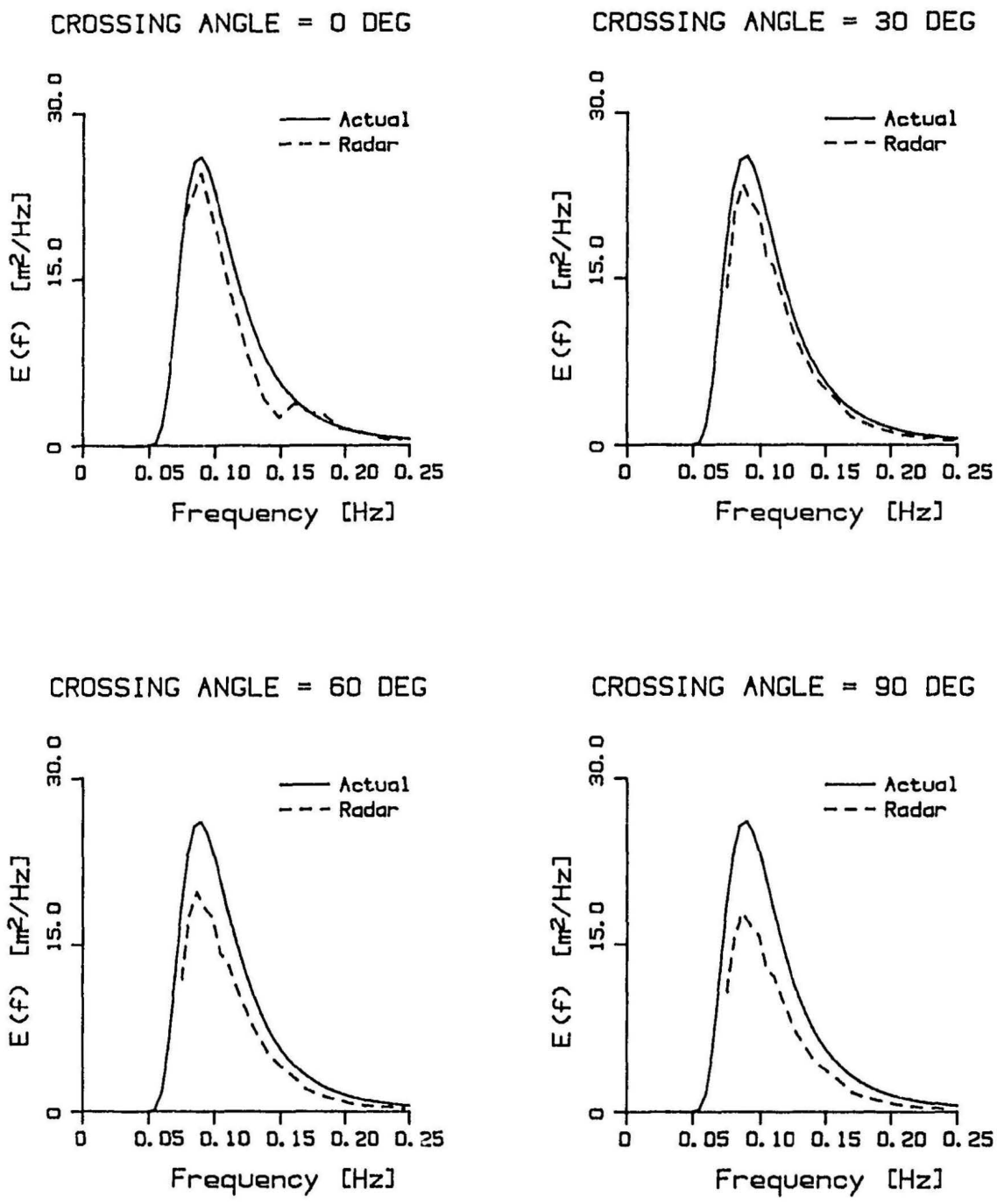

Figure 4.1: Single radar inversion solution for $e(f)$ obtained from simulated 25.4 MHz radar data for $\phi_c = [0°, 30°, 60°, \text{and } 90°]$, $U_w = 30$ knots, and $s = 2$.

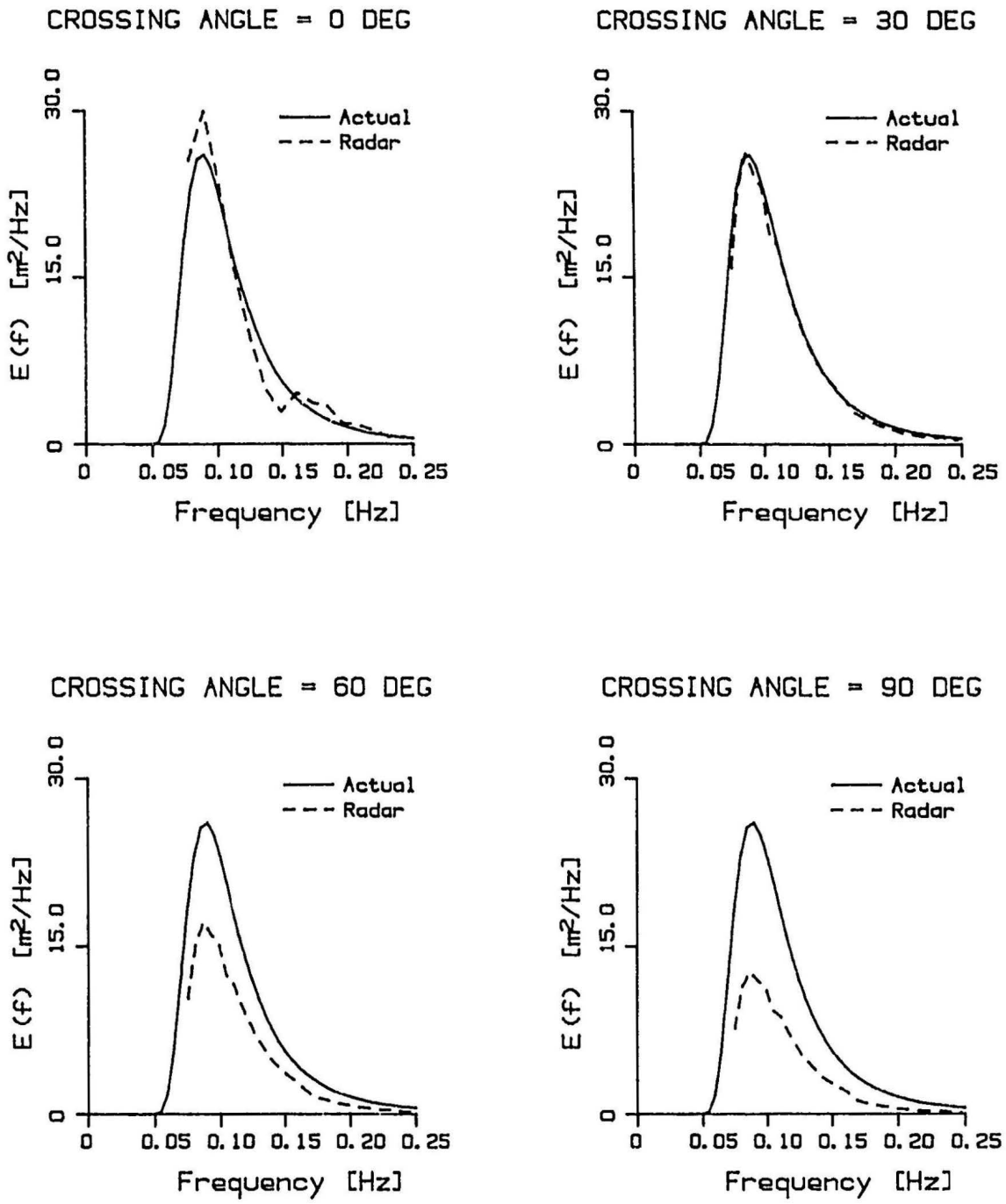

Figure 4.2: Single radar inversion solution for $e(f)$ obtained from simulated 25.4 MHz radar data for ϕ_c = [0°, 30°, 60°, and 90°], U_w = 30 knots, and $s = 4$.

conditions as one-half of the radar spectrum for Bragg wave directions close to zero or 180° will lie at such a low level that it will be likely buried in noise. As only two sidebands are used, the accuracy of the inversion should lessen somewhat. It may be observed from Figs. 4.1 and 4.2 that although the inversion solution compares well with the original data for $\phi_c = 0°$, the shape of this estimated spectrum substantially differs from the actual spectrum in comparison to the inversion results for other wave directions.

It may also be observed from Figs. 4.1 and 4.2 that the accuracy of estimates for $c(f)$ made by a single radar will vary substantially depending upon the directional distribution. In general, the best results are achieved when most of the wave energy is concentrated along the radar beam but becomes progressively underestimated as a greater percentage of the wave energy is distributed about the orthogonal to the beam. Although the overall scale of the estimate for $c(f)$ spectrum varies considerably, its basic shape is preserved.

The physical cause for this behaviour was outlined in section 2.6. Due to the properties of the integral equation's kernel function C, a narrow beam radar will be weakly coupled to those wave components travelling in directions distributed about the perpendicular to the beam. Since the radar is largely unaware of these waves it will tend to underpredict the total wave energy.

Two wave spectrum parameters affect this variation in accuracy. The most obvious of these is the mean direction parameter $\overline{\theta}$. This parameter represents the orientation of the directional distribution and is the most responsible for controlling the accuracy of $c(f)$ estimates. To a lesser but still appreciable extent, the spread parameter s also influences this accuracy. This parameter determines how concentrated the directional distribution is about $\overline{\theta}$. From comparison of the $\phi_c = 90°$ cases of Figs. 4.1 and 4.2 it may be observed that Fig. 4.1 with its lower value of s, and hence wider distribution, provides the better estimate for $c(f)$. With this wider distribution, less energy will

be distributed about the orthogonal to the radar beam while more will travel along the beam. A better estimate for the spectrum may then be obtained.

The width of the distribution as determined by the parameter s affects the accuracy of the inversion in another way. From comparison of the $\phi_c = 0^o$ cases of Figs. 4.1 and 4.2 it may be observed that the total wave energy estimated for the $s = 2$ case is comparable to that of the true spectrum but is overpredicted for the $s = 4$ case. A possible explanation for this effect is the simple fact the inversion was performed with the wave spectrum approximated by its first five Fourier terms only. For a cardioid distribution with $s = 2$ the Fourier series expansion for the wave spectrum will have exactly five non-zero terms (see (4.6)and (4.7)). For $s = 4$ the expansion has exactly nine such terms. Since the inversion has tried to fit five Fourier terms to the data where in fact nine are required, it will tend to produce less accurate estimates for these five coefficients with overprediction taking place for the $a_0(f)$ coefficient. This overprediction should increase as the directional distribution narrows.

Further insight into the behaviour of the single radar inversion solution for $e(f)$ may be obtained if the percentage error of h_s estimates are plotted against ϕ_c. These plots for both $s = 2$ and $s = 4$ are shown respectively in Figs. 4.3 and 4.4. Both of these error plots demonstrate the properties of the solution determined thus far, i.e., the accuracy of h_s estimates inversely depend upon ϕ_c with this inverse dependence becoming stronger with increasing s. However, these plots demonstrate the startling result that this dependence is strongly linear. The $\phi_c = 0^o$ case was not included in the regression fit for these plots as it was generated using only two sidebands while the other results used four.

This linear trend for the accuracy of the inversion suggests the possibility that the estimate for $e(f)$ may be empirically "corrected" to give it the proper scale with knowledge of the directional distribution of the wave spectrum. This would require

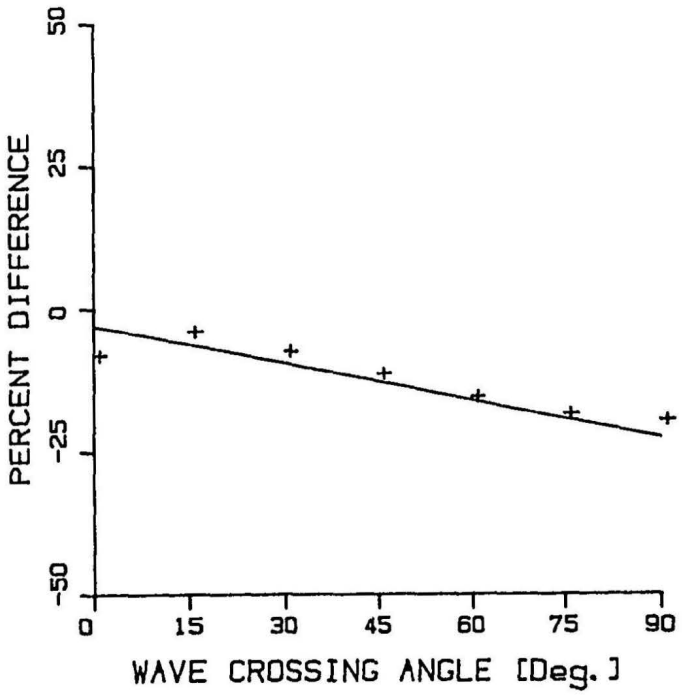

Figure 4.3: Plot of the percentage error of h_s estimates made by a single radar versus ϕ_c for the $s = 2$ simulation tests of Fig. 4.1. Also shown is the linear regression fit to these error values with the exclusion of the $\phi_c = 0$ case. The correlation coefficient of this fit is -0.99.

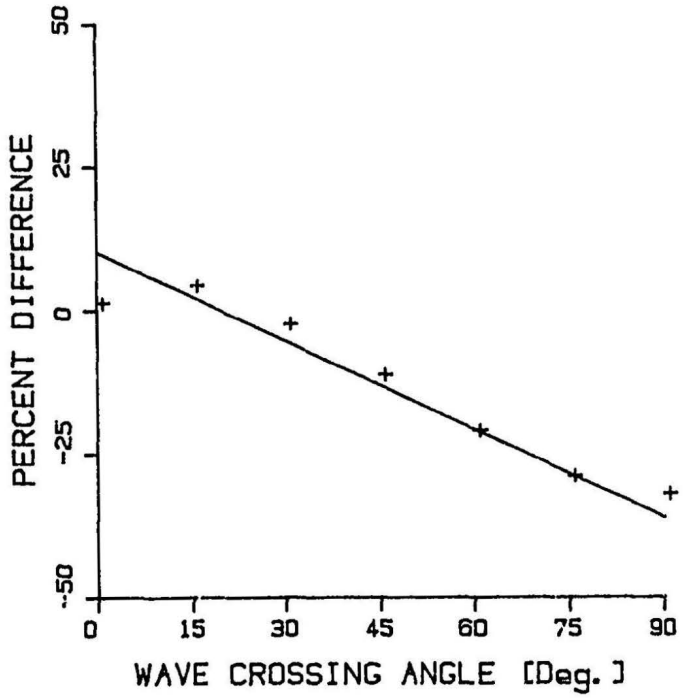

Figure 4.4: Plot of the percentage error of h_s estimates made by a single radar versus ϕ_c for the $s = 4$ simulation tests of Fig. 4.2. Also shown is the linear regression fit to these error values with the exclusion of the $\phi_c = 0$ case. The correlation coefficient of this fit is -0.99.

the extraction of detailed directional information from the inversion results. It is not required to resolve the left/right ambiguity for estimates of $\overline{\theta}$ inherent to a single radar as the parameter ϕ_c is unaffected by this ambiguity.

The extraction of directional information from a single radar is a difficult task. One aspect of this problem is that the only data available to determine the cardioid parameters are the even Fourier coefficients. For many situations, several equally valid solutions to (4.6) are possible when fitting these coefficients to this equation. For example, there is virtually no difference for the values of the even Fourier coefficients resulting from a cardioid distribution with $\overline{\theta} = \pm 19.5^o$ and $s = 1$ as for $\overline{\theta} = \pm 45^o$ and $s = 2$. In other words, the directional distribution represented by these two cases is indistinguishable if it is folded.

Another more important problem is that the accuracy of the "directional" Fourier coefficients $a_1(f)$ and $a_2(f)$ will probably be much less than the $a_o(f)$ coefficient. This is due to the fact that the radar is really only aware of those wave components travelling in directions distributed about the beam. This will introduce a bias into the inversion solution for these coefficients as they are dependent upon the behaviour of the wave spectrum over all directions.

Based upon these two problems, it is expected that, in general, the accuracy of cardioid parameter estimates using a single radar will be poor. Thus far, parameter estimates obtained from a least squares fit of the even coefficients to (4.6) have indeed been poor. These results will not be presented here.

It may be possible that more elaborate techniques can be developed to better interpret directional information from the measured even Fourier coefficients. This problem will not be considered in this thesis.

For all the 25.4 MHz cases shown thus far, the wind speed parameter for the Pierson-Moskowitz spectrum was selected to be 30 knots. In general, the properties and accuracy of the inversion for a single radar is independent of the total energy of

the wave spectrum with the exception of low sea states (wind speeds of 10 knots or less). It is worthwhile to note that the error plots shown in Figs. 4.3 and 4.4 are very much the same for all wind speeds.

For low sea states, the assumption of saturation for the Bragg waves used to linearize the integral equation is no longer appropriate. This does not represent a limitation of the inversion algorithm as there is little interest to perform measurements for such cases. In any event, it may not be possible to process the radar spectrum resulting from such low sea states as it will have a very low signal-to-noise ratio.

4.3.3 Results Using Two Radars

Shown in Fig. 4.5 are the dual-radar inversion results for $e(f, \theta)$ obtained from 25.4 MHz simulated data for $2\phi = 60°$, $U_w = 30$ knots, various wave directions relative to the bisector, and $s = 2$. A similar set of test results are shown in Fig. 4.6 for $s = 4$.

Overall, the inversion results presented in Figs. 4.5 and 4.6 are very good. This demonstrates the increased accuracy that two radars may provide. The use of two radars also eliminates the left/right ambiguity of wave direction estimates inherent to a single radar. This is confirmed by the successful estimation of $\overline{\vartheta}$ over frequency for all cases shown.

The estimate for $e(f)$ also corresponds well with the true spectrum. Several properties of the inversion solution for this parameter are evident in Figs. 4.5 and 4.6. One such property is that the accuracy of estimates for $e(f)$ will depend upon the number of Fourier coefficients that is employed to represent the wave spectrum. Like the single radar inversion, the best results are obtained for the $s = 2$ case (Fig. 4.5) as the wave spectrum will contain exactly five coefficients. The $s = 4$ case (Fig. 4.6), however, requires more coefficients to represent the spectrum. Consequently, over-prediction occurs for wave directions along the bisector.

Another important property of the dual-radar inversion solution for $e(f)$ is that the

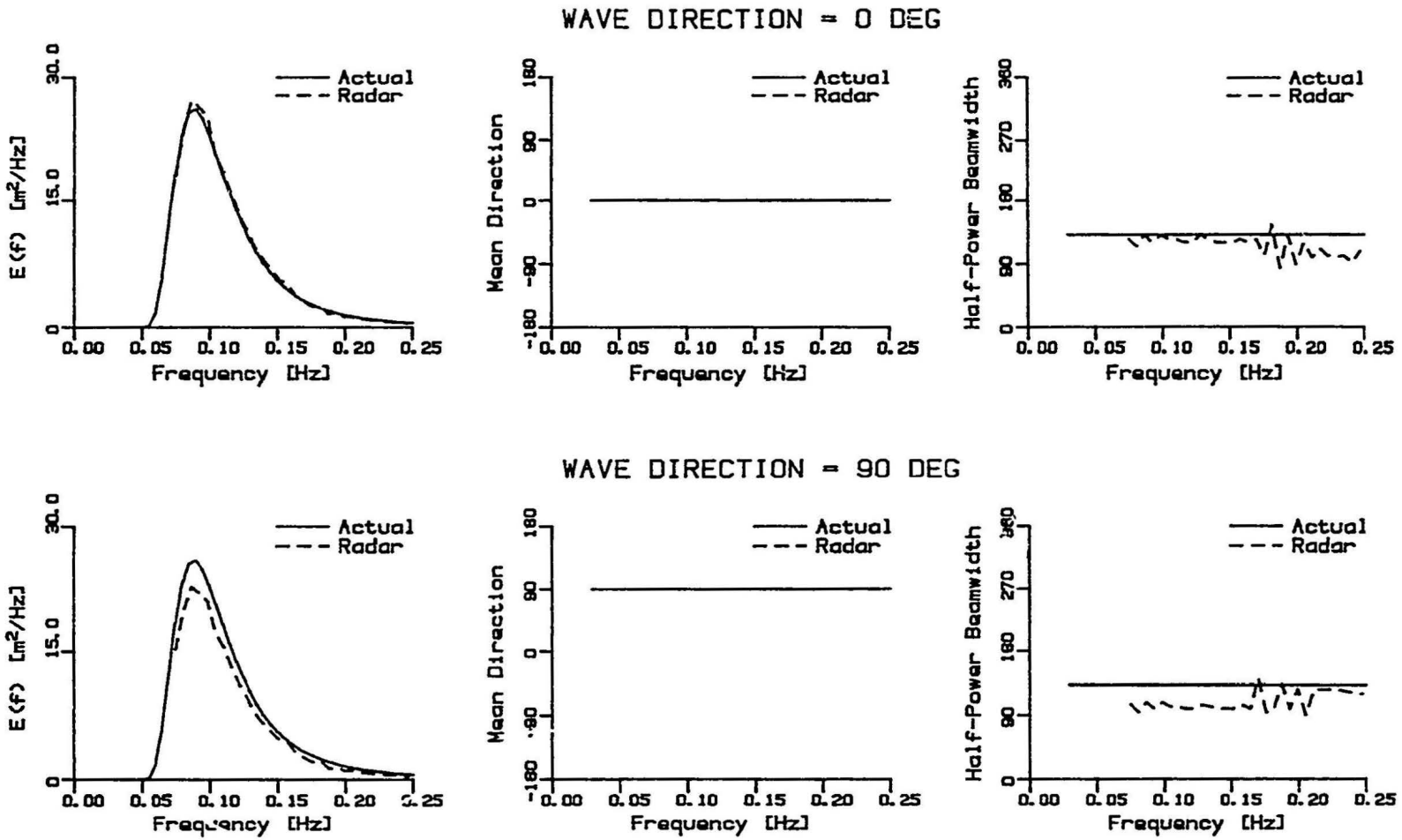

Figure 4.5: Dual-radar inversion solution for $e(f, \theta)$ obtained from simulated 25.4 MHz radar data with $2\phi = 60°$, $U_w = 30$ knots, and $s = 2$.

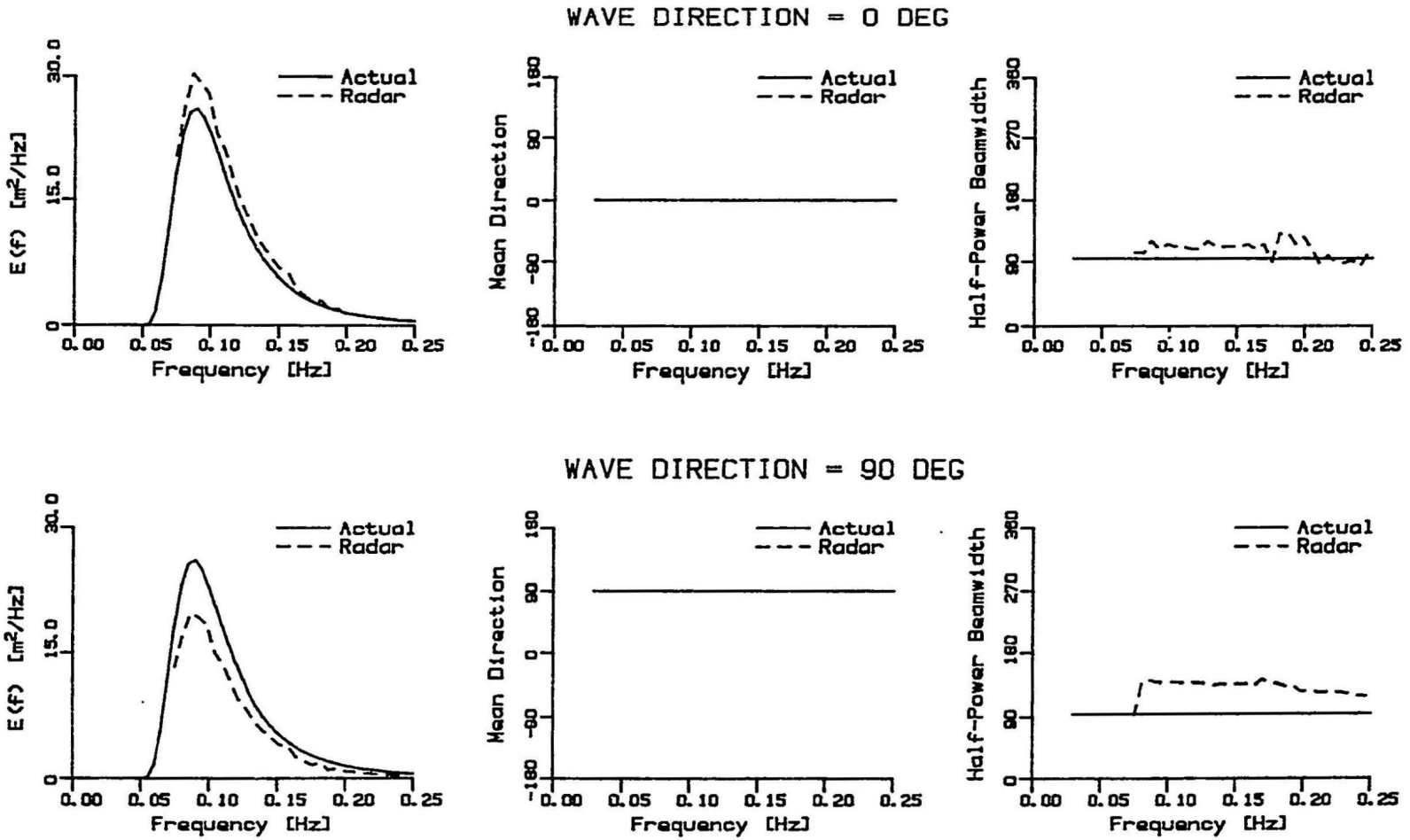

Figure 4.6: Dual-radar inversion solution for $e(f, \theta)$ obtained from simulated 25.4 MHz radar data with $2\phi = 60°$, $U_w = 30$ knots, and $s = 4$.

accuracy of this solution will moderately depend upon the orientation of the wavefield with respect to the bisector. This is simply due to the fact that although two radars separated by 60° can monitor wave energy travelling over an extensive range of wave directions, this information is still incomplete. The best results are obtained when the wavefield is travelling along the bisector. Both radars will then be highly sensitive to the bulk of the total wave energy. However, progressive underestimation occurs as the wavefield direction approaches orthogonality to the bisector. This underestimation increases for increasing s.

The dependence upon the orientation of the wavefield for inversion results is substantially reduced if the two radar beams are orthogonal to one another. On the other hand, this problem worsens as the angular separation between beams decrease. In general, the inversion will still display a high degree of accuracy if the angular separation is 40° or more. For angles less than this the accuracy of the inversion descends rapidly. It is recommended for practical measurements using two radars that the angular separation between beams should be as close as possible to 90° but not less than 40°.

In general, the estimates for $\Delta\theta$ using two radars are good. The accuracy of this parameter depends upon the number of Fourier coefficients used to represent the wave spectrum. For the $s = 2$ case (Fig. 4.5) the beamwidth parameter is well estimated since the wave spectrum can be represented by exactly five coefficients. For the $s = 4$ case (Fig. 4.6) more coefficients are required and as a result the directional distribution is estimated to be wider than it actually is.

As with the single radar results, the general properties of the inversion solution presented here apply over a large range of sea states. Low sea states are excluded however, as they violate the assumptions used to linearize the integral equation.

4.4 Results Using Data from CASP

4.4.1 Introduction

During the winter of 1986, two narrow-beam ground wave radars were deployed on the coast of Nova Scotia, Canada as part of the Canadian Atlantic Storms Program (CASP). Each of these pulse Doppler radars were operated at 25.4 MHz and were equipped with a 3-element Yagi antenna for transmission and a 12-element linear array with three-quarter wavelength spacing for reception. The half-power beamwidth of each receive beam was 6°. Both beams were aimed such that they intersected at the location of a WAVEC directional wave buoy. The angular separation between receive beams was 56°.

The position of all sensors as well as the coverage provided by each receive beam out to a range of 40 km is shown in Fig. 4.7. In this diagram, the receive beams are shown to be divided over range into uniform lengths of 1.2 km. These "cells" represent distinct areas of the ocean surface for which wave measurements are performed.

In this experiment, eight sets of approximately $2\frac{1}{2}$ hour long dual-radar observations were collected over a 10 day period from March 19 to March 28, 1986. For those periods within this time frame that the radars operated, the WAVEC estimated the significant waveheight to have varied between 1.28 and 4.32 metres. In all, a good range of sea states were collected.

The inversion algorithm to be applied to the CASP radar data is identical to that used in the preceding section to process simulated data. The only change made was to set the water depth to the CASP value of 50 m. The Doppler resolution of the CASP data as well as the number of frequency bands used to perform the inversion are given in section 4.1.

As before, wave information is collected for the frequency range 0.07 to 0.25 Hz. The frequency resolution for most of the wave data is 0.006 Hz. This is comparable to the WAVEC resolution of 0.005 Hz. For those single radar cases where the data of

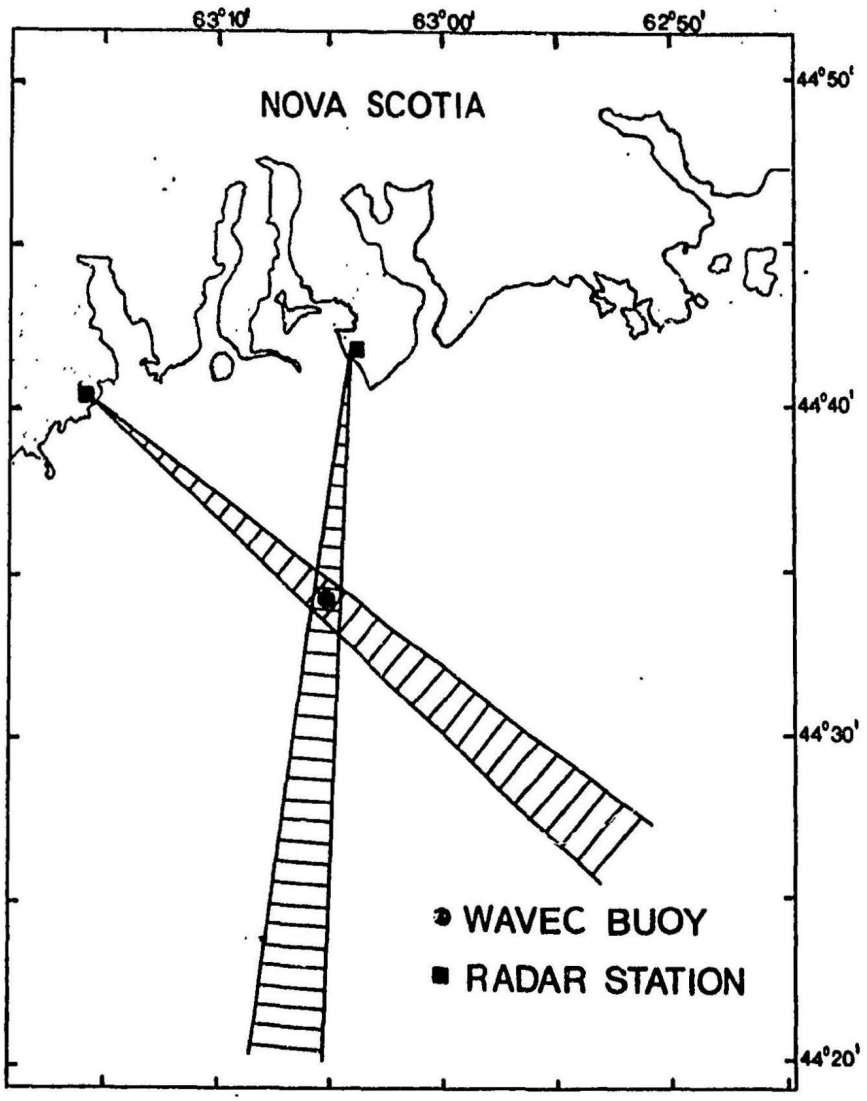

Figure 4.7: Diagram of the 1986 CASP experiment site. Also shown is the coverage provided by the 6° receive beam of each radar after division into 1.2 km long "range cells".

only two sidebands were available, the frequency resolution was set to 0.012 Hz.

4.4.2 Results Using the Barrick and Lipa/Srivastava Model

Shown in Fig. 4.8 is a comparison of CASP wave spectra estimates obtained from the WAVEC buoy and the narrow beam radars. The radar inversion results were generated using the BL/S model for the second order cross section. Radar estimates include the 1-D spectrum $e(f)$ (for both one and two radars) and the cardioid directional distribution parameters of $\overline{\theta}$ and $\Delta\theta$ (two radars only).

From Fig. 4.8 it may be observed that the general behaviour of CASP dual-radar estimates for $e(f)$, in comparison to those of the WAVEC, corresponds to that of simulated data. When using the data of two radars very good correspondence with the buoy's estimate for $e(f)$ exists. For dual-radar estimates made on March 20 (both sets), 21, 24, 27, and 28 there is little difference from the buoy for $e(f)$ estimates. Some noticeable differences arise however, for such days as March 19 and 26. For these cases the radars predict a much broader 1-D spectrum than the buoy and as a result there is a wide disparity between the overall height of the spectral peak. However, the total energy of the spectrum and the location of the spectral peak is consistent with the buoy's estimate.

The general behaviour of single radar estimates for $e(f)$ also corresponds to what was expected from the simulation tests. From Fig. 4.8 it may be observed that the chief difference between the waveheight spectrum estimated by each radar and the buoy is not one of shape, but rather of scale. In general, the shape of the 1-D spectrum predicted by each radar is consistent with that predicted using both radars and the buoy. Upon closer examination of these spectra it may be seen that changes in the overall energy levels of the spectrum varies inversely with the wave crossing angle ϕ_c.

The cardioid directional distribution parameters of $\overline{\theta}$ and $\Delta\theta$, estimated using two radars, also demonstrates good agreement with the buoy. From Fig. 4.8 it may be

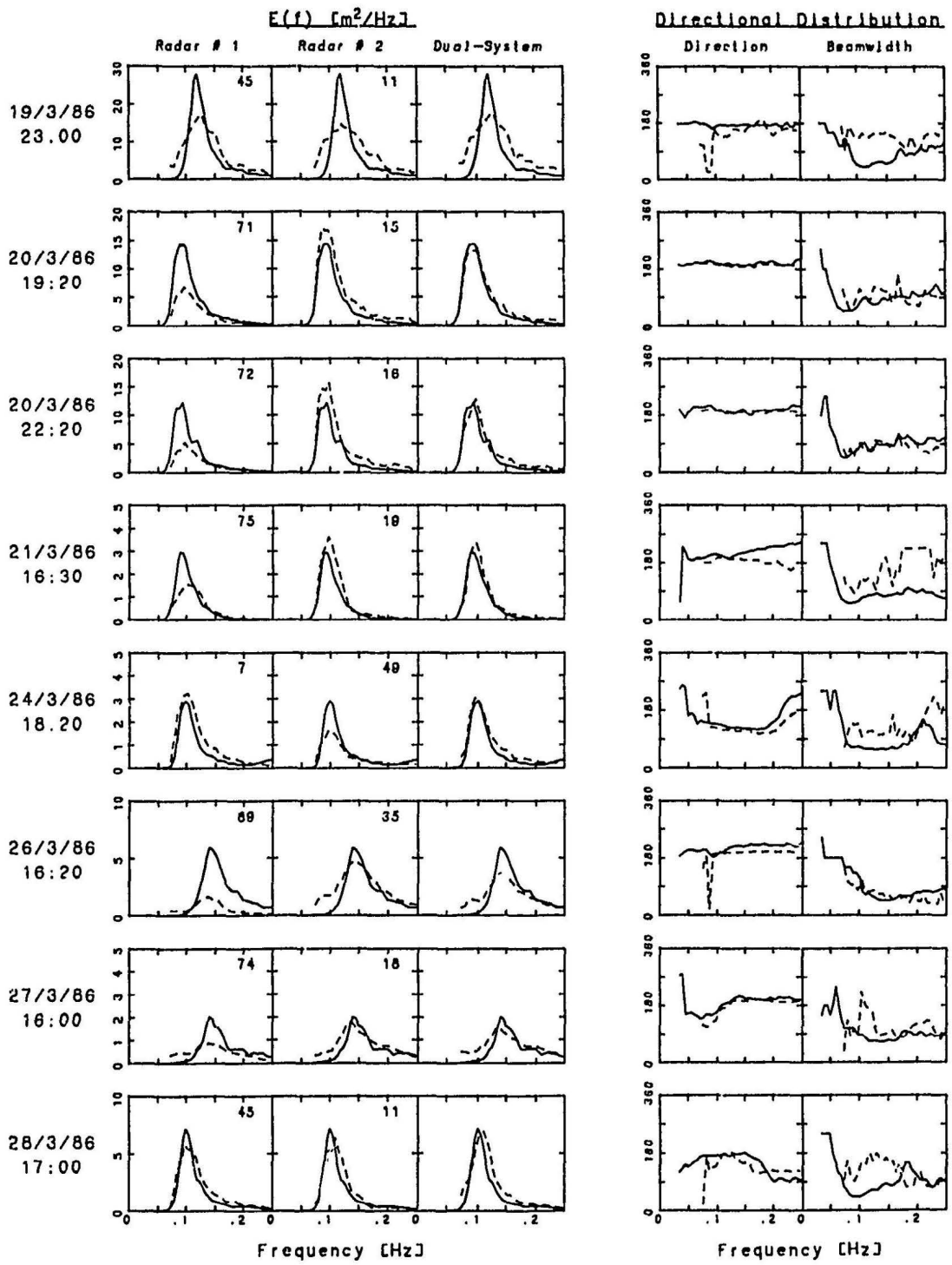

Figure 4.8: Comparison of radar measured wave spectra at CASP (dotted line) using the Barrick and Lipa/Srivastava model with those of the WAVEC buoy (solid line). Separate estimates for $e(f)$ are presented for measurements made by each radar alone and in combination. Radar estimates of the cardioid directional distribution parameters have been made using two radars only. The number appearing in upper right hand corner of single radar estimates for $e(f)$ is ϕ_c. The date and start time (GMT) of each approximately 2.5 hour long observation is indicated on the left.

observed that dual-radar estimates of $\bar{\theta}$ for all cases closely matches that made by the buoy.

Although the comparison of dual-radar estimates of $\Delta\theta$ with the buoy is good overall, this agreement is not consistent. For cases such as March 20 (both sets) and 26 there is close agreement with the buoy for this parameter. On the other hand, for cases such as March 19, 21, and 28 the radar predicts the directional distribution to be much broader than that estimated by the buoy. For the other cases of March 24 and 27 there is reasonable agreement with the buoy for $\Delta\theta$ estimates.

As well as comparing the overall wave spectrum, it will also be useful to compare some of its main statistical parameters. By comparing such parameters, it will be possible to quantify some of the important differences between each sensor's wave spectrum estimates.

Shown in Table 4.1 is a comparison of h_s and f_p estimates made by the buoy and a single radar using the BL/S second order theory. An estimate of ϕ_c for each radar as obtained from the buoy's estimate for θ_d is also presented in this table. The mean and standard deviation of absolute value differences from the buoy for both parameters is shown in Table 4.2.

From both Table 4.1 and Table 4.2 it may be seen that single radar estimates for f_p correspond well with the buoy. The average difference of 0.0048 Hz is reasonably low and is within the buoy's resolution of 0.005 Hz for the wave spectrum.

As expected, the accuracy of single radar estimates for h_s varies substantially. From Table 4.1 it may be observed that significant waveheight estimates are overestimated in comparison to the buoy for values of ϕ_c close to zero but progress to underestimation as ϕ_c approaches 90°. For the CASP data set and this second order model, the mean difference from the buoy (Table 4.2) for h_s estimates is 16.5% with a standard deviation of 10.2%. For many practical applications (e.g., marine forecasts) this level may be deemed acceptable and may already be more accurate then present

Table 4.1: Single radar (Barrick and Lipa/Srivastava model) and WAVEC buoy estimates for significant waveheight (h_s) and peak frequency (f_p) from CASP. Also shown is the wave crossing angle (ϕ_c).

	h_s (m)			f_p (Hz)			ϕ_c (deg)	
Date	Buoy	Radar 1	Radar 2	Buoy	Radar 1	Radar 2	Radar 1	Radar 2
3/19/86	4.24	4.48	4.58	0.120	0.128	0.122	45	11
3/20/86	3.33	2.40	3.88	0.095	0.098	0.086	71	15
3/20/86	2.93	2.08	3.54	0.095	0.098	0.098	72	16
3/21/86	1.37	1.18	1.58	0.090	0.101	0.098	75	19
3/24/86	1.43	1.68	1.22	0.100	0.104	0.098	7	49
3/26/86	2.34	1.30	2.64	0.140	0.140	0.146	89	35
3/27/86	1.36	1.17	1.53	0.140	0.140	0.134	74	18
3/28/86	2.11	2.27	2.19	0.100	0.098	0.110	45	11

Table 4.2: Statistical summary of absolute value differences from the buoy for single radar parameter estimates of Table 4.1.

	h_s	f_p
Mean	16.5 %	0.0048
Standard Deviation	10.2 %	0.0035

techniques (e.g., model predictions for wave heights using meteorological data as input). However, it is still desirable to improve the accuracy of single radar estimates for h_s.

A possible means of improving this accuracy was suggested from the simulation tests after studying the relationship between this accuracy and the directional distribution. Recall from these simulation tests (Figs. 4.3 and 4.4) that the accuracy of h_s estimates was found to have an linear inverse dependence upon ϕ_c with the slope of the line being determined by the width of the distribution. With knowledge of the directional distribution it may be possible to empirically "correct" the estimate for h_s. The problem of extracting the necessary directional information from the data of a single radar and how that data may be used to improve h_s will not be considered here.

To demonstrate that this property of the inversion solution also holds for actual radar observations, the percentage difference of radar derived h_s estimates from the buoy are plotted versus ϕ_c in Fig. 4.9. It may be seen from Fig. 4.9 that there is indeed a strong linear dependence upon ϕ_c for h_s estimates. This is evident from the high value of -0.895 for the correlation coefficient of the linear regression line.

In Fig. 4.9 there is a wide amount of variability about the regression line. This is due in part that the accuracy of h_s estimates also depend upon the width of the directional distribution of the wavefield. Another prominent effect is the statistical variability of estimates made by both the WAVEC buoy and the radars. Both the radar Doppler spectrum and the buoy motion spectrum are subject to statistical variability due to finite record lengths and the random nature of the wave field.

Another interesting feature about Fig. 4.9 is that the regression line has a value of 25% for $\phi_c = 0°$. Although the CASP data set is characterized by a narrow directional distribution for its most energetic frequency components, this amount of overestimation is more than was expected from the study of simulated data. From the

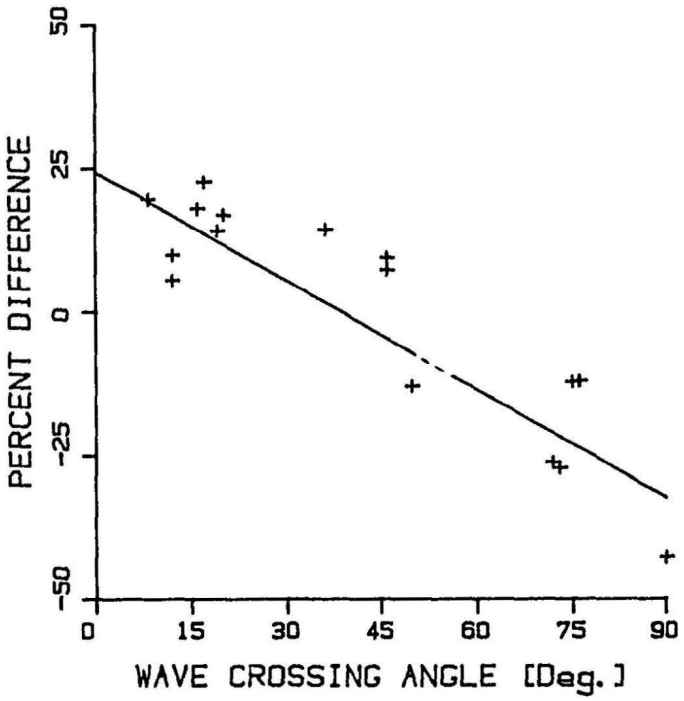

Figure 4.9: Plot of the percentage difference from the buoy versus ϕ_c for CASP single radar h_s estimates made using the Barrick and Lipa/Srivastava model. The correlation coefficient of the linear regression line is -0.895.

last section it was determined that for $s > 2$ the regression line should overestimate h_s at $\phi_c = 0$. In general, the upper limit for this overshoot is expected to be $\approx 10\%$. This was determined from simulated data tests for very large values of s. Although a value of 25% for $\phi_c = 0$ may only be an coincidence it may reflect upon the accuracy of the BL/S second order model. This property will be examined further when studying the inversion results for the WII second order model.

Shown in Table 4.3 is a comparison of h_s, f_p, and θ_d estimates from CASP made by the buoy and dual-radar system based upon the BL/S second order theory. The mean and standard deviation of absolute value differences from the buoy for all parameters is shown in Table 4.4.

The results presented in Tables 4.3 and 4.4 further demonstrate the increased accuracy that two radars may provide. Like the single radar results, the comparison of f_p estimates is very good. Estimates for θ_d are also well correlated with the buoy and have an average difference of only 13.75°. Perhaps the most dramatic result is the much improved accuracy for h_s estimates. The mean difference for this critical parameter is only 9.1% with a 3.5% standard deviation. This is a significant improvement over a single radar and it highlights the greater stability of dual-radar estimates for h_s with its much lower standard deviation value.

Overall, the test of the inversion algorithm using the BL/S model and the CASP data set has been largely successful. This is especially true for wave measurements made by two radars. For this case, wave measurements made by the radars and the WAVEC buoy have good correlation. Not only does this demonstrate that the inversion algorithm is an effective means of recovering wave data from the radar return, it also shows that the BL/S second order model provides a good fit to the radar spectrum.

Table 4.3: Dual-radar (Barrick and Lipa/Srivastava model) and WAVEC buoy estimates for significant waveheight (h_s), peak frequency (f_p), and dominant direction (θ_d) from CASP.

Date	h_s (m)		f_p (Hz)		θ_d (deg, T)	
	Buoy	Radar	Buoy	Radar	Buoy	Radar
3/19/86	4.24	4.84	0.120	0.128	171	153
3/20/86	3.33	3.48	0.095	0.098	199	193
3/20/86	2.93	3.12	0.095	0.098	201	194
3/21/86	1.37	1.48	0.090	0.098	203	188
3/24/86	1.43	1.60	0.100	0.098	132	123
3/26/86	2.34	2.24	0.140	0.140	218	198
3/27/86	1.36	1.48	0.140	0.134	201	188
3/28/86	2.11	2.40	0.100	0.110	173	151

Table 4.4: Statistical summary of absolute value differences from the buoy for dual-radar parameter estimates of Table 4.3.

	h_s	f_p	θ_d
Mean	9.1 %	0.005	13.75°
Standard Deviation	3.5 %	0.0035	6°

4.4.3 Results Using the Walsh and Howell Model

Shown in Fig. 4.10 is a comparison of CASP wave spectra estimates obtained from the WAVEC buoy and the dual-radar inversion algorithm for the WH second order model. Radar estimates include the 1-D spectrum $e(f)$ (for one and two radars) and the cardioid directional distribution parameters of $\overline{\theta}$ and $\Delta\theta$ (two radars only).

A comparison of the main statistical parameters describing the wave spectrum are shown in Tables 4.5 (one radar) and 4.7 (two radars). The mean and standard deviation of absolute value differences from the buoy for these parameters is shown in Tables 4.6 (one radar) and 4.8 (two radars).

From Fig. 4.10 it may be observed that many of the properties of of the inversion solution based upon the WH model is the same as that using the BL/S model. In fact, Fig. 4.10 is very similar to Fig. 4.8. However, there are several important differences between these two sets of inversion results.

One such difference is the better agreement with the buoy for h_s estimates generated using the WH model over that of the BL/S model. In general, the 1-D spectrum estimated by one or two radars using either model will be very similar (with the exception of the dual-radar case of March 19). However, the overall spectral energy predicted by the WH model better compares with the buoy than the other models. This is not readily apparent for single radar estimates of h_s (see Tables 4.5 and 4.6) as they are only slightly better than that of the other models (compare a mean difference of 14.4% with 16.5%). It is apparent from the dual-radar results (see Tables 4.7 and 4.8) that this new model provides better h_s estimates for almost all cases (compare a mean difference of 4.6% with 9.1%). The general accuracy of f_p estimates for all models is roughly the same.

One possible explanation for this better agreement for h_s estimates is the fact that the WH model predicts a slightly higher second order spectrum than the BL/S model (this is especially so for wave directions along the radar beam, i.e., $\phi_c = 0°$). As a

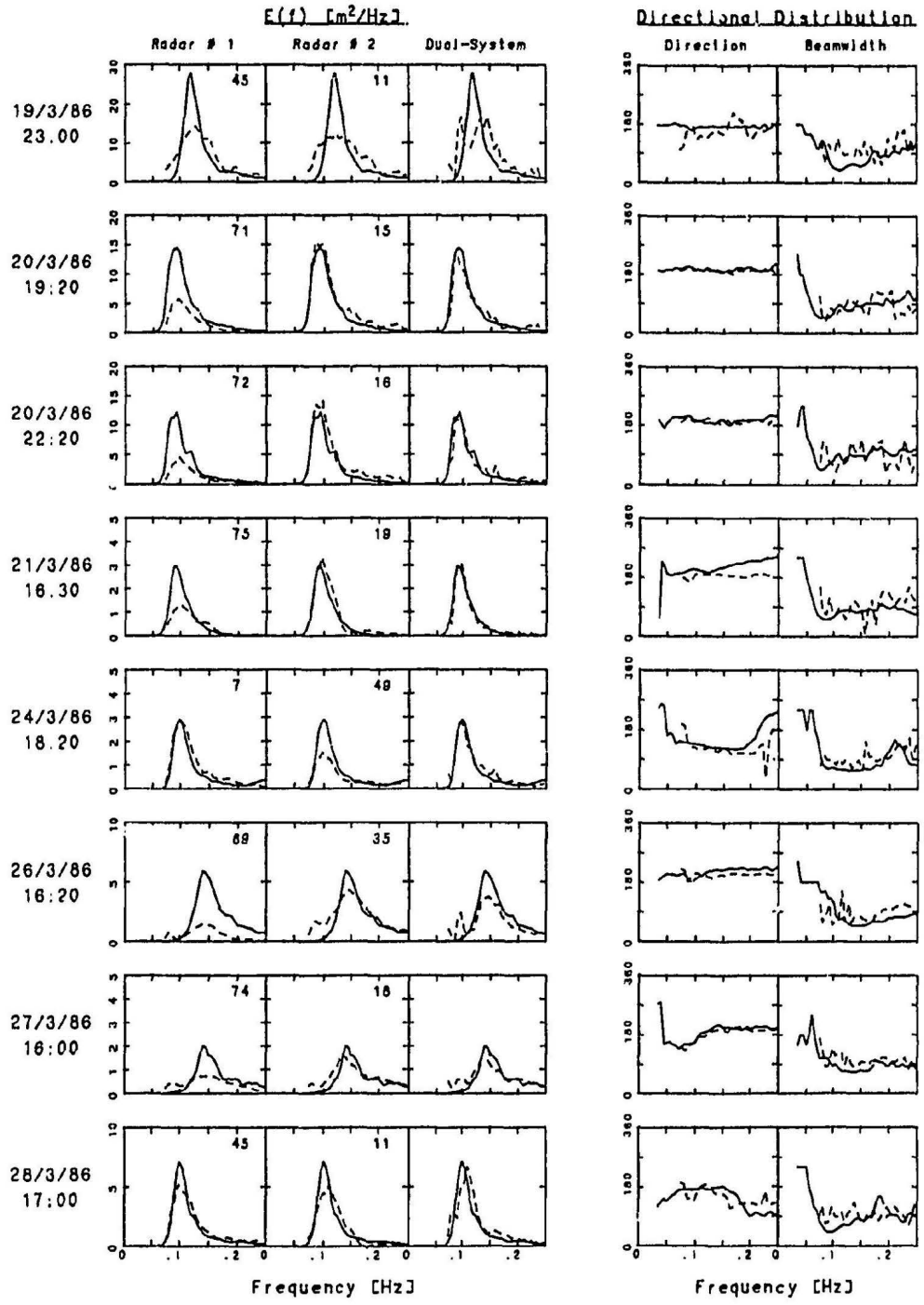

Figure 4.10: Comparison of radar measured wave spectra at CASP (dotted line) using the Walsh and Howell model with those of the WAVEC buoy (solid line). Separate estimates for $e(f)$ are presented for measurements made by each radar alone and in combination. Radar estimates of the cardioid directional distribution parameters have been made using two radars only. The number appearing in upper right hand corner of single radar estimates for $e(f)$ is ϕ_c. The date and start time (GMT) of each approximately 2.5 hour long observation is indicated on the left.

Table 4.5: Single radar (Walsh and Howell model) and WAVEC buoy estimates for significant waveheight (h_s) and peak frequency (f_p) from CASP. Also shown is the wave crossing angle (ϕ_c).

Date	h_s (m)			f_p (Hz)			ϕ_c (deg)	
	Buoy	Radar 1	Radar 2	Buoy	Radar 1	Radar 2	Radar 1	Radar 2
3/19/86	4.24	4.18	4.30	0.120	0.128	0.122	45	11
3/20/86	3.33	2.24	3.62	0.095	0.098	0.086	71	15
3/20/86	2.93	1.94	3.32	0.095	0.098	0.098	72	16
3/21/86	1.37	1.10	1.47	0.090	0.101	0.098	75	19
3/24/86	1.43	1.57	1.15	0.100	0.098	0.098	7	49
3/26/86	2.34	1.24	2.50	0.140	0.140	0.146	89	35
3/27/86	1.36	1.12	1.44	0.140	0.152	0.134	74	18
3/28/86	2.11	2.12	2.02	0.100	0.098	0.110	45	11

Table 4.6: Statistical summary of absolute value differences from the buoy for single radar parameter estimates of Table 4.5.

	h_s	f_p
Mean	14.4 %	0.0054
Standard Deviation	13.5 %	0.0038

Table 4.7: Dual-radar (Walsh and Howell model) and WAVEC buoy estimates for significant waveheight (h_s), peak frequency (f_p), and dominant direction (θ_d) from CASP.

Date	h_s (m)		f_p (Hz)		θ_d (deg, T)	
	Buoy	Radar	Buoy	Radar	Buoy	Radar
3/19/86	4.24	4.48	0.120	0.146	171	149
3/20/86	3.33	3.20	0.095	0.086	199	193
3/20/86	2.93	2.88	0.095	0.092	201	194
3/21/86	1.37	1.32	0.090	0.092	203	185
3/24/86	1.43	1.48	0.100	0.098	132	126
3/26/86	2.34	2.08	0.140	0.146	218	202
3/27/86	1.36	1.40	0.140	0.140	201	187
3/28/86	2.11	2.24	0.100	0.110	173	162

Table 4.8: Statistical summary of absolute value differences from the buoy for dual-radar parameter estimates of Table 4.7.

	h_s	f_p	θ_d
Mean	4.6 %	0.0072	12.5°
Standard Deviation	3.3 %	0.0084	6°

result, the WH model will tend to estimate lower values of h_s than the other models when interpreting wave information from the radar spectrum. This would explain why there is a general trend for the BL/S model to overestimate h_s (see Table 4.3) whereas this is much less so for the WH model (see Table 4.7). This suggests, but is by no means certain, that the WH second order model may provide a better description for the radar spectrum.

If the WH model does better represent the second order return it is expected that the problem of single radar overestimation of h_s using the BL/S model should be most severe when $\phi_c = 0°$. Shown in Fig. 4.11 is a plot of the percentage difference of single radar h_s estimates from the buoy versus ϕ_c for the WH model. It may be seen from Fig. 4.11 that like Fig. 4.9 (BL/S model) that there is a strong linear dependence upon ϕ_c for h_s estimates. An important difference between Figs. 4.9 and 4.11 is that the value of the regression line at $\phi_c = 0°$ is only 16% for Fig. 4.11 while it is 25% for Fig. 4.9. Recall from section 4.3.1 that this value is generally expected to be 10%. This again lends credence to the supposition that the Walsh and Howell model provides a better estimate of the second order spectrum.

With regards to the directional distribution, the WH model also displays better agreement with the buoy than the other models. In general, $\overline{\theta}$ estimates made by all models is virtually the same. Compare a mean difference of 12.5° for θ_d estimates made by the WH model (see Table 4.8) with the 13.75° value obtained using the other models. The important difference with the other models is the much improved comparison with the buoy for $\Delta\theta$ estimates. From examination of Fig. 4.10 it may be observed that all eight CASP observations correlate well with the buoy for this parameter whereas less than half the cases had such good agreement for the other models (see Fig. 4.8).

Overall, the CASP dual-radar results obtained using the WH model are well correlated with the WAVEC's estimates. Better in fact than the results obtained using

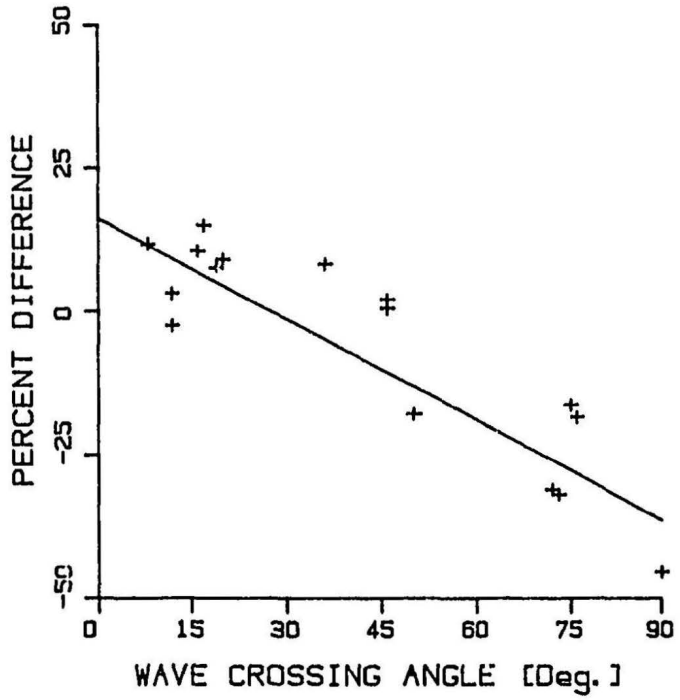

Figure 4.11: Plot of the percentage difference from the buoy versus ϕ_c for CASP single radar h_s estimates made using the Walsh and Howell model. The correlation coefficient of the linear regression line is -0.891.

the BL/S model. This is largely due to the WH model's better estimates for h_s and $\Delta\theta$. This indicates that the WH model for the second order cross section may better represent the radar spectrum than the BL/S model. Due to the somewhat small size of the CASP data set, this finding may be considered only as preliminary. More experiment data will be required in order to be statistically confident of this result.

With the good test results obtained from CASP using the WH model, especially for two radars, the inversion algorithm has been further demonstrated to be an effective means of recovering wave information from the radar spectrum. Based upon the good results found for all models at CASP, the basic feasibility of ground wave radar for wave sensing has been established.

Chapter 5

Conclusions

5.1 General Summary

5.1.1 Solution Method

In this thesis, a data interpretation technique is developed and tested to recover ocean spectral information from the backscatter return of one or more narrow beam HF radars. The basis of this method is the numerical inversion of the first kind integral equation representing the second order radar cross section of the ocean surface at HF. In order to apply the method of Lipa and Barrick (1982) to linearize the equation and to avoid third order effects, the inversion is restricted to that region of the radar spectrum close to the first order peaks ($u < 0.4$).

In linearizing the integral equation, each Doppler half of the radar spectrum is divided by the power contained in its first order peak. Not only does this serve to linearize the equation it has the important advantage of normalizing it as well, i.e., all transmission factors are divided out. Hence, HF radar is a device which requires no calibration of its wave measurement to take into account the path gains and losses of the received signal. For many microwave systems this is a worrisome problem (e.g., Young et al., 1985).

To prepare the linearized integral equation for inversion, it is approximated as a linear algebraic equation at each Doppler frequency point by discretizing the wave spectrum. This is accomplished by expanding the ocean wave spectrum in a trun-

cated Fourier series versus direction and assuming that the Fourier coefficients remain constant over equal length bands of ocean frequency. The system of equations corresponding to a range of Doppler frequencies will then represent a matrix equation whose variables are the Fourier coefficients.

Due to the folding of the wave spectrum about the radar beam, the matrix equation for a single radar will only have even Fourier coefficients as its variables. Consequently, a single radar may only extract ambiguous directional information regarding the wave spectrum. The use of two or more radars overcomes this problem as its matrix equation is dependent upon both even and odd Fourier coefficients.

The solution to the matrix equation is found, in a direct manner, by calculating its pseudo-inverse using a singular value decomposition. A general procedure is outlined to determine how many singular values (r) should be retained to calculate the solution. Overall, there is a great deal of flexibility available for the choice of r. That the solution remains stable over a large range of r and that the singular values decay at a slow rate suggests that this problem is reasonably well conditioned.

As a direct solution is found to the integral equation, the problem of processing radar spectra to recover wave data will become a computationally swift task. All that is required for this analysis is to retrieve the appropriate inverse matrix from computer memory and multiply it with a column vector of radar spectral values. Relatively little time will be required to carry out this simple procedure. Consequently, the proposed algorithm is suitable for near real-time analysis of radar data.

For the most part, this thesis has been concerned with developing an inversion algorithm that is suitable for general use at high HF frequencies ($\approx$ 20 to 30 MHz). Although this algorithm may still be employed for relatively low HF frequencies ($<$ 10 MHz), it is limited at these frequencies to measurement of large sea states only. This limitation is required in order to satisfy the assumption of saturation for the k' wave components used in the linearization technique. As an example of this sea state

limit, at 7 MHz the algorithm may be applied if, in general, $h_s > 5$ m.

That the inversion algorithm is limited in this manner for low HF frequencies does not represent a critical problem as the most crucial task for such systems is to monitor large sea state conditions. However, it would be desirable to modify the linearization method so that the algorithm may perform measurements for a larger range of sea states at lower operating frequencies.

Another important concern for Low HF measurement of wave spectra is the limited range of frequencies that ocean spectral information may be obtained for. To extract information for a greater frequency range a greater range of Doppler frequency must be examined then the present limit of $u < 0.4$. At 10 MHz and $u < 0.4$, spectral information can be extracted for frequencies ranging from 0.044 to 0.157 Hz which will provide a good estimate of significant waveheight for only very large sea state conditions. This contrasts with 25 MHz measurements where information can be extracted for the frequency range 0.07 to 0.25 Hz which, in general, will contain the bulk of the ocean spectral energy.

5.1.2 Test Results

The principal source of data used to test the inversion algorithm in this thesis are the 25.4 MHz dual-radar observations collected during the 1986 CASP experiment. Simulated radar data is used as well to confirm some of the trends observed in the CASP inversion results and to provide additional testing of the algorithm.

With regards to single radar measurements of wave spectra, the principal information that has been extracted so far is the 1-D wave spectrum $e(f)$. The problem of developing a set of techniques to interpret directional information from the single radar inversion results has not been considered in this thesis. It should be cautioned that a single radar may only provide partial directional information as it suffers from a left/right directional ambiguity. This is a result of fact that a single radar folds the

wave spectrum about the radar beam so that it depends only upon $e(f,\theta) + e(f,-\theta)$. Without independent information or the use of at least one other radar this ambiguity cannot be resolved.

For both measured and simulated radar data, it was observed that the accuracy of single radar estimates for $e(f)$ depends, in a strong linear fashion, upon the orientation of the wavefield with respect to the radar beam. In general, the best results are obtained if the directional distribution is aligned with the radar beam ($\phi_c = 0°$) but becomes progressively underestimated as the wavefield approaches directions that are orthogonal to the beam ($\phi_c = 90°$). Although the scale of the estimate for $e(f)$ changes with ϕ_c its basic shape is preserved. This fact suggests that $e(f)$ estimates may be semi-empirically corrected to give it the proper scale with knowledge of several important directional parameters, particularly ϕ_c.

Even with this directional dependence on the accuracy of single radar estimates for $e(f)$, the comparison of several important statistical parameters with the CASP WAVEC buoy have been very encouraging. Using the BL/S second order model, average differences (in an absolute value sense) from the WAVEC buoy are 16.5% for h_s and 0.0048 Hz for f_p. For the WH second order model these differences are 14.4% for h_s and 0.0054 Hz for f_p. For many practical applications (e.g., marine forecasts) this level of accuracy may be considered acceptable and is perhaps already better or comparable with present estimation techniques (e.g., wave model forecasts using meteorological data as input).

In addition to providing full directional information, the use of two radars also provides more accurate estimates of $e(f)$. As to be expected, the accuracy of dual-radar wave spectra estimates will depend upon the angular separation between radar beams with the best results being obtained if the beams are orthogonal. For practical deployments, it is recommended that this angular separation should be as close to 90° as possible but not less than 40°. At CASP this angular separation was 56°.

Overall, there is a high degree of correlation between the CASP dual-radar system and the WAVEC buoy for directional wave spectrum estimates. This is evidenced by the good agreement with the WAVEC buoy for several important statistical parameters. For the BL/S second order model the average difference from the buoy for these parameters are: 9.1% for h_s; 0.005 Hz for f_p; and 13.75° for θ_d. For the WH second order model these average differences are: 4.6% for h_s; 0.007 Hz for f_p; and 12.5° for θ_d.

Although all three second order models produced estimates that agree well with the buoy, it was the WH model which had the best agreement. This is largely due to this model's consistently better estimates for h_s and the directional distribution's angular width. Based upon this better agreement there is evidence to support the claim that the Walsh and Howell (1990) second order model better represents the radar spectrum than the mutually agreeing Barrick and Lipa (1986) and Srivastava (1984) models. Owing to the the relatively small size of the CASP data set it is not yet possible to draw a firm conclusion in this regard.

On the basis of the positive results obtained from the the CASP experiment, the proposed inversion algorithm has demonstrated itself to be a suitable means of analysing HF radar data. In addition, the basic feasibility of ground wave radar for wave sensing has been established.

5.2 Suggestions for Future Work

For many practical situations it is desired to perform wave measurements at operating frequencies generally less than 10 MHz. One of the advantages obtained by operating at such low frequencies is the large sensing range that may be achieved. In order to adapt the present algorithm for general use at low HF frequencies several modifications are recommended:

1. Develop a more general linearization method that does not require the assumption of saturation.

2. Extend the range of ocean frequencies that spectral information is collected for by analysing a greater Doppler frequency range. This will be a especially difficult problem as it will require the inclusion of third order effects into the inversion algorithm (Walsh and Howell, 1990).

It was suggested from the algorithm tests that, with knowledge of the directional distribution, single radar estimates for $e(f)$ may be semi-empirically corrected to give it the proper scale. To accomplish this, a set of techniques must be developed to interpret directional information from the measured even Fourier coefficients. It is not yet certain how much useful directional information may be obtained from a single radar, but it is hoped that it will at least be able to provide reasonable estimates of ϕ_c.

As the radar data is subject to statistical fluctuations due to noise and the stochastic nature of the ocean surface, the algorithm's estimate for the wave spectrum will also be subject to statistical variability. In order to better investigate the accuracy of the solution, it is recommended that a technique be developed to determine confidence intervals for the inversion estimate. This will require a careful study of the integral equation to relate the statistics of the radar data with that of the estimate.

Bibliography

[1] Baker, C. T. H. (1977), *The Numerical Treatment of Integral Equations.* Oxford University Press, Oxford, 1034 pp.

[2] Barrick, D. E. (1972), "Remote sensing of sea state by radar," in *Remote Sensing of the Troposphere*, Edited by V. E. Derr, pp. 12-1–12.46, NOAA Environmental Research laboratories, Boulder, Colo.

[3] Barrick, D. E. (1977), "Extraction of wave parameters from measured HF sea echo Doppler spectra," *Radio Sci.*, vol. 12, pp. 415-424.

[4] Barrick, D. E. and B. J. Lipa (1979), "A compact transportable HF radar system for directional coastal wavefield measurements," in *Ocean Wave Climate.* M. D. Earle and A. Malahoff, Eds., pp. 153-201, Plenum, New York.

[5] Barrick, D. E. and B. J. Lipa (1986), "The second-order shallow-water hydrodynamic coupling coefficient in interpretation of HF radar sea echo," *IEEE J. Oceanic Eng.*, vol. OE-11, no. 2, pp. 310-315.

[6] Crombie, D. D. (1955), "Doppler spectrum of sea echo at 13.56 Mc/s," *Nature*, vol. 175, pp. 681-682.

[7] Delves, L. M. and J. L. Mohamed (1985), *Computational Methods for Integral Equations.* Cambridge University Press, Cambridge, 376 pp.

[8] Dongarra, J. J., C. B. Moler, J. R. Bunch, and G. W. Stewart (1979), *LINPACK Users' Guide.* SIAM, Philadelphia.

[9] Earle, M. D. and J. M. Bishop (1984), *A Practical Guide to Ocean Wave Measurement and Analysis.* ENDECO Inc., Marion MA, U.S.A., 77 pp.

[10] Gill (1990), E. W., *An Algorithm for the Extraction of Ocean Wave Parameters from Wide Beam HF Radar (CODAR) Backscatter.* M. Eng. thesis, Memorial Univ. of Newfoundland, St. John's, NF, Canada, 111 pp.

[11] Gladwell, I. (1974), "Numerical linear algebra," in *Numerical Solution of Integral Equations*, Edited by L. M. Delves and J. Walsh, pp. 23 - 40, Oxford University Press, London.

[12] Hasselmann, K. (1962), "On the non-linear energy transfer in a gravity-wave spectrum; Part 1. General theory," *J. Fluid Mech.*, vol. 12, pp. 481-500.

[13] Hasselmann, K. (1971), "Determination of ocean wave spectra from Doppler radio return from the sea surface," *Nature Phys. Sci.*, vol. 229, pp. 16-17.

[14] Hasselmann, K., D. B. Ross, P. Muller, and W. Sell (1976), "A parametric wave prediction model," *J. Geophys. Res.*, vol. 6, pp. 200-228.

[15] Howell, R., R. S. Srivastava, S. K. Srivastava and J. Walsh (1987), "Remote sensing of sea state using ground wave radars," *Proc. IEEE Oceans '87*, Halifax, Canada, pp. 1085-1090.

[16] Howell, R. and J. Walsh (1988), "Extraction of ocean wave spectra from HF radar returns," *Proc. Canadian Conf. on Electrical and Computer Engineering*, Vancouver, Canada, pp. 719-722.

[17] Howell, R. and J. Walsh (1989), "Measurement of ocean wave spectra using narrow beam HF radar," *Proc. IGARSS '89*, Vancouver, Canada, vol. 5, pp. 2969-2972.

[18] Howell, R. and J. Walsh (1990), "Measurement of ocean wave spectra using a ship-mounted HF radar," *Proc. NECEC '90*, St. John's, Canada, in press.

[19] *IMSL Math/Library User's Manual* (1987), vol. 1, ch. 1, IMSL Inc., 398. pp.

[20] Kinsman, D. (1965), *Wind Waves.* Prentice-Hall, Englewood Cliffs, N.J., 676 pp.

[21] Lipa, B. J. and D. E. Barrick (1980), "Methods for the extraction of long-period ocean wave parameters from narrow beam HF radar sea echo," *Radio Sci.*, vol. 15, pp. 843-853.

[22] Lipa, B. J. and D. E. Barrick (1982), *Analysis Methods for Narrow-Beam High-Frequency Radar Sea Echo.* NOAA Tech. Rep. ERL 420-WPL 56, Boulder, Colo., 54 pp.

[23] Lipa, B. J. and D. E. Barrick (1986), "Extraction of sea state from HF radar sea echo: Mathematical theory and modelling," *Radio Sci.*, vol. 21, pp. 81-100.

[24] Lipa, B. J., D. E. Barrick, and J. W. Maresca Jr. (1981), " HF radar measurements of long ocean waves," *J. Geophys. Res.*, vol. 86, no. c5, pp. 4089-4102.

[25] Longuet-Higgins, M. S., D. E. Cartwright, and N. D. Smith (1963), "Observations of the directional spectrum of sea waves using the motions of a floating buoy," in *Ocean Wave Spectra*, Prentice-Hall, pp. 111-136.

[26] Maresca, J. W., Jr., and T. M. Georges (1980), "Measuring rms waveheight and the scalar ocean wave spectrum with HF skywave radar," *J. Geophys. Res.*, vol. 85, no. c5, pp. 2759-2771.

[27] Miller, G. F. (1974), "Fredholm equations of the first kind," in *Numerical Solution of Integral Equations*, Edited by L. M. Delves and J. Walsh, pp. 175 - 188, Oxford University Press, London.

[28] Phillips, D. L. (1962), "A technique for the numerical solution of certain integral equations of the first kind," *J. Assoc. Comput. Mach.*, vol. 9, pp. 84-97.

[29] Phillips, O. M. (1966), *The Dynamics of the Upper Ocean.* Cambridge University Press, London, 261 pp.

[30] Pierson, W. J. and L. Moskowitz (1964), "A proposed spectral form for fully developed seas based upon the similarity theory of S. A. Kitaigorodskii," *J. Geophys. Res.*, vol. 69(24), pp. 5181-5190.

[31] Rice, S. O. (1951), "Reflection of electromagnetic waves from slightly rough surfaces," in *Theory of Electromagnetic Waves*, Edited by M. Kline, pp. 351-378, Interscience, New York.

[32] Srivastava, R. S. (1987), *Contribution of Multipathing Effects in Ground Wave Radar Return from the Sea Surface.* M. Eng. thesis, Memorial Univ. of Newfoundland, St. John's, NF, Canada, 98 pp.

[33] Srivastava, S. K. (1984), *Scattering of High-Frequency Electromagnetic Waves from an Ocean Surface: An Alternative Approach Incorporating a Dipole Source.* Ph.D. dissertation, Memorial Univ. of Newfoundland, St. John's, NF, Canada, 305 pp.

[34] Stewart, G. W. (1973), *Introduction to Matrix Computations.* Academic Press, New York, 441 pp.

[35] Strang, G. (1976), *Linear Algebra and its Applications.* Academic Press, New York, 374 pp.

[36] Twomey, S. (1963), "On the numerical solution of Fredholm integral equations of the first kind by inversion of the linear system produced by quadrature," *J. Assoc. Comput. Mach.*, vol. 10, pp. 97-101.

[37] van Heteren, J., D. M. A. Schaap, and H. C. Peters (1986), "Rijkswaterstaat's interest in HF radar," *IEEE J. Oceanic Eng.*, vol. OE-11, no. 2, pp. 235-240.

[38] Walsh, J. (1980), *On the Theory of Electromagnetic Propagation Across a Rough Sea and Calculations in the VHF Region.* Tech. rep. prepared for the Def. Res. Estab. Atlantic (DREA), Dep. of Supply and Serv., Govt. of Canada (available from the Ocean Eng. Inform. Centre, Rep. N00232, Memorial Univ. of Newfoundland, St. John's, Nfld, A1B 3X5,Canada), 200 pp.

[39] Walsh, J. and R. Howell (1990), *Model Development for Evaluation Studies of Ground Wave Radar.* Tech. Rep. prepared for the Dept. of National Defence, Govt. of Canada, DSS contract No. W7714-8-5655/01-ss.

[40] Walsh, J. and S. K. Srivastava (1987a), "Rough surface propagation and scatter 1. General formulation and solution for periodic surfaces," *Radio Sci.*, vol. 22, no. 2, pp. 193-208.

[41] Walsh, J. and S. K. Srivastava (1987b), "Rough surface propagation and scatter with applications to ground wave remote sensing in an ocean environment," *Proc. AGARD (NATO) 40th EPP Specialist Meeting*, Conf. Proc. no. 419, pp. 23.1 - 23.15.

[42] Wyatt, L. R. (1984), "The measurement of significant waveheight and mean period from HF radar Doppler spectra," Memo 508, Dept. of Electron. and Electric. Eng., Univ. of Birmingham, Birmingham, U. K..

[43] Wyatt, L. R. (1986), "The measurement of the ocean wave directional spectrum from HF radar Doppler spectra," *Radio Sci.*, vol. 21, no. 3, pp. 473-485.

[44] Wyatt, L. R. (1987), "Ocean wave parameter measurement using a dual-radar system: A Simulation Study," *Int. J. Remote Sensing*, vol. 8, no. 6, pp. 881-891.

[45] Wyatt, L. R., J. Venn, G. D. Burrows, A. M. Ponsford, M. D. Moorhead, and J. van Heteren (1986), "HF radar measurements of ocean wave parameters during NURWEC," *IEEE J. Oceanic Eng.*, vol. OE-11, no. 2, pp. 219-234.

[46] Young, I. R., W. Rosenthal, and F. Ziemer (1985), "A three-dimensional analysis of marine radar images for the determination of ocean wave directionality and surface currents," *J. Geophys. Res.*, vol. 90, no. c1, pp. 1049-1059.